



**ΕΘΝΙΚΟ ΜΕΤΣΟΒΙΟ ΠΟΛΥΤΕΧΝΕΙΟ**

**ΣΧΟΛΗ ΗΛΕΚΤΡΟΛΟΓΩΝ ΜΗΧΑΝΙΚΩΝ**

**ΚΑΙ ΜΗΧΑΝΙΚΩΝ ΥΠΟΛΟΓΙΣΤΩΝ**

**ΤΟΜΕΑΣ ΣΥΣΤΗΜΑΤΩΝ ΜΕΤΑΔΟΣΗΣ ΠΛΗΡΟΦΟΡΙΑΣ**

**ΚΑΙ ΤΕΧΝΟΛΟΓΙΑΣ ΥΛΙΚΩΝ**

**A BIOMECHATRONIC EPP UPPER-LIMB PROSTHESIS  
AND ITS PERFORMANCE COMPARISON TO OTHER  
CONTROL TOPOLOGIES**

**ΜΙΑ ΒΙΟ-ΜΗΧΑΝΟΤΡΟΝΙΚΗ ΕΡΡ ΤΟΠΟΛΟΓΙΑ ΕΛΕΓΧΟΥ  
ΑΝΩ ΠΡΟΣΘΕΤΙΚΟΥ ΑΚΡΟΥ ΚΑΙ Η ΠΕΙΡΑΜΑΤΙΚΗ  
ΣΥΓΓΡΚΡΙΣΗ ΤΗΣ ΑΠΟΔΟΣΗΣ ΤΗΣ ΜΕ ΑΛΛΕΣ  
ΤΟΠΟΛΟΓΙΕΣ ΕΛΕΓΧΟΥ**

**ΔΙΠΛΩΜΑΤΙΚΗ ΕΡΓΑΣΙΑ**

**Σπυρίδων Γ. Κοντογιαννόπουλος**

**Επιβλέπων :** Δ. Δ. Κουτσούρης  
Καθηγητής Ε.Μ.Π.

Αθήνα, Οκτώβριος 2018





**ΕΘΝΙΚΟ ΜΕΤΣΟΒΙΟ ΠΟΛΥΤΕΧΝΕΙΟ**

**ΣΧΟΛΗ ΗΛΕΚΤΡΟΛΟΓΩΝ ΜΗΧΑΝΙΚΩΝ**

**ΚΑΙ ΜΗΧΑΝΙΚΩΝ ΥΠΟΛΟΓΙΣΤΩΝ**

**ΤΟΜΕΑΣ ΣΥΣΤΗΜΑΤΩΝ ΜΕΤΑΔΟΣΗΣ ΠΛΗΡΟΦΟΡΙΑΣ**

**ΚΑΙ ΤΕΧΝΟΛΟΓΙΑΣ ΥΛΙΚΩΝ**

**A BIOMECHATRONIC EPP UPPER-LIMB PROSTHESIS  
AND ITS PERFORMANCE COMPARISON TO OTHER  
CONTROL TOPOLOGIES**

**ΜΙΑ ΒΙΟ-ΜΗΧΑΝΟΤΡΟΝΙΚΗ ΕΡΡ ΤΟΠΟΛΟΓΙΑ ΕΛΕΓΧΟΥ  
ΑΝΩ ΠΡΟΣΘΕΤΙΚΟΥ ΑΚΡΟΥ ΚΑΙ Η ΠΕΙΡΑΜΑΤΙΚΗ  
ΣΥΓΓΡΚΡΙΣΗ ΤΗΣ ΑΠΟΔΟΣΗΣ ΤΗΣ ΜΕ ΑΛΛΕΣ  
ΤΟΠΟΛΟΓΙΕΣ ΕΛΕΓΧΟΥ**

**ΔΙΠΛΩΜΑΤΙΚΗ ΕΡΓΑΣΙΑ**

**Σπυρίδων Γ. Κοντογιαννόπουλος**

**Επιβλέπων :** Δ. Δ. Κουτσούρης  
Καθηγητής Ε.Μ.Π.

Εγκρίθηκε από την τριμελή εξεταστική επιτροπή την 29<sup>η</sup> Οκτωβρίου 2018.

.....  
Δ. Δ. Κουτσούρης  
Καθηγητής Ε.Μ.Π.

.....  
Γ. Ματσόπουλος  
Αν. Καθηγητής Ε.Μ.Π.

.....  
Ε. Παπαδόπουλος  
Καθηγητής Ε.Μ.Π.

Αθήνα, Οκτώβριος 2018

.....  
Σπυρίδων Γ. Κοντογιαννόπουλος

Διπλωματούχος Ηλεκτρολόγος Μηχανικός και Μηχανικός Υπολογιστών Ε.Μ.Π.

Copyright © Σπυρίδων Γ. Κοντογιαννόπουλος, 2018

Με επιφύλαξη παντός δικαιώματος. All rights reserved.

Απαγορεύεται η αντιγραφή, αποθήκευση και διανομή της παρούσας εργασίας, εξ ολοκλήρου ή τμήματος αυτής, για εμπορικό σκοπό. Επιτρέπεται η ανατύπωση, αποθήκευση και διανομή για σκοπό μη κερδοσκοπικό, εκπαιδευτικής ή ερευνητικής φύσης, υπό την προϋπόθεση να αναφέρεται η πηγή προέλευσης και να διατηρείται το παρόν μήνυμα. Ερωτήματα που αφορούν τη χρήση της εργασίας για κερδοσκοπικό σκοπό πρέπει να απευθύνονται προς τον συγγραφέα.

Οι απόψεις και τα συμπεράσματα που περιέχονται σε αυτό το έγγραφο εκφράζουν τον συγγραφέα και δεν πρέπει να ερμηνευθεί ότι αντιπροσωπεύουν τις επίσημες θέσεις του Εθνικού Μετσόβιου Πολυτεχνείου.



## Περίληψη

Η τεχνολογία των προσθετικών άνω άκρων έχει αλλάξει άρδην τα τελευταία χρόνια. Οι διαθέσιμες συσκευές και αυτές που είναι υπό εξέλιξη προσεγγίζουν όλο και περισσότερο την λειτουργικότητα του ακρωτηριασμένου άκρου. Παρ' όλα αυτά, λόγω έλλειψης ανάδρασης της κατάστασής τους, αποτυγχάνουν να ενεργοποιήσουν την ιδιοδεκτική αισθητικότητα του ακρωτηριασμένου.

Η Εκτεταμένη Φυσιολογική Ιδιοδεκτικότητα (Extended Physiological Proprioception-EPP) προσφέρει την δυνατότητα ασυναίσθητου ελέγχου θέσης του άκρου, καθώς τα σήματα ανάδρασης που παρέχει στον ακρωτηριασμένο, ενεργοποιούν την ιδιοδεκτική του αισθητικότητα. Στα μειονεκτήματα, η απευθείας μηχανική σύνδεση με το προσθετικό άκρο, μέσω ντιζών, έχει αποδειχθεί αισθητικά μη αποδεκτή από τους χρήστες, ενώ απαιτείται και ειδικό χειρουργείο κινησιοπλαστικής. Τα παραπάνω οδήγησαν σταδιακά στην εγκατάλειψη της μεθόδου αυτής.

Στο Εργαστήριο Αυτομάτου Ελέγχου της Σχολής Μηχανολόγων Μηχανικών έχει προταθεί μια νέα τοπολογία EPP, που ονομάστηκε Biomechatronic EPP, η οποία δεν απαιτεί τη χρήση ντιζών και χειρουργείου κινησιοπλαστικής. Ο πυρήνας της πρότασης αυτής βασίζεται στην τεχνολογία της τηλερομποτικής και του τηλεχειρισμού. Στο προτεινόμενο σύστημα, εφαρμόζεται ένα master-slave σχήμα ελέγχου θέσης-δύναμης το οποίο περιλαμβάνει την εμφύτευση γραμμικών επενεργητών οι οποίοι συνδέονται σε σειρά κατά τη διάρκεια του χειρουργείου ακρωτηριασμού με τους εναπομείναντες μύες, αποτελώντας τα κύρια (master) ρομπότ του συστήματος τηλεχειρισμού και τη χρήση ενός προσθετικού άκρου, που είναι το ρομπότ υπηρέτης (slave). Το εμφυτευμένο ρομπότ δέχεται ένα σήμα δύναμης από τον μύ στον οποίο είναι προσδεμένο. Αυτή η εντολή δύναμης μεταδίδεται ασύρματα στο ρομπότ υπηρέτη, το οποίο κινείται στο χώρο. Αυτό μεταδίδει το σήμα ανάδρασης της θέσης του πίσω στον ελεγκτή του κυρίου ρομπότ, το οποίο με τη σειρά του κινείται. Ο ελεγκτής του συστήματος εγγυάται τη δυναμική σύζευξη των master και slave ρομπότ, ενεργοποιώντας την ιδιοδεκτική αισθητικότητα του ακρωτηριασμένου.

Στην παρούσα διπλωματική εργασία, παρουσιάζουμε μια πειραματική σύγκριση μεταξύ της προτεινόμενης τοπολογίας, της κλασσικής EPP διάταξης, μιας μυοηλεκτρικής μεθόδου ελέγχου και ενός ελεγκτή ροπής που δεν παρέχει ανάδραση. Περιγράφεται η πειραματική διάταξη, καθώς και η υλοποίηση των κατάλληλων ελεγκτών. Για την πειραματική σύγκριση των προαναφερόμενων μεθόδων ελέγχου χρησιμοποιήσαμε μια δοκιμασία επίτευξης στόχων, η οποία υλοποιήθηκε με βάση το νόμο του Fitts, ως ένα μοντέλο επίδοσης για τη σύγκριση διαφορετικών στρατηγικών ελέγχου άνω άκρων.

Τα αποτελέσματα που παρήχθησαν μέσω της έρευνας και των πειραμάτων που διεξήχθησαν κατά την εκπόνηση της παρούσας Διπλωματικής Εργασίας, αποδεικνύουν την ισοδυναμία της προτεινόμενης Biomechatronic EPP τοπολογίας ελέγχου σε σχέση με την κλασσική EPP διάταξη. Ακόμη, αναδεικνύουν την υπεροχή της έναντι των διατάξεων που δεν παρέχουν στο χρήστη αισθητική ανατροφοδότηση.

## Λέξεις κλειδιά

Τεχνητά μέλη, Προσθετικά άνω άκρων, Έλεγχος, Εκτεταμένη Φυσιολογική Ιδιοδεκτικότητα, Μυοηλεκτρικός έλεγχος, Ηλεκτρομυογράφημα, Νόμος του Fitts, Πειραματική σύγκριση

## Abstract

Upper-limb prosthetic technology has significantly changed in recent years. The devices available and those under development are more and more able to approximate the function of the lost limb. However, most of them fail to activate the proprioception of the amputee, as they do not provide the user with the adequate feedback information. Current externally powered upper-limb prostheses are difficult to use because of the lack of sensory feedback, while Neuroprostheses which have recently been developed for people with upper-limb amputation are complicated, expensive, and still under investigation.

The Extended Physiological Proprioception (EPP) topology has proven the best scheme in terms of control, as the feedback it provides to the amputee, stimulates his proprioceptive sense, enabling subconscious control. On the downside, the required connection cables are aesthetically unacceptable by the users while an additional post-amputation surgery is required for their installation. The aforementioned attributes gradually led to the abandonment of EPP control, and the propagation and eventually establishment of myoelectric control, which is a noninvasive method. Subsequently, the advantage of subconscious control also vanished.

At the Control Systems Laboratory of the School of Mechanical Engineering, a new topology of EPP, coined as Biomechatronic EPP, was proposed to eliminate the drawback of cineplasty and Bowden cables, which render the EPP unaesthetic for the user. The core of this concept is based on principles of the field of Telerobotics and Teleoperation. In the proposed system, a master - slave position-force control scheme is applied, using an implanted linear actuator as the Master at the time of the amputation surgery, and the prosthetic hand as the Slave. The implant takes a force command signal from the muscle/tendon attached to. The force command then is transmitted wirelessly to the Slave, and a position feedback comes back from the Slave to the linear actuator controller, which then moves. The controller of the topology guarantees the dynamic conjunction of the master and slave robots, enabling amputee's proprioception. The proposed system is expected to provide a modern EPP-equivalent control scheme for upper-limb prostheses without the disadvantages of previous EPP configurations, but with the control advantages of proprioceptive feedback.

In this thesis, we present an experimental comparison among the proposed control topology, the Classic EPP topology, an EMG control method and a torque controller without feedback, coined "Unconnected". The experimental setup used for the evaluation of the experiments along with the implementation of the appropriate controllers, are described. The test used to experimentally compare the aforementioned control methods was a target acquisition test, built accordingly to Fitts' Law.

The results conducted during this thesis, prove the equivalency of the proposed Biomechatronic EPP control topology to the Classic EPP configuration and also reveal its superiority over the two other control methods, which do not provide the user with the adequate sensory feedback.

## Key words

Artificial limbs, Upper-Limb Prosthetics, Prosthesis, Control, Extended Physiological Proprioception, Myoelectric control, EMG, Fitts' law, Experimental comparison

*Αφιερώνεται στους γονείς μου, Γιώργο και Βάσω,  
τον αδελφό μου, Χρήστο,  
την κοπέλα μου Γιάννα  
και τους φίλους μου, Γιάννη, Αντώνη,  
Κυριάκο, Δημήτρη και Βαγγέλη.*

## Preface

Nowadays, robotics has reached a high level of maturity driven by the cutting-edge technology innovation. This has also affected the field of upper-limb prostheses. Recently, technical innovations have combined to make artificial limbs much more comfortable, efficient, and lifelike than earlier versions. However, in the majority of these advanced, multi-degree of freedom prosthetic systems, the quality of the interface between the limb remnants and the artificial prosthesis is in doubt. This lack of somatosensory connection has led many amputees around the world to abandon their prosthetics and therefore lose the hope for a normal life. For me, finding of a viable solution for those people is a matter of necessity. This fact along with the vast field of knowledge that the prosthetics could offer were the main reasons why I decided to choose this diploma thesis topic.

The current diploma thesis is part of a bigger project running the last years at the Control System Laboratory of NTUA, which introduces a novel prosthetic system for below the elbow amputations. An in principle evaluation of the control quality provided by the proposed control topology has been realized in previous related theses in both simulation and experimental environments. Following these works, this thesis presents an experimental comparison among our proposal and traditional control strategies that are used in upper-limb prostheses.

In order to pursue the objectives of the current work, a lot of demands had to be satisfied. This forced me to investigate several aspects of different scientific fields. Control systems, human computer interaction, circuit design, biology and statistics were combined during the realization of this thesis. Apart from the theoretical skills that I obtained, I also became extensively familiar with MATLAB/Simulink and dSpace DS1103, a powerful tool for control systems implementation and experimentation. Finally, the interactive nature of the experiments conducted, provided me with the spirit of collaboration and teamwork.

At this point it would be appropriate to thank my supervisor, Prof. Evangelos Papadopoulos, who gave me the opportunity to work on this thesis. At his laboratory I had the chance to meet and collaborate with magnificent people and every single one of his subordinates that helped me through this thesis. Furthermore, I would like to thank Postdoctoral Fellow Dr. Georgios A. Bertos, who has proposed the Biomechatronic EPP concept, for his advising during the stages of this thesis and his motivational and inspiring critique. Finally, I would like to express my thanks to Nikolaos Koukoulas for the harmonious and constructive collaboration we had during our meetings in the laboratory.

# Table of Contents

Περίληψη .....	1
Abstract .....	2
Preface .....	4
Table of Contents .....	5
Figure Index .....	8
Table Index .....	12
Εκτεταμένη Περίληψη .....	14
Εισαγωγή .....	14
Ο Νόμος του Fitts .....	15
Πειραματική Διάταξη .....	15
Στρατηγικές Ελέγχου .....	17
Πειραματική Φάση .....	19
Αποτελέσματα .....	21
Συμπεράσματα .....	21
<b>1 Introduction .....</b>	<b>23</b>
1.1 Purpose .....	25
1.2 Literature Review .....	25
1.3 Thesis Structure .....	28
<b>2 Fitts' Law .....</b>	<b>30</b>
2.1 Information Theory Foundation .....	30
2.2 Original Model Formulation .....	30
2.3 The Original Experiments and Emerging Problems .....	32
2.4 Variations of Fitts' Law and Adjustment for Accuracy .....	34
2.5 The Standard for Building a Fitts' Law Model .....	34
<b>3 Experimental Setup .....</b>	<b>37</b>
3.1 The Mechanical Setup .....	37
3.2 Force Transducer .....	40
3.3 Hardware Connectivity .....	42
<b>4 Control topologies .....</b>	<b>48</b>
4.1 Classic EPP control topology .....	48
4.2 Biomechatronic EPP control topology .....	51
<b>5 EMG Setup and Controller .....</b>	<b>57</b>
5.1 Anatomy of the Forearm .....	57
5.2 EMG Sensors .....	60
5.3 EMG Signal Acquisition and Configuration .....	61
<b>6 Target experiment .....</b>	<b>66</b>
6.1 Protocol .....	66
6.2 Results .....	69
<b>7 Experimental Data Evaluation .....</b>	<b>88</b>

7.1	Transparency-Equivalency Test .....	88
7.2	Force Application Test .....	95
7.3	EMG signals comparison .....	98
<b>8</b>	<b>Conclusion and Future Work .....</b>	<b>101</b>
8.1	Conclusion .....	101
8.2	Future Work .....	101
<b>9</b>	<b>References .....</b>	<b>103</b>
<b>10</b>	<b>Appendix A .....</b>	<b>106</b>
10.1	Psychophysics Toolbox Version 3 (PTB-3) .....	106
10.2	Myo Mex SDK MATAB Wrapper .....	109
10.3	ASAM XIL API-dSPACE .....	112
10.4	Target Experiment Script .....	116
<b>11</b>	<b>Appendix B .....</b>	<b>122</b>



## Figure Index

Figure 1.1.	EMG control topology. ....	23
Figure 1.2.	EPP prosthesis control for forearm amputee with biceps cineplasty. ....	24
Figure 1.3.	Proposed control topology of Biomechatronic EPP. ....	25
Figure 1.4.	Schematic illustration of the traditional body-powered prosthesis for forearm amputations. ....	26
Figure 1.5.	Schematic diagram of a myoelectric controller for upper-limb prosthetics. ....	27
Figure 2.1.	Movement task of a distance A and a target width W. ....	31
Figure 2.2.	The reciprocal tapping paradigm(Fitts,1954). ....	32
Figure 2.3.	Scatter plot of movement time vs. index of difficulty using data from Fitts' (1954) 1-oz tapping experiment. ....	33
Figure 3.1.	Schematic illustration of Classic EPP setup. ....	37
Figure 3.2.	Setup for the Classic EPP configuration. ....	38
Figure 3.3.	3D printed shaft. ....	38
Figure 3.4.	Schematic design of the proposed Biomechatronic EPP setup. ....	39
Figure 3.5.	Setup for the Biomechatronic EPP configuration. ....	39
Figure 3.6.	Final setup. ....	40
Figure 3.7.	(a) The Force Sensitive Resistor used in the setup. (b) Resistance vs Force diagram. ....	40
Figure 3.8.	Operational Amplifier LT1495. ....	41
Figure 3.9.	Signal Conditioning Circuit (SCC). Modified from [4]. ....	41
Figure 3.10.	Hameg7042-5. Two of these power suppliers (totally five channels) used for the power supply of the whole setup. ....	42
Figure 3.11.	DS1103 expansion box and the 50 pin D-SUB male connectors cables. ....	42
Figure 3.12.	AZBDV10A4 analog servo drive. ....	43
Figure 3.13.	HEDS 5540 500 Counts per turn encoder pins mapping. ....	43
Figure 3.14.	Schematic Design for the Slave Motor Division. ....	44
Figure 3.15.	DRV8833 motor driver. ....	45
Figure 3.16.	The ENX10 EASY 512IMP encoder pins mapping. ....	45
Figure 3.17.	Schematic Design for the Master Motors Subsystem. ....	46
Figure 3.18.	Schematic Design for the FSRs' Subsystem. ....	47
Figure 4.1.	Schematic structure of the Classic EPP topology. ....	48
Figure 4.2.	Schematic diagram of the Classic EPP controller. ....	49
Figure 4.3.	Processing of the acquired force signals. ....	49
Figure 4.4.	Upper and Lower Bounds of the FSR sensor Output. From [4]. ....	49
Figure 4.5.	Position limits and direction change ....	50
Figure 4.6.	Normalization of the input for the motor driver. ....	51
Figure 4.7.	Schematic structure of the Biomechatronic EPP topology. ....	51
Figure 4.8.	Biomechatronic EPP control scheme. ....	52
Figure 4.9.	PD Control of DC motor plant. ....	53
Figure 4.10.	Block diagram of model based feedforward friction compensation. ....	55
Figure 4.11.	Feedforward loop. ....	56
Figure 5.1.	The superficial muscles of the anterior forearm. ....	58
Figure 5.2.	The muscles in the superficial layer of the posterior forearm. ....	59



Figure 5.3.	The Thalmic Labs Myo Armband. ....	60
Figure 5.4.	(a) Numbering of sensor pods. (b) The Myo Armband mounted on the forearm. ....	61
Figure 5.5.	EMG configuration stages. ....	62
Figure 5.6.	High-Pass filter magnitude and phase responses. ....	62
Figure 5.7.	Low-Pass filter magnitude and phase responses. ....	63
Figure 5.8.	EMG signal excerpt from Extensor Carpi Radialis during configuration. (a) Raw EMG signal, (b) High-Pass Filtered, (c) Rectified and (d) Low-Pass Filtered. ....	63
Figure 5.9.	Normalization of EMG signal. ....	64
Figure 5.10.	Threshold of the input signals. ....	65
Figure 6.1.	(a) Shaft added to imitate wrist movement. (b) Extension and flexion of the wrist. ....	66
Figure 6.2.	Fitts' Paradigm. ....	67
Figure 6.3.	Fitts' Law application in Human Computer Interaction. ....	67
Figure 6.4.	Subjects during the experiments. ....	67
Figure 6.5.	Monitor display during experiments. ....	68
Figure 6.6	The distribution of end-points for a pair of targets with $W=15$ and $D=27.5$ . With green color the end-points for forward movement and with red color for backward. The end-points that lie on the right side of the left circle and on the left side of the right circle are considered as outliers. ....	69
Figure 6.7.	Movement time by control method. ....	77
Figure 6.8.	Bonferroni's Confidence Intervals for Movement Time. ....	78
Figure 6.9.	Error rate by control method. ....	79
Figure 6.10.	Bonferroni's Confidence Intervals for Error Rate. ....	80
Figure 6.11.	Throughput by control method. ....	81
Figure 6.12.	Bonferroni's Confidence Intervals for Throughput. ....	82
Figure 6.13.	Linear regression model for Biomechatronic EPP. ....	84
Figure 6.14.	Linear regression model for Classic EPP. ....	85
Figure 6.15.	Linear regression model for Unconnected method. ....	86
Figure 6.16.	Linear regression model for EMG method. ....	87
Figure 7.1.	(a) Responses of the FSR sensors connected to the agonist (red line) and the antagonist muscle (blue line) (b) Difference ( $F_{ag}-F_{ant}$ ) between the FSR responses of the antagonistic muscle pair. ....	88
Figure 7.2.	(a) Current and (b) torque of the slave motor. ....	89
Figure 7.3.	(a) Current and (b) torque of the agonistic master motor. ....	89
Figure 7.4.	(a) Current and (b) torque of the antagonistic master motor. ....	90
Figure 7.5.	Torque response of the slave motor (blue line), master motors (red line) and the difference between them (yellow dotted line). ....	90
Figure 7.6.	(a) Angular position and (b) velocity of the slave motor. ....	91
Figure 7.7.	Displacement of the Bowden cable terminals in Classic EPP topology: Terminal connected to the (a) Agonistic (b) Antagonistic muscle. ....	91
Figure 7.8.	(a) Displacement and (b) velocity responses of the agonistic linear actuator in Biomechatronic EPP topology. ....	92
Figure 7.9.	(a) Displacement and (b) velocity responses of the antagonistic linear actuator in Biomechatronic EPP topology. ....	92
Figure 7.10.	(a) Comparison of the agonistic terminal displacement responses during Biomechatronic (blue line) and Classic EPP (red dotted line) and (b) their respective error. ....	93

Figure 7.11.	(a) Comparison of the antagonistic terminal displacement responses during Biomechatronic (blue line) and Classic EPP (red dotted line) and (b) their respective error .....	93
Figure 7.12.	Measurement of the delay between the applying force and the displacement of the prosthesis motor.....	94
Figure 7.13.	Power losses of the agonist (blue line) and antagonist (red line) master motors. Yellow line represents the total power losses. ....	95
Figure 7.14.	The weight attached to the shaft of the slave motor. ....	95
Figure 7.15.	FSRs output with the weight (a) not attached and (b) attached to the shaft of the slave motor. ....	96
Figure 7.16.	Reaction time among subjects for Biomechatronic EPP. ....	97
Figure 7.17.	Reaction time among subjects for Classic EPP.....	98
Figure 7.18.	Five sections of the Activation Level (AL) of Extensor Carpi Radialis recorded during the realization of the target experiments.....	99
Figure 7.19.	Five sections of the Activation Level (AL) of Flexor Carpi Rasdialis recorded during the realization of the target experiments.....	99
Figure 10.1.	Schematic diagram showing the connection between the dSPACE products and software tools.....	113



## Table Index

Table 2.1.	Data from Fitts' (1954) Tapping Task Experiment with 1-oz Stylus.....	32
Table 2.2.	Variations of Fitts' Law.....	34
Table 3.1.	Analog Servo Drive AZBDC10A4 connectivity map.....	44
Table 3.2.	ENCODER HEDS5540 500 Counts per turn connectivity map.....	44
Table 3.3.	DRV8833 Dual Motor Driver Carrier connectivity map.....	45
Table 3.4.	Sensor - ENX10 EASY 512IMP connectivity map for Master Motor Right.....	45
Table 3.5.	Sensor - ENX10 EASY 512IMP connectivity map for Master Motor Left.....	46
Table 3.6.	FSR Sensors connectivity map.....	47
Table 4.1.	The values of the parameters of the system.....	53
Table 4.2.	Logic table of DRV883 Inputs.....	56
Table 6.1	Possible widths and distances.....	69
Table 6.2.	Target widths and distances before and after adjustment.....	70
Table 6.3.	Summary Data for Biomechatronic EPP.....	71
Table 6.4.	Summary data for Classic EPP.....	72
Table 6.5.	Summary data for Unconnected method.....	73
Table 6.6.	Summary data for EMG.....	74
Table 6.7.	ANOVA table.....	75
Table 6.8.	Data for Movement Time.....	77
Table 6.9.	ANOVA table for Movement Time.....	78
Table 6.10.	Bonferroni's Method for Movement Time.....	78
Table 6.11.	Results for Error Rate.....	79
Table 6.12.	ANOVA table for Error Rate.....	80
Table 6.13.	Bonferroni's Method for Error Rate.....	80
Table 6.14.	Results for Throughput.....	81
Table 6.15.	ANOVA table for Throughput.....	82
Table 6.16.	Bonferroni's Method for Throughput.....	82
Table 6.17.	Summary of the Model for Biomechatronic EPP.....	84
Table 6.18.	ANOVA table for Biomechatronic EPP.....	84
Table 6.19.	Coefficients of model for Biomechatronic EPP.....	84
Table 6.20.	Summary of the Model for Classic EPP.....	85
Table 6.21.	ANOVA table for Classic EPP.....	85
Table 6.22.	Coefficients of model for Classic EPP.....	85
Table 6.23.	Summary of the Model for Unconnected.....	86
Table 6.24.	ANOVA table for Unconnected.....	86
Table 6.25.	Coefficients of model for Unconnected.....	86
Table 6.26.	Summary of the Model for EMG.....	87
Table 6.27.	ANOVA table for EMG.....	87
Table 6.28.	Coefficients of model for EMG.....	87
Table 7.1.	Answers given by the five subjects through the experiment. Each cell corresponds to a collision. With green color are the positive answers and with red color are the negative ones.....	97

Table 7.2. Mean activation levels of the flexor muscle. .... 99

Table 7.3. Mean activation levels of the extensor muscle. .... 100

# Εκτεταμένη Περίληψη

## Εισαγωγή

Η αντικατάσταση των ανθρώπινων άνω άκρων από μηχανικά αποτελεί μία σοβαρή επιστημονική πρόκληση. Οι μηχανικές απαιτήσεις και περιορισμοί αυτού του στόχου είναι σημαντικοί. Ωστόσο, ο πιο κρίσιμος παράγοντας για τη σωστή λειτουργία του άνω άκρου είναι ο έλεγχός του. Ο σχεδιασμός του ελεγκτή ορίζει την επικοινωνία - σύνδεση μεταξύ του ακρωτηριασμένου ατόμου και του προσθετικού άνω άκρου. Η πρόκληση αυτή συνήθως περιορίζεται από την έλλειψη επαρκούς επικοινωνίας η οποία πραγματοποιείται μόνο με οπτική ανατροφοδότηση, μεταξύ του ακρωτηριασμένου και του προσθετικού άνω άκρου.

Μία μέθοδος ελέγχου που κυριάρχησε στο πεδίο των προσθετικών και χρησιμοποιήθηκε ευρέως είναι ο Αναλογικός Μυοηλεκτρικός Έλεγχος. Ένα σύστημα αναλογικού μυοηλεκτρικού ελέγχου αποτελείται από έναν μικροελεγκτή ή έναν υπολογιστή που καταγράφει τα μυοηλεκτρικά σήματα (“EMG”) από αισθητήρες στους μύες και στη συνέχεια ενεργοποιεί τον αντίστοιχο ενεργοποιητή άρθρωσης ανάλογα με το σήμα “EMG”.

Αν και τα μυοηλεκτρικά σήματα θεωρούνται ευρέως ως η καλύτερη διαθέσιμη διασύνδεση ελέγχου για προσθετικά άκρα, πολλοί ακρωτηριασμένοι εγκαταλείπουν τις συσκευές τους από απογοήτευση λόγω της έλλειψης ακρίβειας των κινήσεων των προσθετικών.

Μία εναλλακτική τοπολογία ελέγχου είναι η Κλασσική Εκτεταμένη Φυσιολογική Ιδιοδεκτικότητα (Classic Extended Physiological Proprioception – “Classic EPP”). Στην τοπολογία αυτή το προσθετικό άκρο συνδέεται απευθείας με τους εναπομείναντες λειτουργικούς μύες του ακρωτηριασμένου, μέσω μηχανικών συνδέσεων, συνήθως ντιζών. Με τον τρόπο αυτό, το προσθετικό άκρο γίνεται επέκταση του εναπομείναντος μέλους.

Ωστόσο, αυτή η μέθοδος ελέγχου έχει το μειονέκτημα ότι δεν είναι αισθητική για τον χρήστη, έχει συχνά περιορισμούς ελέγχου (που σχετίζονται με την κατεύθυνση της κίνησης) και επιπλέον απαιτείται πλαστική χειρουργική.

Κατά τη διάρκεια των τελευταίων ετών, στο εργαστήριο Αυτομάτου Ελέγχου του Ε.Μ.Π., όπου η παρούσα διπλωματική εργασία εκπονήθηκε, έχει πραγματοποιηθεί έρευνα πάνω σε μία πρωτοποριακή μέθοδο ελέγχου άνω προσθετικών άκρων, που ονομάστηκε “Biomechatronic EPP”, η οποία δεν απαιτεί τη χρήση ντιζών και χειρουργείου κινησιοπλαστικής. Η νέα αυτή πρόταση αποσκοπεί στην ενεργοποίηση της φυσιολογικής ιδιοδεκτικότητας του χρήστη. Η κεντρική ιδέα βασίζεται στην ανάπτυξη και εξέλιξη ενός διαφορετικού κλάδου της Ρομποτικής, αυτόν της Τηλερομποτικής- Τηλεχειρισμού (Telerobotics-Teleoperation), και περιλαμβάνει χρήση εμφυτευμάτων, που σκοπός τους είναι η ενεργοποίηση των νευρικών υποδοχέων των μυών κατά την λειτουργία του άκρου μέσω μιας αρχιτεκτονικής ελέγχου master-slave.

Στην παρούσα διπλωματική εργασία, παρουσιάζουμε μια πειραματική σύγκριση μεταξύ της προτεινόμενης τοπολογίας, της κλασσικής EPP διάταξης, μιας μυοηλεκτρικής μεθόδου ελέγχου και ενός ελεγκτή ροπής που δεν παρέχει ανάδραση (“Unconnected”). Περιγράφεται η πειραματική διάταξη, καθώς και η υλοποίηση των κατάλληλων ελεγκτών. Για την πειραματική σύγκριση των προαναφερόμενων μεθόδων ελέγχου χρησιμοποιήσαμε μια δοκιμασία επίτευξης στόχων, η οποία

υλοποιήθηκε με βάση το νόμο του Fitts, ως ένα μοντέλο επίδοσης για τη σύγκριση διαφορετικών στρατηγικών ελέγχου άνω άκρων.

## Ο Νόμος του Fitts

Στην εργονομία, ο Νόμος του Fitts είναι ένα μοντέλο της ανθρώπινης κίνησης, το οποίο προβλέπει τον χρόνο που απαιτείται για την γρήγορη μετακίνηση από μια θέση εκκίνησης σε μιας τελική περιοχή-στόχο, ως συνάρτηση της απόστασης από το στόχο και το μέγεθος του στόχου. Ο Νόμος του Fitts χρησιμοποιείται κατά τη δημιουργία μαθηματικών υποδειγμάτων για την πράξη της κατάδειξης τόσο στον φυσικό κόσμο (π.χ. τείνοντας χέρι ή δάχτυλο) όσο και στο περιβάλλον των υπολογιστών (π.χ. μετακινώντας το δείκτη στην οθόνη με το ποντίκι).

Μαθηματικά, ο Νόμος του Fitts έχει διατυπωθεί με αρκετούς διαφορετικούς τρόπους. Μια συνηθισμένη μορφή είναι η διατύπωση Σάνον (προτεινόμενη από τον Σκοτ Μακ Κένζι, καθηγητή του Πανεπιστημίου του Γιορκ, και ονομασμένη έτσι για την ομοιότητά της με το θεώρημα Σάνον-Χάρτλεϊ) για κίνηση σε μία διάσταση:

$$MT = a + b \log_2(2D/W) \quad (1)$$

Όπου: MT - ο μέσος χρόνος που χρειάζεται για την ολοκλήρωση της κίνησης

a, b - εμπειρικές σταθερές

D - απόσταση από το σημείο εκκίνησης μέχρι το κέντρο του στόχου

W - πλάτος του στόχου μετρημένο κατά μήκος του άξονα της κίνησης

Ο Νόμος του Fitts είναι ένα ασυνήθιστα επιτυχές και καλά μελετημένο μαθηματικό υπόδειγμα. Πειράματα τα οποία αναπαράγουν τα αποτελέσματα του Fitts και αποδεικνύουν την εφαρμογή του νόμου του σε κάπως διαφορετικές περιπτώσεις δεν είναι δύσκολο να εκτελεστούν. Οι μετρήσεις από αυτά τα πειράματα συχνά σχηματίζουν μια ευθεία γραμμή με συντελεστή συσχέτισης ίσο με 0,95 ή μεγαλύτερο, πράγμα που υποδεικνύει ότι το υπόδειγμα είναι πολύ ακριβές.

Ο λογάριθμος στο νόμο του Fitts καλείται δείκτης δυσκολίας (ID) για το στόχο, και μετριέται σε bits. Μπορούμε να ξαναγράψουμε το νόμο ως:

$$ID = \log_2 \left( \frac{D}{W} + 1 \right) \quad (2)$$

## Πειραματική Διάταξη

Η πειραματική διάταξη που χρησιμοποιήθηκε για την υλοποίηση των “Classic EPP”, “Biomechatronic EPP” και “Unconnected” τοπολογιών ελέγχου παρουσιάζεται στην Εικόνα 1. Οι τοπολογίες αυτές μοιράζονται τον ίδιο μηχανισμό ο οποίος στις “Classic EPP” και “Unconnected” τοπολογίες αποτελεί το προσθετικό άκρο, ενώ στην Biomechatronic το slave robot. Όπως περιγράφεται και παρακάτω η είσοδος του συστήματος και στις τρεις περιπτώσεις ελέγχου πραγματοποιείται από δύο σημεία τα οποία ουσιαστικά προσομοιώνουν το ζεύγος ανταγωνιστικών μυών που είναι υπεύθυνο για τον έλεγχο του προσθετικού άκρου. Σημειώνεται ότι ο έλεγχος πραγματικού χρόνου και για τις δύο διατάξεις επιτυγχάνεται μέσω του προγράμματος MATLAB/Simulink κάνοντας χρήση του DSpace control board.

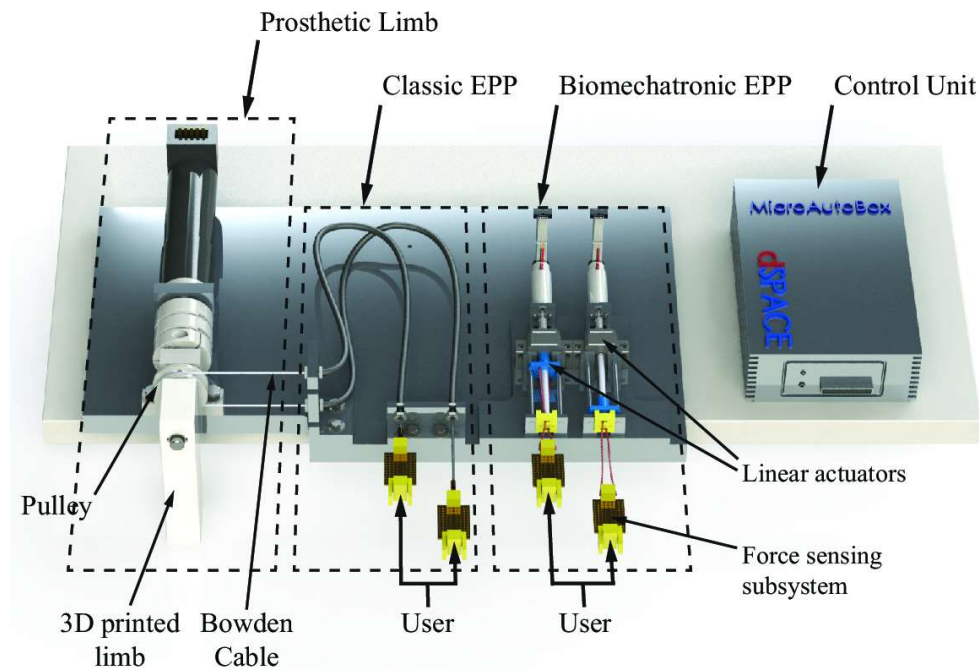
“**Classic EPP**”: Η “Classic EPP” διάταξη αποτελείται από την ντίζα ελέγχου (Bowden Cable) και το προσθετικό άκρο. Η ντίζα προσδένεται πάνω στην τροχαλία του προσθετικού άκρου και στερεώνεται

με έναν κοχλία σύσφιξης. Ο χρήστης της τοπολογίας ασκεί δυνάμεις τραβώντας σχοινάκια που δένονται στους ακροδέκτες της ντίζας, και οι δυνάμεις αυτές, αφού διαβαστούν από αισθητήρες, οδηγούν τον κινητήρα του προσθετικού. Με αυτόν τον τρόπο, η μετατόπιση του ακροδέκτη της ντίζας στο σημείο επικοινωνίας με τον χρήστη είναι απευθείας ανάλογη της ακτίνας της τροχαλίας πάνω στην οποία είναι προσδεμένη. Για την καταγραφή των ασκούμενων δυνάμεων χρησιμοποιούνται Force Sensitive Resistors (FSRs).

**“Biomechatronic EPP”:** Στην “Biomechatronic EPP” διάταξη ο χρήστης έρχεται σε επαφή και αλληλοεπιδρά με το master ρομπότ. Συγκεκριμένα, ασκεί απευθείας δυνάμεις τραβώντας τα περικόχλια κίνησης του γραμμικού επενεργητή (linear actuator). Ενδιάμεσα παρεμβάλλονται οι αισθητήρες δύναμης (FSRs), ώστε το σήμα δύναμης του χρήστη να διαβάζεται και να τροφοδοτεί τον ελεγκτή της τοπολογίας. Η επικοινωνία του master και slave ρομπότ γίνεται με την κάρτα ελέγχου dSpace, μέσω της οποίας πραγματοποιείται ο έλεγχος που εγγυάται την δυναμική σύζευξη του χρήστη με το προσθετικό άκρο.

**Unconnected:** Στην “Unconnected” τοπολογία ελέγχου η μόνη ειδοποιός διαφορά σε σχέση με την “Classic EPP” είναι ότι οι αισθητήρες δύναμης προσδένονται σε σταθερά σημεία, με αποτέλεσμα να μην υπάρχει ανατροφοδότηση στον χρήστη

**Αισθητήρες Δύναμης :** Για την καταγραφή των ασκούμενων δυνάμεων χρησιμοποιούνται Force Sensitive Resistors (FSRs). Η τιμή των αντιστάσεων αυτών μεταβάλλεται ανάλογα με την πίεση που ασκείται στη αισθητήρια επιφάνειά τους. Οι αισθητήρες δύναμης βρίσκονται κλεισμένοι μέσα σε μία θήκη, η οποία, καθώς ο χρήστης τραβάει τα σχοινάκια στα οποία είναι συνδεδεμένος, παράγει κάθετη δύναμη στην αισθητήρια περιοχή του. Η θήκη είναι σχεδιασμένη ώστε να προσαρμόζεται πάνω της ένα ηλεκτρικό κύκλωμα που ενισχύει το σήμα που παράγεται από τους αισθητήρες. Αυτό γίνεται για να μειωθούν οι επιπτώσεις του θορύβου κατά την μεταφορά του σήματος στην απόσταση του ελεγκτή.



Εικόνα 1. Εργαστηριακή πειραματική διάταξη.



**Μυοηλεκτρική μέθοδος ελέγχου (“EMG” topology):** In the “EMG” control method, the reference input is provided by myoelectric signals, acquired from the muscles of interest. The Myo armband, developed by Thalmic Labs, was used to record these signals.

Στην μυοηλεκτρική μέθοδο ελέγχου, η είσοδος στο σύστημα παρέχεται μέσω μυοηλεκτρικών σημάτων, τα οποία καταγράφονται από τους κατάλληλους μύες. Για την καταγραφή των σημάτων αυτών χρησιμοποιείται το Myo Armband (Εικόνα 2).



**Εικόνα 2. Myo Armband, κατασκευασμένο από την Thalmic Labs.**

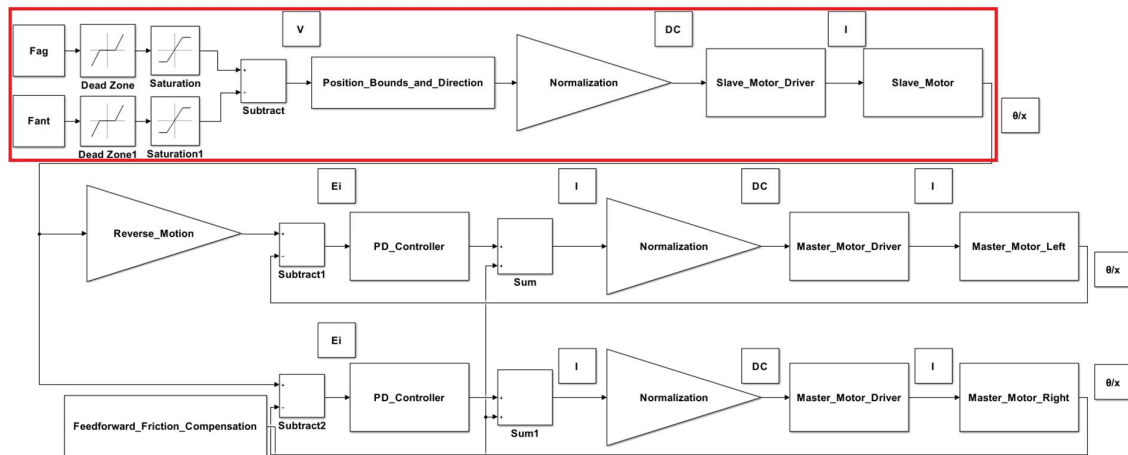
### **Στρατηγικές Ελέγχου**

Πηγή ελέγχου για τις “Biomechatronic EPP”, “Classic EPP” και “Unconnected” τοπολογίες είναι η διαφορά μεταξύ των δυνάμεων που καταγράφονται από τα FSRs. Το σχήμα ελέγχου για αυτές τις τοπολογίες παρουσιάζεται στην Εικόνα 3. Το κομμάτι μέσα στο κόκκινο κουτί χρησιμοποιείται ως ελεγκτής για τις “Classic EPP” και Unconnected μεθόδους. Το σήμα που παρέχεται από τον αισθητήρα δύναμης κυμαίνεται μεταξύ 0 και 5V. Το στάδιο του “dead zone” μοντελοποιεί το όριο κάτω από το οποίο η τιμή της εισόδου δεν προκαλεί την κίνηση του προσθετικού, ενώ το στάδιο του “saturation” χρησιμοποιείται για προστασία σε περίπτωση που η είσοδος προσπεράσει τα όρια που έχουν τεθεί. Έπειτα, η απόλυτη διαφορά μεταξύ των δυνάμεων των ανταγωνιστικών μυών κανονικοποιείται και παρέχεται σαν είσοδος στον driver του κινητήρα, ελέγχοντας με αυτόν τον τρόπο την ταχύτητα του προσθετικού. Η φόρα κίνησης ορίζεται από το πρόσημο της διαφοράς. Στη περίπτωση της “Classic EPP” τοπολογίας, η ιδιοδεκτικότητα του χρήστη διατηρείται μέσω του Bowden cable, ενώ στην “Unconnected” μέθοδο δε υπάρχει ανατροφοδότηση. Όσον αφορά την “Biomechatronic EPP” διάταξη, η θέση του slave κινητήρα παρέχεται σαν είσοδος στους PD ελεγκτές των δύο master κινητήρων, οι οποίοι κινούνται σε αντίθετες κατευθύνσεις προκειμένου να μιμηθούν την κίνηση των άκρων του Bowden cable στην “Classic EPP” τοπολογία. Πέρα από τους PD ελεγκτές, χρησιμοποιείται επίσης η λειτουργία της αντιστάθμισης τριβής με προς τα εμπρός τροφοδότηση (Feedforward friction compensation), προκειμένου να βελτιστοποιηθεί η κίνηση των master κινητήρων.

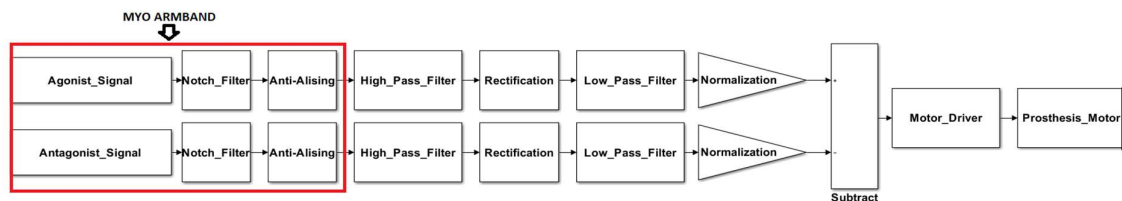
Τα επιφανειακά μυοηλεκτρικά σήματα συλλέγονται από τον Ωλένιο Εκτείνων τον καρπό μυ (έκταση καρπού) και τον Ωλένιο Καμπτήρα του καρπού μυ (κάμψη καρπού), χρησιμοποιώντας το Myo Armband. Τα δυναμικά που παρέχονται από το Armband κυμαίνονται μεταξύ του -128 και 128 σε μονάδες ενεργοποίησης. Η ροή της πληροφορίας του ηλεκτρομυογραφήματος γίνεται στα 200Hz. Το Myo ενσωματώνει επίσης anti-aliasing φίλτρο και Notch φίλτρο στα 50Hz. Τα μυοηλεκτρικά σήματα μεταφέρονται στο περιβάλλον του MATLAB για περαιτέρω επεξεργασία. Ο ελεγκτής που υλοποιήθηκε φαίνεται στην Εικόνα 4. Τα στάδια επεξεργασίας των δεδομένων είναι με τη σειρά : υπερεπατό φίλτρο, ανόρθωση και χαμηλοπερατό φίλτρο. Η συχνότητα αποκοπής για το υπερεπατό φίλτρο είναι στα 30Hz και για το χαμηλοπερατό στα 6Hz. Έπειτα υπολογίζονται οι μέσες απόλυτες τιμές (Mean Absolute Values - MAVs) των μυοηλεκτρικών σημάτων μέσω της τεχνικής “sliding windows”. Το εύρος των παραθύρων που χρησιμοποιούνται είναι 100 ms με μετατόπιση 50 ms. Τα MAVs του ανταγωνιστικού ζεύγους μυών κανονικοποιούνται κάνοντας χρήση της τεχνικής Maximum Voluntary Isometric Contraction (MVIC) και τίθενται τα κατάλληλα όρια. Η διαφορά στο πλάτος των σημάτων χρησιμεύει για να τεθεί το Duty Cycle του driver του κινητήρα. Η σχέση αυτή περιγράφεται παρακάτω.

$$\%DC = \left| \left[ \frac{M_1}{G_1} - T_1 \right] - \left[ \frac{M_2}{G_2} - T_2 \right] \right| \times 100\% \quad (3)$$

όπου M1 είναι η μέση απόλυτη τιμή του πρώτου μύος, G1 είναι αντίστοιχη τομή που εξάχθηκε κατά τη διαδικασία της MVIC και T1 είναι το όριο που τέθηκε κάτω από το οποίο δε ενεργοποιείται κίνηση στον αντιστοίχο μυ. Ομοίως και για τον δεύτερο μυ του ανταγωνιστικού ζεύγους. Σημειώνεται ότι τα όρια τέθηκαν χειροκίνητα με γνώμωμα την ελαχιστοποίηση σκούσιας ενεργοποίησης της κίνησης του προσθετικού.



**Εικόνα 3. Σχήμα ελέγχου για την “Biomechatronic EPP” τοπολογία.**



**Εικόνα 4. Σχήμα ελέγχου τοπολογίας “EMG”.**

## Πειραματική Φάση

Προκειμένου να αναπαραστήσουμε την κίνηση που πραγματοποιεί το χέρι κατά την έκταση και κάμψη του καρπού, προσθέσαμε στην κεφαλή του slave κινητήρα έναν 3D τυπωμένο άξονα. Τα όρια κίνησης τέθηκαν τοποθετώντας δύο μηχανικά εμπόδια. Το πρώτο στις 90 μοίρες στην κατεύθυνση της έκτασης του καρπού και το δεύτερο στις 75 μοίρες στην κατεύθυνση της κάμψης. Με αυτόν τον τρόπο, ο άξονας παίζει τον ρόλο του προσθετικού άκρου και ο slave κινητήρας αυτόν του επενεργητή κινήσεως.

Στόχος του πειράματος είναι να καθορίσουμε την ικανότητα των χρηστών να ελέγξουν την μετατόπιση του προσθετικού χρησιμοποιώντας τις τέσσερις προαναφερόμενες τοπολογίες ελέγχου.

**Συμμετέχοντες :** Στο πείραμα συμμετείχαν 14 αρτιμελή άτομα, 12 άντρες και 2 γυναίκες, μεταξύ 20 και 33 ετών.

**Διαδικασία :** Οι συμμετέχοντες πραγματοποίησαν πολλαπλές προσπάθειες σε μια απλή δοκιμασία χρησιμοποιώντας τις τέσσερις εναλλακτικές τοπολογίες ελέγχου. Χρησιμοποιήθηκε ειδικός νάρθηκας που επέτρεπε μόνο την κάμψη και έκταση του καρπού. Για τις τοπολογίες "Classic EPP", "Biomechatronic EPP" και "Unconnected", οι αισθητήρες FSR συνδέθηκαν μέσω ενός συστήματος σχοινιών και τροχαλίας στον νάρθηκα, ενώ για την τοπολογία "EMG" οι συμμετέχοντες χρησιμοποίησαν τόσο τον νάρθηκα όσο και το Myo Armband. Η Εικόνα 5. Χρήστης κατά την εκτέλεση του πειράματος. παρουσιάζει έναν χρήστη κατά τη διάρκεια του πειράματος. Οι συμμετέχοντες εξασκήθηκαν με την διάταξη πριν την έναρξη των πειραμάτων.

Μια οθόνη υπολογιστή χρησιμοποιήθηκε για την αναπαράσταση της τρέχουσας θέσης του προσθετικού, ως την θέση του κέρσορα. Οι συμμετέχοντες στόχευαν εναλλάξ ένα ζεύγος κυκλικών στόχων. Οι θέσεις των στόχων περιορίστηκαν στην περιφέρεια ενός ημικυκλίου που αντιστοιχούσε στην τροχιά που εκτελούσε το προσθετικό άκρο. Ο ένας στόχος αντιστοιχούσε στο σημείο έναρξης (Γκρι χρώμα) και ο άλλος στο σημείο τερματισμού (Κόκκινο χρώμα) (Εικόνα 6). Οι συμμετέχοντες έχοντας οπτική επαφή μόνο με την οθόνη του υπολογιστή έπρεπε να μετακινήσουν τον κέρσορα από το σημείο έναρξης στον στόχο και να παραμείνουν εντός αυτού για 1s (dwell time). Μετά το πέρας κάθε επανάληψης, οι δυο στόχοι εναλλάσσονταν σε χρώμα, κατευθύνοντας έτσι τον χρήστη μέσα από τα διαφορετικά στάδια του πειράματος.

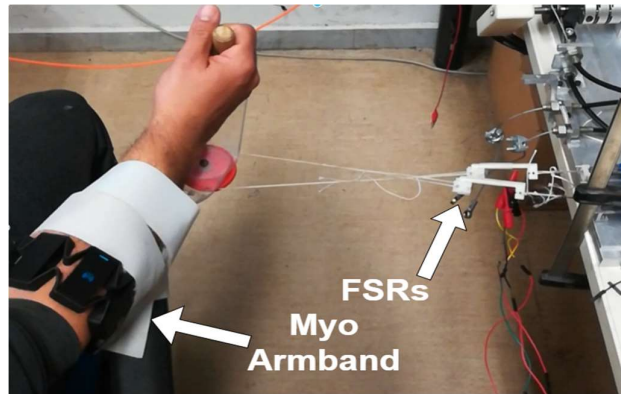
**Σχεδιασμός :** Για την οργάνωση του πειράματος χρησιμοποιήθηκε «εντός των υποκειμένων» σχεδιασμός. Ανεξάρτητες μεταβλητές ήταν η μέθοδος ελέγχου, η δοκιμασία, η απόσταση μεταξύ των στόχων και το πλάτος των στόχων. Ο Πίνακας 1 αναλύει τους διαφορετικούς συνδυασμούς απόστασης-πλάτους στόχων που χρησιμοποιήθηκαν. Ο κάθε χρήστης έκανε 15 προσπάθειες για κάθε συγκεκριμένη συνθήκη (συνδυασμός απόστασης-πλάτους). Το πείραμα ξεκινούσε από τα μεγαλύτερα πλάτη και κατέληγε στα μικρότερα. Μετά το πέρας των πειραμάτων για όλες τις μεθόδους ελέγχου, κάθε χρήστης είχε ολοκληρώσει συνολικά 1500 προσπάθειες.

**Μετρικές απόδοσης :** Για την αξιολόγηση των μεθόδων ελέγχου έγινε χρήση τριών διαφορετικών μετρικών απόδοσης οι οποίες όλες πηγάζουν από τον Νόμο του Fitts. Αυτές είναι ο χρόνος από την έναρξη της κίνησης μέχρι την ολοκλήρωσή της (MT), το ποσοστό αποτυχίας (% Error), το οποίο αναφέρεται στο ποσοστό των αποτυχημένων προσπαθειών (Εξ. 4) και το Throughput (TP), το οποίο υπολογίζεται με βάση την Εξ. 5.

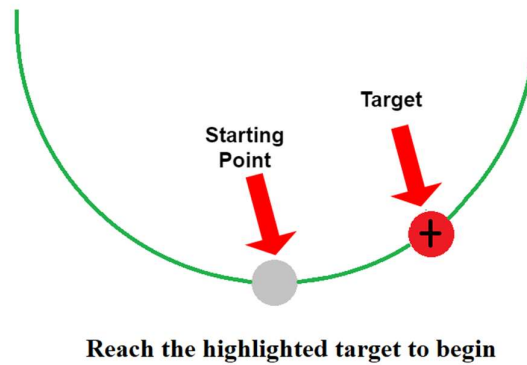
$$\%Error = \frac{\#Trials - \#Hits}{\#Trials} \times 100 \quad (4)$$

$$TP = ID / MT \quad (5)$$

Η μετρική του Throughput χρησιμοποιείται για την ποσοτικοποίηση της απόδοσης του εκάστοτε χρήστη στο πλαίσιο της δοκιμασίας, της συσκευής και του περιβάλλοντος που εκτελείται κάποιο πείραμα.



Εικόνα 5. Χρήστης κατά την εκτέλεση του πειράματος.



Εικόνα 6. Αναπαράσταση της οθόνης κατά τη διάρκεια του πειράματος.

Πίνακας 1. Συνδυασμοί πλάτους (W), απόστασης (D) και οι αντίστοιχοι βαθμοί δυσκολίας (ID).

W(Degrees)	D(Degrees)				
	27.5	67.7	80	90	135
2	3.88	5.12	5.36	5.60	6.10
3	3.34	4.56	4.80	5.03	5.52
5	2.70	3.86	4.09	4.32	4.81
10	1.91	2.95	3.17	3.39	3.86
15	1.50	2.46	2.67	2.87	3.32

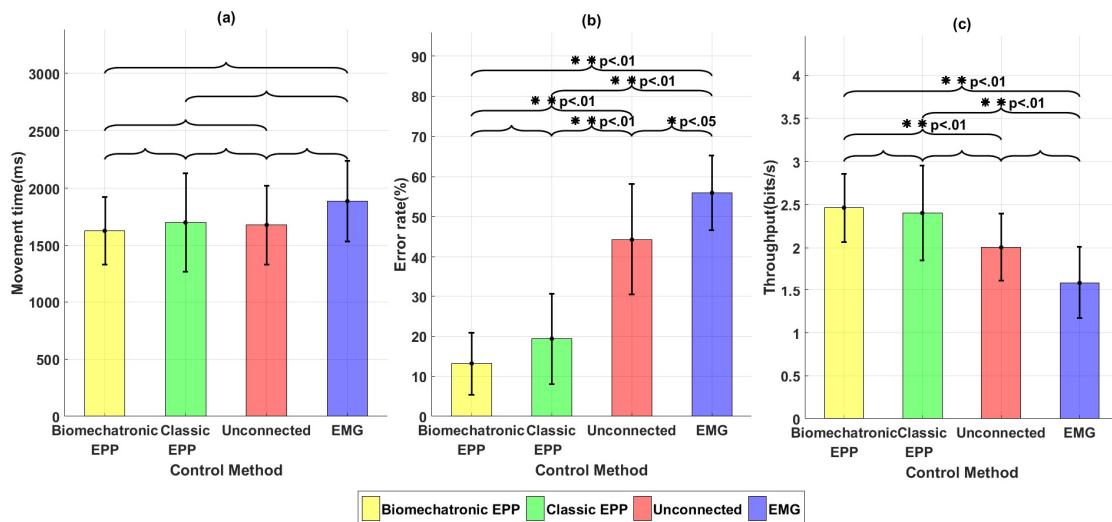
**Στατιστική Ανάλυση** : Η ανάλυση των δεδομένων που συλλέχθηκαν έγινε με τη χρήση του λογισμικού MATLAB. Έγιναν τεστ για την επίδραση της μεθόδου ελέγχου σε τρεις διαφορετικές εξαρτημένες μεταβλητές : χρόνο κίνησης (MT), ποσοστό αποτυχίας και Throughput (TP), χρησιμοποιώντας την μέθοδο της ανάλυσης ANOVA ως προς έναν παράγοντα (one-way ANOVA). Το επίπεδο συνολικής «εμπιστοσύνης» τέθηκε στο 0,05. Επίσης, εκτελέσαμε Post-hoc tests (Bonferroni corrections) για να διακρίνουμε τις διαφορές μεταξύ των μεθόδων ελέγχου.

## Αποτελέσματα

Ο Πίνακας 2 και η Εικόνα 7 συνοψίζουν την απόδοση (μέση τιμή  $\pm$  διακύμανση) κάθε μεθόδου ελέγχου μεταξύ των διαφορετικών μετρικών απόδοσης.

Πίνακας 2. Σύνοψη μετρικών απόδοσης.

	MT(ms)	Error(%)	TP(bits/s)
“Biomechatronic EPP”	1628.1 $\pm$ 294.6	13.2 $\pm$ 7.8	2.461 $\pm$ 0.398
“Classic EPP”	1702.3 $\pm$ 428.2	19,3 $\pm$ 11.2	2.402 $\pm$ 0.547
“Unconnected”	1679.9 $\pm$ 342.8	44.3 $\pm$ 13.9	2.00 $\pm$ 0.388
“EMG”	1886.9 $\pm$ 350.9	56,0 $\pm$ 9.3	1.589 $\pm$ 0.419



Εικόνα 7. Απόδοση μεθόδων ελέγχου με βάση την εκάστοτε μετρική απόδοσης : (a) Χρόνος κίνησης, (b) Ποσοστό αποτυχίας, (c) Throughput. Με μονό αστερίσκο (\*) σημειώνεται η σημαντική διαφορά μεταξύ των μέσω τιμών για συνολική «εμπιστοσύνη» 0,05 και με διπλό αστερίσκο (\*\*) για 0,01.

## Συμπεράσματα

Η χρήση της EPP μεθόδου ως σχήμα ελέγχου για προσθετικές συσκευές άνω άκρων έχει απορριφθεί τις τελευταίες δεκαετίες. Η επιφανειακή ηλεκτρομυογραφία έχει αποτελέσει την βάση για τα υπάρχοντα προσθετικά συστήματα χάρις στην ευκολία εφαρμογής της και την μη επεμβασιμότητά της.

Στη Διπλωματική αυτή εργασία πραγματοποιήσαμε μια συγκριτική αξιολόγηση του “Biomechatronic EPP”, μιας καινοτόμου τοπολογίας ελέγχου, του “Classic EPP”, της “Unconnected” μεθόδου και της “EMG” μεθόδου ελέγχου. Η διαδικασία σύγκρισης έγινε στα πλαίσια ενός, πραγματικού χρόνου, πειράματος επίτευξης στόχων που βασίστηκε στον Νόμο του Fitts.

Η στατιστική ανάλυση που πραγματοποιήθηκε ανέδειξε την υπεροχή του “Biomechatronic EPP” έναντι των δύο μεθόδων που δεν παρείχαν αισθητική ανατροφοδότηση στον χρήστη: της «Unconnected» και της “EMG”. Ειδικότερα, εξήγαμε το συμπέρασμα αυτό μέσα από τα αποτελέσματα που λάβαμε για την μετρική του Throughput, η οποία είναι ενδεικτική της συνολικής απόδοσης του χρήστη. Από την άλλη μεριά, δεν αναδείχθηκε κάποια στατιστικά σημαντική διαφορά όσον αφορά την

προτεινόμενη τοπολογία και την “Classic EPP”, κάτι το οποίο αναδεικνύει την μεταξύ τους ισοδυναμία και έρχεται να επιβεβαιώσει πειραματικά, προηγούμενες συναφείς μελέτες.

Οφείλουμε να σημειώσουμε πως παρότι τα αποτελέσματα της εργασίας αυτής αποδεικνύονται ιδιαίτερος ενθαρρυντικά, είναι ένα από τα αρχικά βήματα της προσπάθειας που γίνεται για τη δημιουργία ενός λειτουργικού εμφυτεύματος που θα δώσει πνοή στο προτεινόμενο σύστημα ελέγχου.

# 1 Introduction

The replacement of the human upper limbs by mechanical ones is a solemn scientific challenge. The mechanical demands and constraints of this aim are significant; however, the most critical factor for the proper function of the upper limb is its control. Elaborating, the controller design defines the communication - connection between the impaired and the upper limb prosthetic. This hindrance is related to the lack of sufficient communication that is restrained only to communication with visual feedback, between the mutilated and the alien upper limb prosthetic.

In the case of the upper limbs of the human body the control is achieved by a practically a infinite number of sensors available. These sensors are called mechanoreceptors and provide information to the neural system on any variations in the state of the upper limb. The ability to sense using these mechanoreceptors is called proprioception, and its absence renders the control of the limbs impossible. Thus, it is pellucid that even though a prosthetic could be highly advanced from an engineering perspective, it would not be functional unless proprioception is achieved. A control method that dominated the field of prosthetics and was widely used is *Proportional Myoelectric Control* [5]. A proportional myoelectric control system employs a microcontroller or computer that inputs electromyography (EMG) signals from sensors on the muscle(s) and then activates the corresponding joint actuator(s) proportionally to the EMG signal, see Figure 1.1.

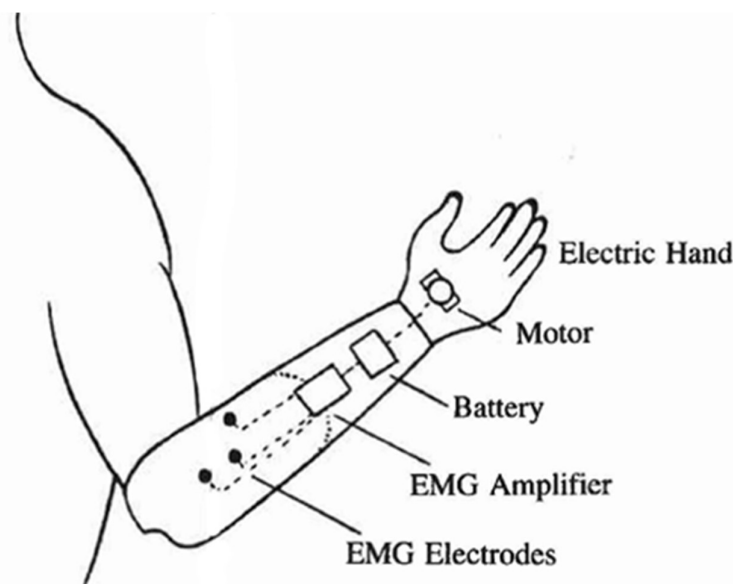


**Figure 1.1. EMG control topology.**

Although myoelectric signals, are widely considered the best available control interface for powered prostheses, many amputees abandon their devices out of frustration due to the lack of precision of the prosthesis' movements. Noisy control signals, derived from the stochastic myoelectric signals, and lack of adequate sensory feedback, are two of the central bottlenecks limiting precision.

Another control method is the *Classic Extended Physiological Proprioception (Classic EPP)* in which the tendons of the arm are connected to cables with the prosthetic limb. More precisely, the limb prosthetic is connected directly to the muscles of the impaired mechanically, using links such as Bowden cables [21], [43]. Thus, the alien prosthetic becomes an extension of the remaining limb, see

Figure 1.2. Consequently, the position, the velocity and the forces that are applied to the prosthetic are transferred from the cables to the muscles, stimulating the neural receptors of the body, activating the proprioception to a certain degree. The EPP control resembles to hydraulic steering. The driver "feels" the state of the wheels and simultaneous assistance is provided for more effortless driving. Nevertheless, the most important factor is that the drive and the wheels are synchronized.

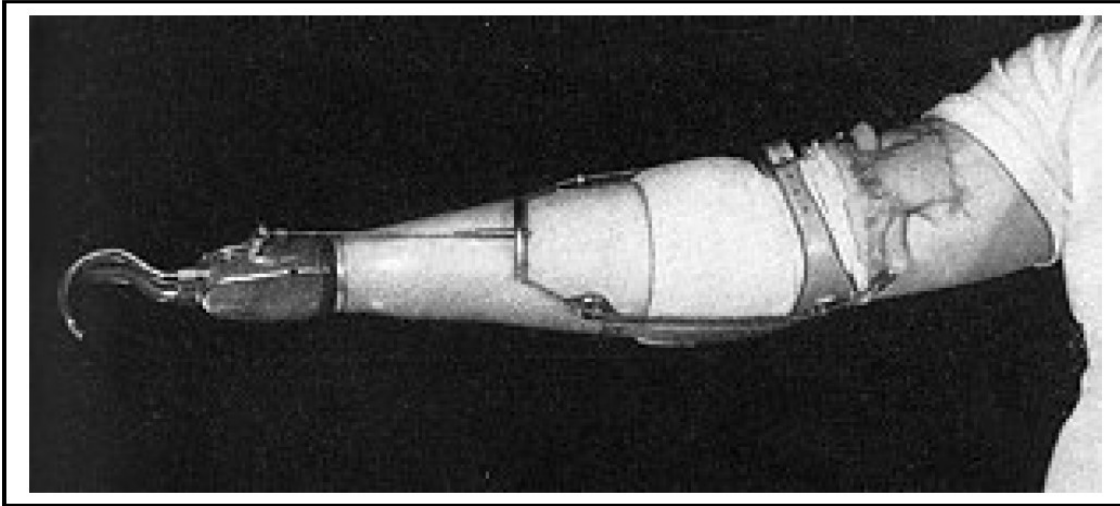


**Figure 1.2. EPP prosthesis control for forearm amputee with biceps cineplasty.**

However, this control method has the disadvantage that it is not aesthetic for the human user, it has often had control constraints (related to the direction of the movement) and finally a plastic surgery is required.

During the last couple of years, at the Control Systems Lab of NTUA, where this thesis was supervised, research was conducted in this field and a new, innovative control proposal was introduced [25]. This proposal was about a novel control topology, with activation of proprioception as well. To be more precise, the core of this concept is based on the field of Telerobotics - Teleoperation. In this field, a master - slave control scheme is designed, using implants that activate the receptors of the limb. This scheme guarantees the connection between the remaining intact muscles of the limb with its prosthetic. It has to be noted that the degrees of freedom of both the master and slave devices must be the same. This topology is considered a successful one, if the impedance of the environment is the same for the user, as if he or she were controlling the slave motor without the master. In this case, the control system is called *transparent* [49].

The new control method is called by the research team of the laboratory as *Biomechatronic Extended Physiological Proprioception (Biomechatronic EPP)*, see Figure 1.3. The main advantage of this method is that feedback is provided to the patient and thus a closed loop system is created (minimizing the systems position error) unlike the open loop system in the previous method.

Two previous Diploma and one MSc students worked on this project. Mablekos-Alexiou Anestis and Vaggelatos Zaharias in their diploma theses [25], [45], established the theoretical foundations of this notion, and designed an experimental setup for the comparison of Classic and Biomechatronic EPP, respectively. MSc student Koukoulas Nikolaos designed and implemented the wireless setup of Biomechatronic EPP [23].



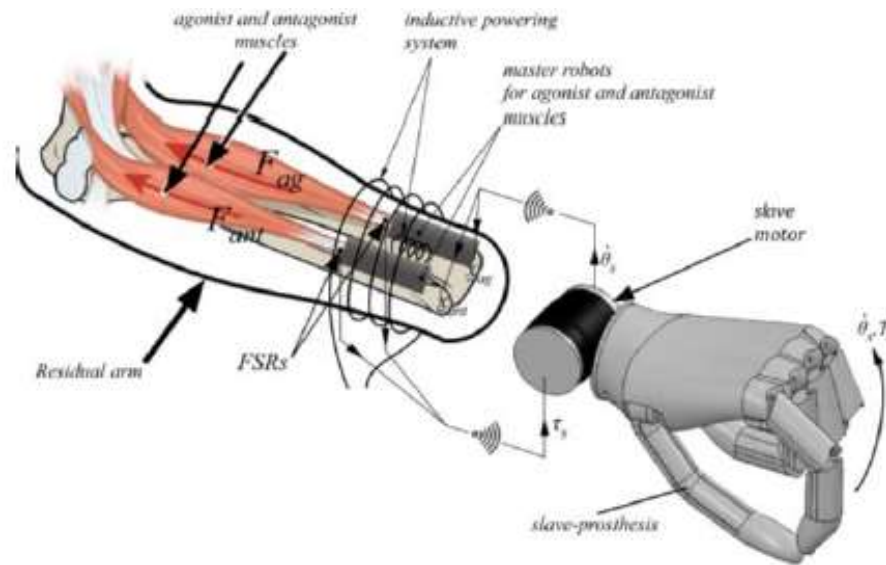


**Figure 1.3. Proposed control topology of Biomechatronic EPP.**

## 1.1 Purpose

The purpose of this thesis is the experimental comparison of the Classic EPP, the “Unconnected”, the Biomechatronic EPP and the EMG prosthesis methods. To achieve this objective, this thesis extends the use of Fitts' law, a psychological model of human movement, as a performance model for these four control topologies.

## 1.2 Literature Review

### 1.2.1 Desirable Attributes of Prosthesis Control

Childress D.S. had presented the requirements for the control scheme of upper limb prosthesis [7], [46]:

1. Low mental loading or subconscious control.
2. User friendly or simple to learn to use.
3. Independence in multifunctional control.
4. Simultaneous, coordinated control of multiple functions.
5. Direct access and instantaneous response.
6. No sacrifice of human functional ability.
7. Natural appearance.

It is obvious that a prosthetic system, along with its operational components, is determined by the choice of the control scheme.

### 1.2.2 Types of prosthesis

There are generally four different types of prosthesis for patients with upper-limb amputation:

1. Body-powered prosthesis
2. Externally-powered prosthesis
3. Passive prosthesis
4. Neuroprosthetics

**Body-powered prostheses** have not changed significantly since developments in 1950s' which were spurred by World War II [16]. They work by using steel cables and harnesses to link the movement of the body to the prosthesis and to control it. This linkage gives to the amputee sensory feedback of the prosthesis, facilitating the subconscious control of the prosthetic. However, they look more archaic, and the shoulder harnesses are uncomfortable and restrictive.

Extended Physiological Proprioception(EPP) is one of the control topologies that were inquired in this thesis and is included in the family of body-powered prostheses. Simpson D.C suggested this topology in 1974 [38]. He was the first that said the phrase "Extended Physiological Proprioception", to imply the use of the sensors of the human body to move the prosthetic limb.

The main notion is that the prosthetic limb is connected directly to the muscles of the amputee using links, such as Bowden Cables, see Figure 1.4. This mechanical connection converts the alien prosthetic limb to an extension of the remaining human body. Thus, the data for the position, the velocity and the forces applied to the prosthetic limb are transferred directly to the muscles, stimulating the neural receptors of the body, activating the proprioception of the user. However, this control method has the disadvantage that it is not aesthetic for the human user, it has often had control constraints (related to the direction of the movement) and finally a plastic surgery is required.

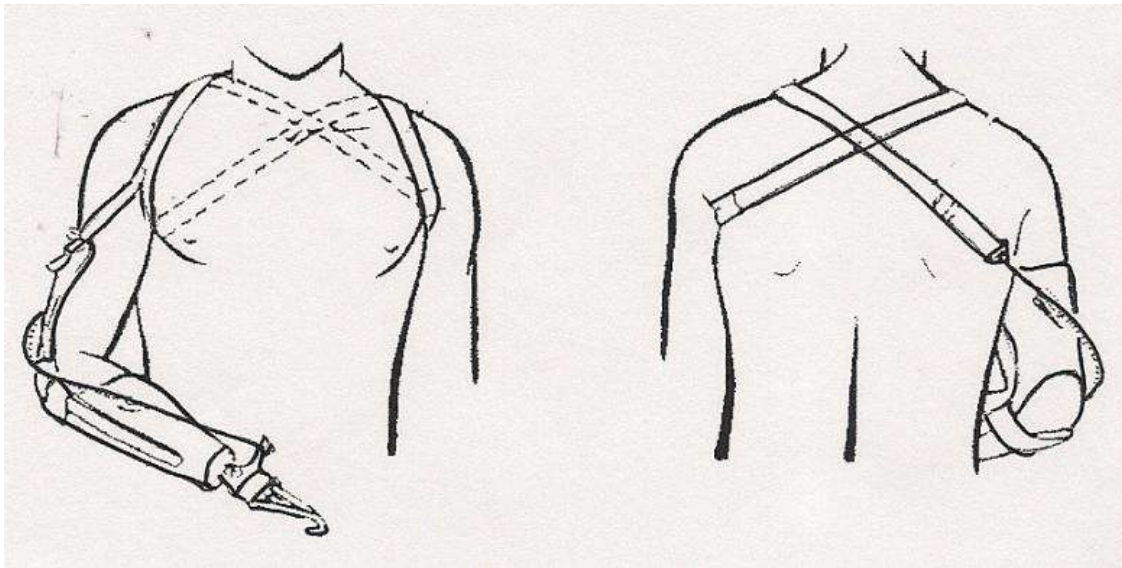


**Figure 1.4. Schematic illustration of the traditional body-powered prosthesis for forearm amputations.**

**Externally-powered prosthetic systems** do not use body force as actuator. Most systems of this type are powered by electricity from a battery and use pneumatic or electrical actuators to assist the movement of the alien prosthetic. Myoelectric control is the most common type of externally-powered prosthesis. In this control topology, the electrical activity of one or more muscles is used to drive the joint(s) actuators, [35]. Surface electrodes record the electromyography (EMG) signal, a biomedical signal that measure electrical currents generated in muscle during its contraction representing neuromuscular activities. After its processing the EMG signal is used to drive the prosthetic limb. The modeling of a system like this is shown in Figure 1.5 and will be discussed thoroughly in the following chapters.

Myoelectric control does not require any invasive operation and is widely studied and used during the last decades. Noisy control signals, derived from the stochastic myoelectric signals, and lack of adequate sensory feedback, are two of the central drawbacks limiting precision.

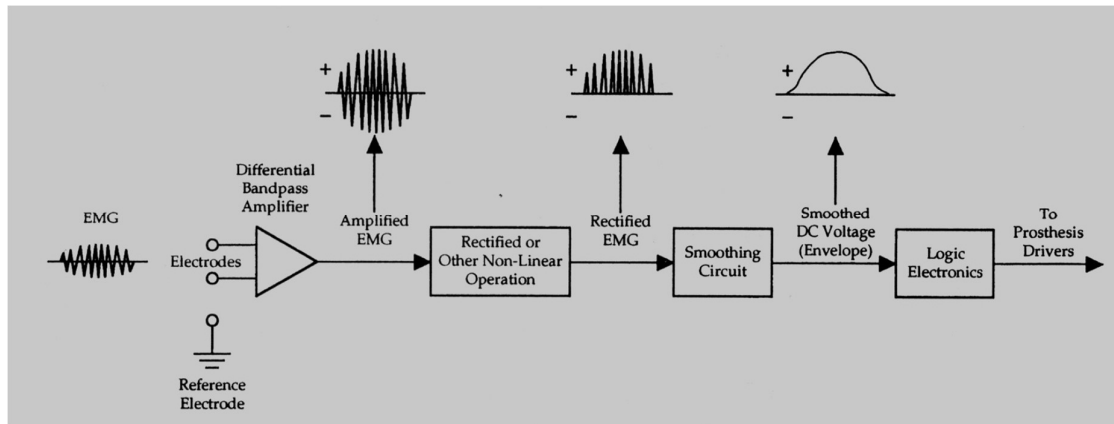


**Figure 1.5. Schematic diagram of a myoelectric controller for upper-limb prosthetics.**

**Passive prosthesis** is a cosmetic restoration. It is another option for upper extremity patients who do not require precise hand control or grasp, but still seek a cosmetically pleasing prosthesis.

**Neuroprosthetics** present one of the newest concentrations of biomedical engineering [10]. These devices may be powered by the human body—that is, they operate from electrical signals sent via electrodes from an external source to the peripheral muscle neuron—or they may be powered externally.

The upper extremities prove a significant challenge in fine-tuned control requirements. The incredible strength and flexibility of complex hand function are difficult to reproduce. The newest in prosthetic design hopes to overcome some of these challenges.

### 1.2.3 Telerobotics - Teleoperation (TT)

TT is the control of a machine or an actuator at a distant area. A system like this consists of the following:

- A master device controlled by the user
- A slave device whose function depends on the master device
- A controller that is the link between the master and the slave devices, allowing the correlation of their displacement and applied forces respectively.

It has to be noted that the degrees of freedom of both the master and the slave devices must be the same. This topology is considered a successful one, if the impedance of the environment is the same for the user, as if he or she was controlling the slave motor without the master. In this case, the control system is called transparent [7].

### 1.2.4 Human Performance Modeling

Human performance modeling (HPM) is a method of quantifying human behavior, cognition, and processes; a tool used by human factors researchers and practitioners for both the analysis of human function and for the development of systems designed for optimal user experience and interaction.

There are several model categories but the one we are interested in is Command and Control. Human performance models of Command & Control describe the products of operator output behavior, and are often also models of dexterity within the interactions for certain tasks.

### **Fitts' Law**

Fitts's Law is an empirical model explaining speed-accuracy tradeoff characteristics of human muscle movement [2]. Following the work of Shannon, Wiener, and other information theorists in the 1940s, "information" models of psychological processes emerged with great fanfare in the 1950s [30]. The terms "probability", "redundancy", "bits", "noise", and "channels" entered the vocabulary of experimental psychologists as they explored the latest technique for measuring and modeling human behavior. Two surviving models are the Hick-Hyman law for choice reaction time [34], and Fitts' law for the information processing capacity of the human motor system [11].

In the decades since Fitts' original publication, his relationship, or "law", has proven one of the most robust, highly cited, and widely adopted model to emerge from experimental psychology. Psychomotor studies in diverse settings – from under a microscope to underwater – have shown a high correlation between Fitts' measure of task difficulty and the time required to complete a movement task. Kinematics and human factors are two fields that are particularly rich in investigations of human performance using Fitts' analogy.

## **1.3 Thesis Structure**

At this point the structure of this thesis is presented.

In the first introductory chapter, the purpose of the Diploma Thesis and a brief literature review are presented.

The second chapter introduces the basic concepts of Fitts' Law, refers to the several forms that has taken through years, and focuses on the standards which should be followed while building a Fitts' Law model.

In the third chapter, the experimental setup used for the evaluation of the Biomechatronic and Classic EPP are presented. The design of the FSRs circuitry and the connection map of the hardware components are also displayed.

The fourth chapter describes the Biomechatronic and Classic EPP topologies and presents the procedures followed to design their control interfaces using MATLAB/Simulink and the DS1103 platform of DSpace.

The fifth chapter is dedicated to the presentation of the setup used and the controller designed for the realization of the EMG control method. A brief description of the anatomy of the forearm and the appropriate placement of the Myo Armband are also presented.

The sixth chapter is separated in two main sections. In the first one, we present the target acquisition task, the main experiment conducted for the evaluation of the control quality of the four control topologies that were compared during this thesis. The second main section describes the way the gathered data were manipulated and presents the results of the target experiment.

In the seventh chapter, three separate experiments conducted are presented. The first one verifies the transparency of the Biomechatronic EPP configuration system and its equivalency to Classic EPP, while the second one tests its operation when disturbances in the environment of the prosthesis motor

are occurred. In the last one, we make a comparison of the EMG signals captured during the operation of the four aforementioned control methods so as to evaluate the fatigue of the muscle of interest during the target experiment.

In the eighth and final chapter, the conclusions of this thesis are presented, with potential recommendations for future research.

Finally, Appendix A presents information for the software tools used in this thesis and excerpts of the written code while in Appendix B datasheets of the most important hardware parts are quoted.

## 2 Fitts' Law

### 2.1 Information Theory Foundation

Fitts' law is a model of human psychomotor behavior based on Shannon's Theorem, a fundamental theorem of communication systems [39]. The realization of movement in Fitts' model is analogous to the transmission of "information" in electronic systems. Movements are assigned an index of difficulty, in "bits", and in carrying out a movement task the human motor system is said to transmit so many "bits of information". If the number of bits is divided by the time to move, then a rate of transmission in "bits per second" can be ascribed.

Fitts' idea was novel for two reasons: first, it suggested that the difficulty of a motor task could be measured using the information metric "bits"; and second, it introduced the idea that in human movement, information is transmitted through a channel – a human channel. With respect to electronic communication systems, the concept of a channel is straight forward: A signal is transmitted through a non-ideal medium (such as copper, air, or glass) and is perturbed by noise. The effect of the noise is to reduce the information capacity of the channel from its theoretical maximum. Shannon's Theorem expresses the effective information capacity  $C$  (in bits/s) of a communications channel of bandwidth  $B$  (in s<sup>-1</sup> or Hz) as:

$$C = B \log_2 \left( \frac{S+N}{N} \right) \quad (2.1)$$

Or in the form:

$$C = B \log_2 \left( \frac{S}{N} + 1 \right) \quad (2.2)$$

where  $S$  is the signal power and  $N$  is the noise power [36].

The notions of "channel" and "channel capacity" are not as straightforward in the domain of human performance. The problem lies in the measurement of human channel capacity. Although electronic communication systems transmit information with specific and optimized codes, this is not true of human "channels". Human coding is ill-defined, personal, and often irrational or unpredictable. Optimization is dynamic, intuitive. Cognitive strategies emerge in everyday tasks through "chunking" which is analogous to "coding" in information theory – the mapping of a diverse pattern (or complex behavior) into a simple pattern (or behavior). Neuromuscular coding emerges through the interaction of nerve, muscle, and limb groups during the acquisition and repetition of skilled behavior. Difficulties in identifying and measuring cognitive and neuromuscular factors confound the measurement of the human channel capacity, causing tremendous variation to surface in different experiments seeking to investigate similar processes.

### 2.2 Original Model Formulation

Fitts sought to establish the information capacity of the human motor system. This capacity, which he called the index of performance or  $IP$ , is analogous to channel capacity  $C$  in Shannon's theorem.  $IP$  is calculated by dividing a motor task's index of difficulty,  $ID$ , by the movement time,  $MT$ , to complete a motor task. Thus,

$$IP = ID / MT \quad (2.3)$$

Eq. (2.3) is analogous to Eq. (2.2), with  $IP$  corresponding to  $C(\text{bits/s})$  and  $MT$  corresponding to  $1/B$  (s).

Fitts claimed that electronic signals are analogous to movement distances or amplitudes ( $A$ ) and that noise is analogous to the tolerance or width ( $W$ ) of the region within which a move terminates. Loosely based on Shannon's logarithmic expression, the following was offered as the index of difficulty for a motor task:

$$ID = \log_2(2A/W) \quad (2.4)$$

Since  $A$  and  $W$  are both distances, their ratio within the logarithm is without units. The notion of "bits" as the unit of task difficulty stems from the somewhat arbitrary choice of base "two" for the logarithm.

A useful variation of Eq. (2.3) places movement time on the left as the predicted variable:

$$MT = ID / IP \quad (2.5)$$

This relationship is tested by devising a series of movement tasks with  $ID$  (that is,  $A$  and  $W$ ) as the controlled variable and  $MT$  as the dependent variable. In an experimental setting, subjects are required to move to and acquire targets of width  $W$  at a distance  $A$  as quickly and accurately as possible, see Figure 2.1.

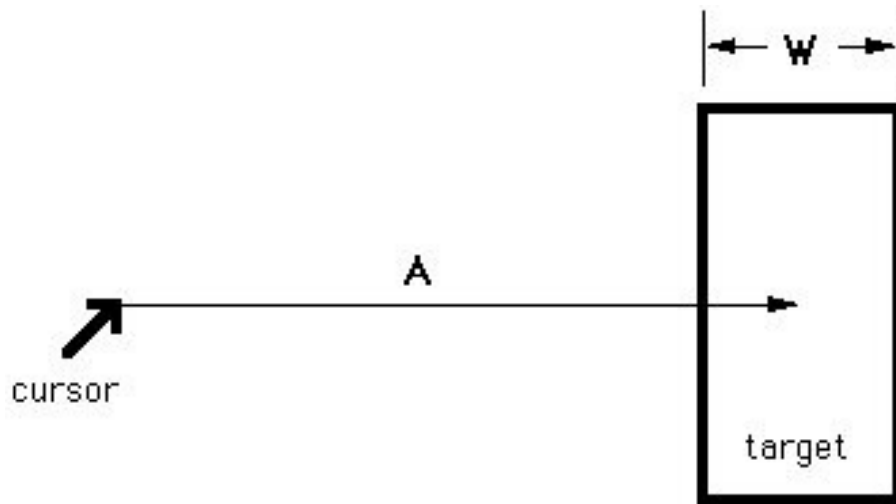


**Figure 2.1. Movement task of a distance  $A$  and a target width  $W$ .**

The index of performance ( $IP$ ) can be calculated directly using Eq. (2.3) by dividing a task's index of difficulty by the observed movement time (averaged over a block of trials), or it can be determined by regressing  $MT$  on  $ID$ . In the latter case, the regression line equation is

$$MT = a + b ID \quad (2.6)$$

where  $a$  and  $b$  are regression coefficients. The reciprocal of the slope coefficient,  $1/b$ , corresponds to  $IP$  in Eq. (2.5), obtained through direct calculation. These two values for  $IP$  will be slightly different due to the different methods of calculation.

The intercept coefficient,  $a$ , is sometimes viewed as an error term. A non-zero intercept is troublesome since it suggests that a movement task with "zero difficulty" has a non-zero predicted completion time. The usual form of Fitts' law is Eq. (2.6) expanded as follows:

$$MT = a + b \log_2(2A/W) \quad (2.7)$$

The factor "2" in the logarithm was added by Fitts as an arbitrary adjustment to ensure that ID was greater than zero for the range of experimental conditions employed in his experiments [11]. The "2" increases the index of difficulty by 1 bit for each task but has no effect on the MT-ID correlation or on the slope of the regression line equation. The constant "1" in Shannon's original equation was omitted by Fitts without justification. More to be said about the intercept and slope coefficients and the form of the logarithm term in the next sections of this chapter.

### 2.3 The Original Experiments and Emerging Problems

Fitts' original investigation (1954) involved four experiments: two reciprocal tapping tasks (1-oz stylus and 1-lb stylus), a disc transfer task, and a pin transfer task. In the tapping experiments the subjects moved a stylus back and forth between two metal bars as quickly as possible and tapped the bars at their centers (see Figure 2.2) [11]. This experimental arrangement is commonly called the "Fitts' paradigm".

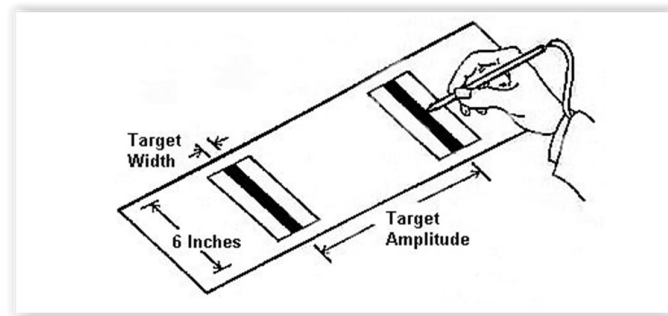


**Figure 2.2.** The reciprocal tapping paradigm(Fitts,1954).

I. Scott McKenzie in his PhD thesis reproduced the data from the 1-oz tapping experiment. This data is summarized in Table 2.1 [30].

**Table 2.1.** Data from Fitts' (1954) Tapping Task Experiment with 1-oz Stylus.

A (in)	W (in)	ID (bits)	MT (ms)	Error Rate (%)	IP (bits/s)
2	2.00	1	180	0.00	5.56
2	1.00	2	212	0.44	9.43
4	2.00	2	203	0.08	9.85
2	0.50	3	281	1.99	10.68
4	1.00	3	260	1.09	11.54
8	2.00	3	279	0.87	10.75
2	0.25	4	392	3.35	10.20
4	0.50	4	372	2.72	10.75
8	1.00	4	357	2.38	11.20
16	2.00	4	388	0.65	10.31
4	0.25	5	484	3.41	10.33
8	0.50	5	469	2.05	10.66
16	1.00	5	481	1.30	10.40
8	0.25	6	580	2.78	10.34
16	0.50	6	595	2.73	10.08
16	0.25	7	731	3.65	9.58
Mean			392	1.84	10.10
SD			157	1.22	1.33



The mean value of  $IP=10.10$  bits/s ( $SD=1.33$ ) is the information processing rate of the human motor system for this task. A high correlation between  $MT$  and  $ID$  emerges with  $r=0.9831(p=0.01)$ . Regressing  $MT$  on  $ID$  yields the following prediction equation for movement time (ms):

$$MT = 12.8 + 94.7 ID \quad (2.8)$$

Despite the high correlation between Index of Difficulty and the observed mean Movement Time, problems with the model have been noted by many researchers through the years.

In 1959 Crossman [8] and Welford in 1960 [47] pointed out a systematic departure of observations from predictions. A scatter plot reveals an upward curvature of movement time away from the regression line for  $ID$ s of 1 and 2 bits (see Figure 2.3). The failure of the model when  $ID$  is small is also evident in Table 2.1. The index of performance rating of 5.56 bits/s when  $ID = 1$  bit is over 3 standard deviations from the mean value of 10.10 bits/s.

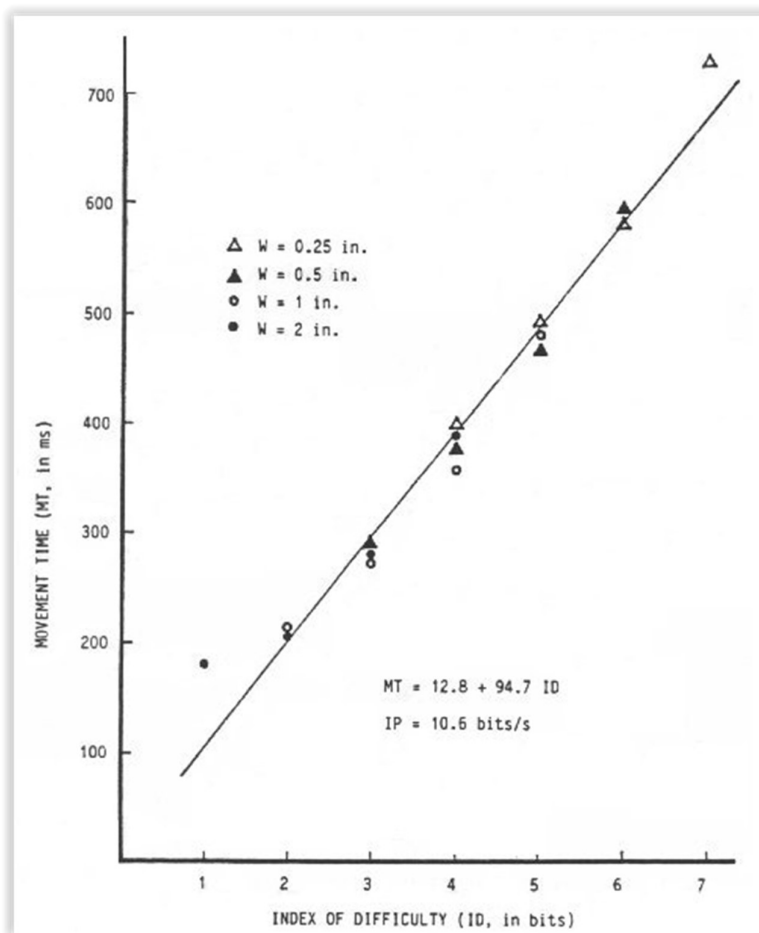


**Figure 2.3. Scatter plot of movement time vs. index of difficulty using data from Fitts' (1954) 1-oz tapping experiment.**

Another problem emerges from the relative contributions of  $A$  and  $W$ . In a detailed analysis of Fitts' four experiments, M. R. Sheridan showed that reductions in target width disproportionately increase in movement time yielded similar increases in target amplitude [37].

## 2.4 Variations of Fitts' Law and Adjustment for Accuracy

To improve the data-to-model fit, alternatives of Fitts' relationship have been used in several studies, see Table 2.2. The following table summarizes these variations.

**Table 2.2. Variations of Fitts' Law.**

Relationship	Suggested by:	Studies
$MT = a + b \log_2(A/W + 0.5)$	Welford(1960) [47]	[3],[12],[19],[22]
$MT = a + b \log_2(A/W + 1)$	Direct analogy with Shannon's information theory	[18], [26],[27],[33]
$MT = a + b_1 \log_2 A + b_2 \log_2 W$	Welford(1968) [48]	[13], [37], [48]

As mentioned in the previous section, analyses of Fitts' experiments revealed an inequitable contribution of movement amplitude and target width. A technique to adjust output measures in order to reflect what a subject actually did (output condition), rather than what a subject was expected to do (input condition) had been introduced by Crossman [9]. This technique proposes the use of effective values  $A_e$  and  $W_e$  instead of  $A$  and  $W$  respectively, in the calculation of  $ID$  (see Eq. (2.4)), to include spatial variability of accuracy in its calculation.

More about this technique and in general the rules for building a Fitts' Law Model are presented in the following section.

## 2.5 The Standard for Building a Fitts' Law Model

Through years, Fitts' law has been used by many researchers in various science fields like ergonomics, psychology, kinematics and HCI (Human-Computer Interaction) for either movement time predictions or for the comparison of conditions in experiment.

In order to improve the robustness of a Fitts' law model, as well as, its comparability and consistency, R. William Soukoreff and I. Scott MacKenzie [39] have presented a series of recommendations the designer is advised to include in his project. As their proposal supports the methods described in ISO 9241-9 standard [40] on the evaluation of pointing devices, the terms Movement Amplitude ( $A$ ) and Index of Performance ( $IP$ ), which have already been mentioned, are replaced by the terms Target Distance ( $D$ ) and Throughput ( $TP$ ), respectively. This terminology will be used as well for the rest of this thesis.

The recommendations are the following:

1. When designing an experiment, researchers should use the Shannon formulation of the index of difficulty ( $ID$ )

$$ID = \log_2 \left( \frac{D}{W} + 1 \right) \quad (2.9)$$

2. The variety of movement distances ( $D$ ) and target widths ( $W$ ) should be chosen so that subjects face a large and representative range of  $ID$  values. A range of  $ID$  values from 2 to 8 bits should suffice for most situations.

Each condition must be presented to each subject many times (15 - 25), so that the central tendency of each subject's performance for each condition can be ascertained.

The experimenter should also collect movement time (MT) data. Movement time refers to the time subjects spend moving the pointing device, and specifically should not include homing time, dwell time and reaction time.

3. A measure of the scatter of subjects' movement end-points must be gathered, either by determining the error rate or by recording the physical end-points of each movement task. Ideally both error rates and end-points should be measured and reported.

The suggestion that experimenters record movement end-points and error rates implies that no filtering of the data (barring the removal of outliers) is performed. Specifically, "peak error-free performance" is an uninformative measure, as speed measurements in the absence of accuracy are meaningless. However, obvious outliers may be removed from the data.

4. The end-point scatter data should be used to perform the adjustment for accuracy for each subject, for each condition. There are two ways to accomplish this. If end-point scatter data has been observed, then the standard deviation ( $s$ ) of the end-point positions should be calculated, and the effective target width is then defined as:

$$W_e = 4.133\sigma \quad (2.10)$$

Alternately, the error rate may be used to approximate the adjustment for accuracy, if the standard deviation of the end-point data is unavailable,

$$W_e = \begin{cases} W \times \frac{2.066}{z(1 - Err / 2)} & \text{if } Err > 0.0049\%, \\ W \times 0.5089 & \text{otherwise.} \end{cases} \quad (2.11)$$

where Err is the error rate corresponding to this specific condition, and  $z(x)$  represents the inverse of the standard normal cumulative distribution.

If the movement end-point data are available, the movement distance parameter  $D$  can also be adjusted for accuracy. The effective distance,  $D_e$ , is calculated as the mean movement distance from the start-of-movement position to the end points. The adjusted width parameter (and adjusted distance—if available) are used to define the effective index of difficulty

$$ID_e = \log_2\left(\frac{D}{W_e} + 1\right) \text{ or } ID_e = \log_2\left(\frac{D_e}{W_e} + 1\right) \quad (2.12)$$

The interpretation of the adjustment for accuracy follows. The ID values calculated via Eq. (2.9) above represent the movement tasks that the experimenter wants subjects to attempt to perform. However, the subjects will not actually perform at these index of difficulty values for two reasons: (i) The spread of movement end-points will not perfectly align with the target widths specified and hence the error rates will not be consistent across the various ID values. (ii) Subjects tend to 'cheat' on easier ID conditions by not moving fast enough, and by not covering the whole distance). The disparity between subjects' performance and the ID values presented by the experimenter is greatest at the extremes—the highest and lowest ID values used. The adjustment for accuracy corrects the ID values so that they match the movements that subjects actually performed.

The adjustment for accuracy must be performed for each condition faced by each subject, because it makes use of within-subject variability. Thus, the movement end-points or error rates used to perform the adjustment for accuracy cannot be pooled together; correct application of the adjustment for accuracy requires separate measurements for each subject, for each condition.

By the end of this step in the analysis, if there were  $y$  subjects and  $x$  conditions, the experimenter should have pairs of movement time and effective index of difficulty data, ( $ID_{eij}$ ,  $MT_{ij}$ ) where  $1 \leq i \leq y$  and  $1 \leq j \leq x$

5. Least-squares linear regression is used to find the intercept ( $a$ ) and slope ( $b$ ) parameters of the Fitts' law equation

$$MT = a + b \times ID_e \quad (2.13)$$

Linear regression serves as a test to measure the goodness of fit and the reasonableness of the results.

6. If the intent of the experimenter is to make movement time predictions using the model, then movement time should be predicted using the following equation

$$MT_{\text{Predicted}} = a + b \times ID \quad (2.14)$$

7. If the purpose of this analysis is the comparison of two or more experiment conditions, then throughput (TP) is calculated first for each subject (as the mean throughput achieved by the subject over all  $x$  movement conditions), and these subject throughputs are averaged to produce the grand throughput,

$$TP = \frac{1}{y} \sum_{i=1}^y \left( \frac{1}{x} \sum_{j=1}^x \frac{ID_{eij}}{MT_{ij}} \right) \quad (2.15)$$

where  $y$  is the number of subjects, and  $x$  represents the number of movement conditions. The units of throughput are bits per second (or bps). Calculated this way, TP is a complete measure encompassing both the speed and accuracy of the movement performance. Speed and accuracy are averaged over the range of  $ID_e$  values used in the study, and as such, this approach combines the effects of the intercept and slope parameters of the regression model into one dependent measure that can easily be compared between conditions (and, indeed, between studies).

Although TP provides a useful over-all measure of performance, movement times (means for each ID condition), error rates (per condition), and end-point variation (the standard deviation of end-point positions, per condition) complete the picture, and should be included in published reports.

### 3 Experimental Setup

This chapter presents the experimental setup used for the simulation of Classic EPP, Biomechatronic EPP and "Unconnected", along with the controllers implemented for these topologies.

#### 3.1 The Mechanical Setup

The design and the construction of the setup had been already realized in a previous thesis [45], so the following sections attempt to present and explain its basic parts.

##### 3.1.1 Classic EPP setup

In Classic EPP, a motor assists the motion of a joint which is moving by means of its connection to muscles. The basic concept of *Classic EPP* setup is illustrated in Figure 3.1.

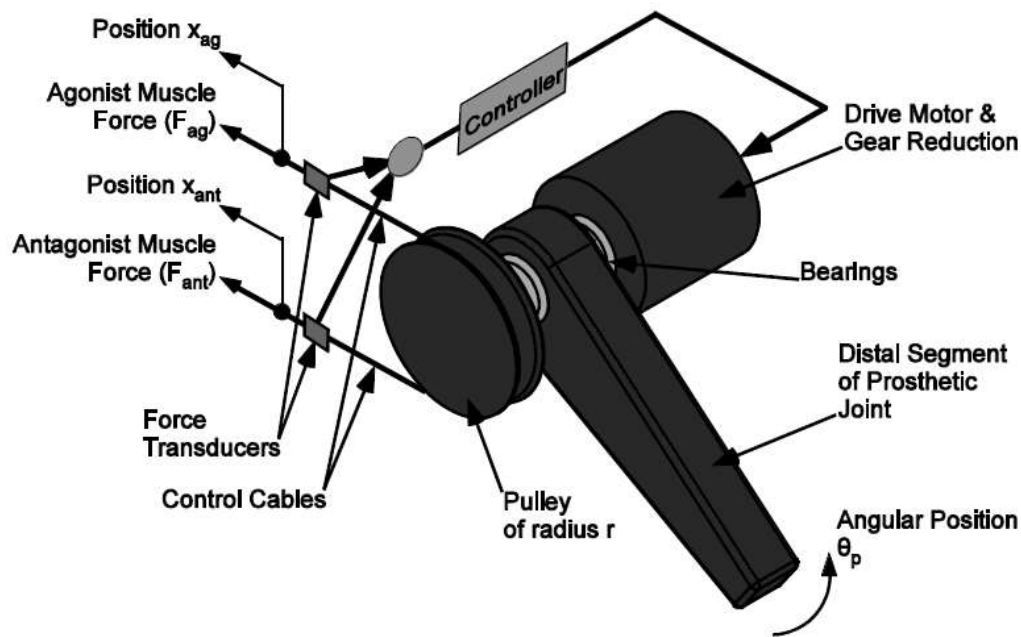


**Figure 3.1.** Schematic illustration of Classic EPP setup.

The setup used for the Classic EPP configuration is presented in Figure 3.2. The system of the motor consists of a brushed DC motor, a gearhead coupling, a shaft and a pulley. The 3D printed part shown in Figure 3.3 is connected to the shaft and simulates the prosthetic joint. Its rotation is driven by the motor of the configuration. In Classic EPP topology a pair of agonist-antagonist muscles is connected to mechanical linkages. As in most situations, the mechanical linkage used in the setup is a Bowden cable. The cable is intertwined with the pulley. This way, the proprioception of the user is preserved.

What remains to be clarified is the way the force is applied in order to achieve the rotation of the motor. The force mechanism consists of two force sensors connected to the terminations of the Bowden cable, between them and the user. The applied force is read and transmitted to the controller of the scheme. More to be said about this after the presentation of the Biomechatronic EPP setup.

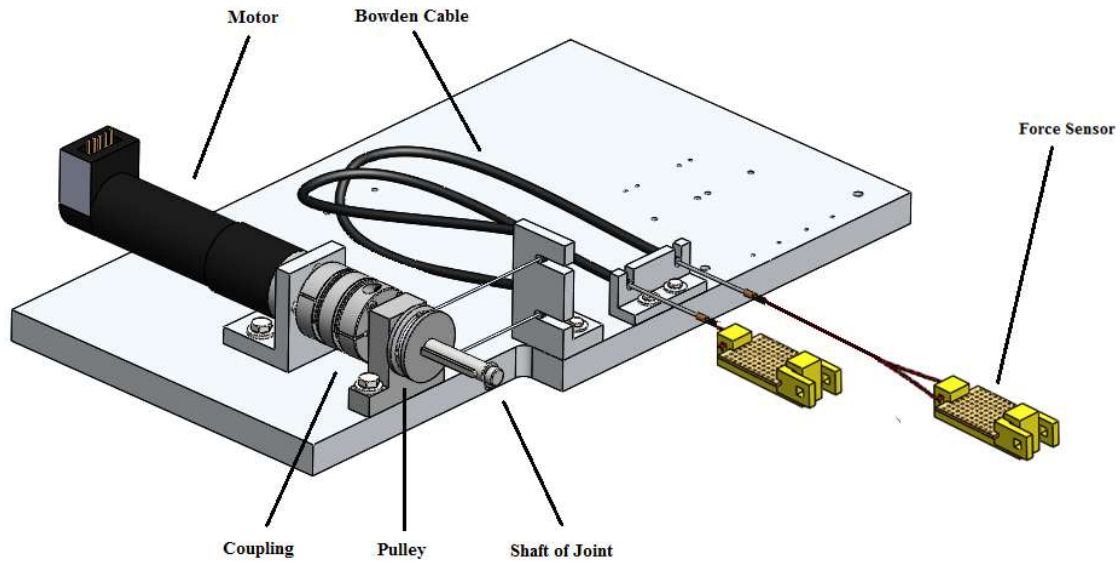


**Figure 3.2.** Setup for the Classic EPP configuration.

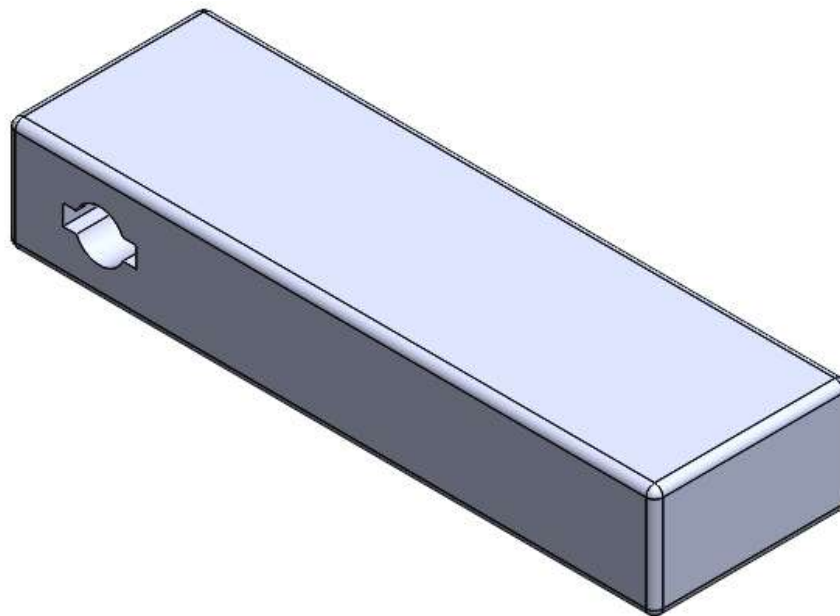


**Figure 3.3.** 3D printed shaft.

### 3.1.2 Unconnected setup

There is not much to say about the setup of the *Unconnected* topology. The only difference in comparison with Classic EPP is that the force sensors are connected to a fixed place and not to the Bowden cable. This way, the user has no feedback for the status of the prosthetic joint.

### 3.1.3 Biomechatronic EPP setup

As it has been previously mentioned, the aim of *Biomechatronic EPP* is to eliminate the disadvantages of Classic EPP, by bypassing the usage of mechanical linkages. A schematic design of the Bomechatronic EPP setup is demonstrated in Figure 3.4.

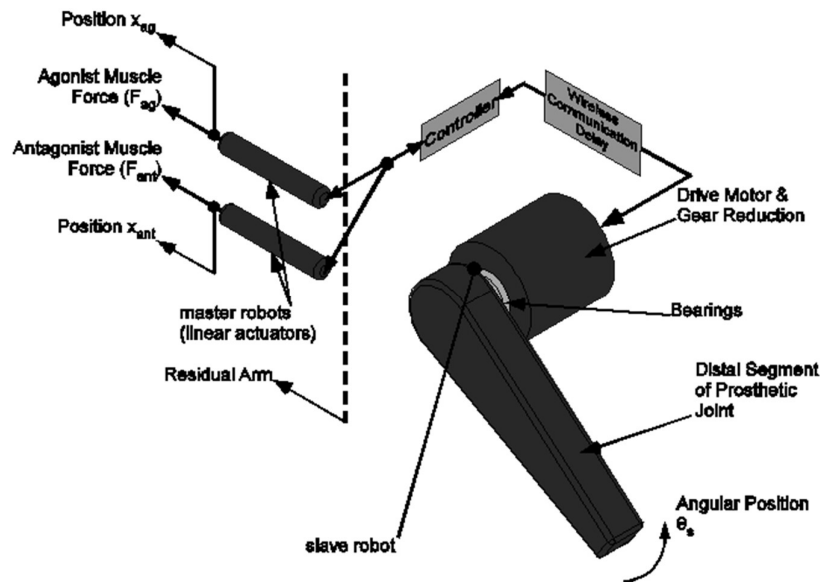


**Figure 3.4. Schematic design of the proposed Biomechatronic EPP setup.**

The experimental setup used for the simulation of Biomechatronic EPP is displayed in Figure 3.5. In this control topology, the slave motor is the one that rotates the joint of the prosthetic limb and the master motors are the ones that are connected to the remaining muscles of the arm. The input of the master motors is the displacement of the slave motor. Both master motors are connected via coupling with power screws (34mm length) acting like linear actuators which convert the rotary displacement to translation. Thus, the master part of the setup, consisting of the master motors and their power screws gives the user the desired proprioception.

The force mechanism is the same used for the Classic EPP setup. However, the force sensors are placed between the power screws and the user.

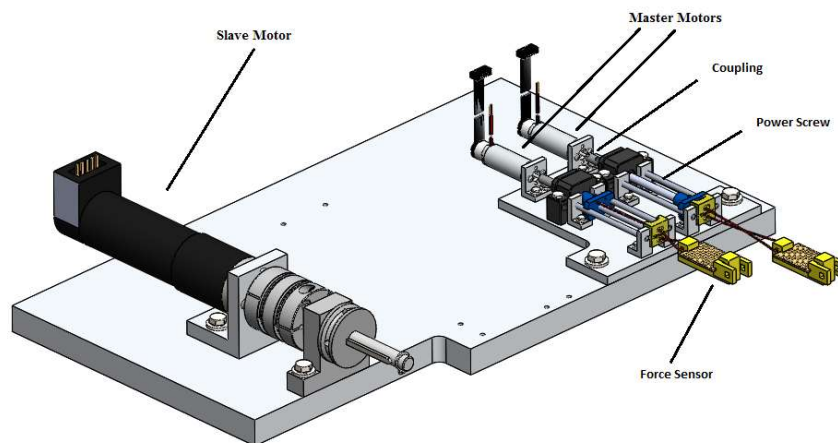


**Figure 3.5. Setup for the Biomechatronic EPP configuration.**

### 3.1.4 Final Setup

All in all, the final setup is displayed in Figure 3.6. To the right of the setup the DSpace DS1103 controller board is displayed, which is connected to the rest of the setup. The DS1103 is an all-rounder for rapid

control prototyping. It can be mounted in a PC or a DSpace Expansion Box to test the control functions in a laboratory. Its processing power and fast I/O are vital for applications that involve numerous actuators and sensors. Used with Real-Time Interface (RTI), the controller board is fully programmable from the Simulink® block diagram environment. A detailed analysis on how to use the most often required material of DS1103 controller board and its graphical environment (ControlDesk 5.6) is presented in Appendix A of [45].

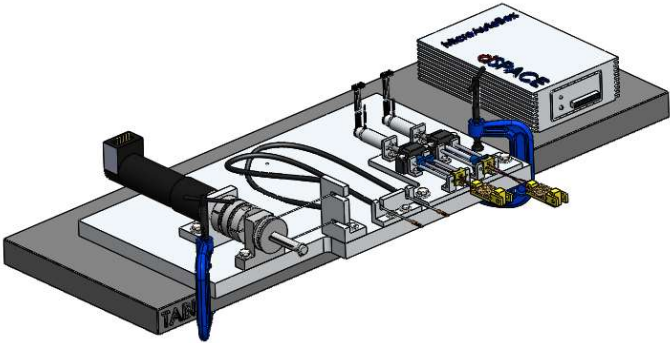


**Figure 3.6. Final setup.**

### 3.2 Force Transducer

An essential part of the experimental setup is the implementation of a force mechanism to provide the reference input to the system. For all the setups presented before, this is the force of the muscles.

For this specific application, the means of converting the applied force to the muscles to a measured signal selected is the Force Sensitive Resistor (FSR) displayed in Figure 3.7(a). The FSR's resistance depends on the applied pressure on its surface (see Figure 3.7(b)) hence it is ideal for the purpose of the setup. The main drawback of FSRs is that they do not have linear response, especially for low forces. This non-linearity was confronted with the construction of the signal conditioning circuit, shown in Figure 3.9. The Linear Technology LT1495 operation amplifier (see Figure 3.8), used in the circuit, is one of the lowest power op amps with precision specifications.

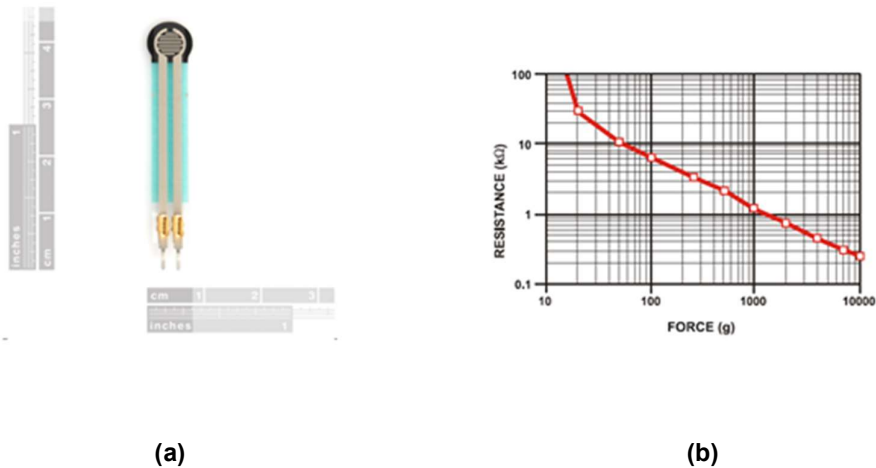


**Figure 3.7. (a) The Force Sensitive Resistor used in the setup. (b) Resistance vs Force diagram.**



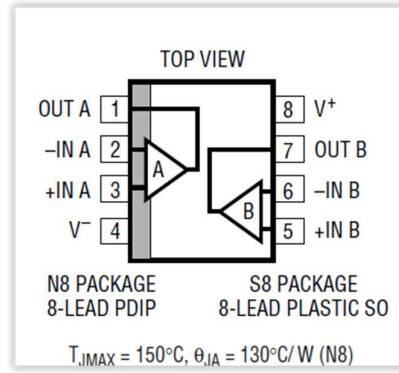


**Figure 3.8. Operational Amplifier LT1495.**

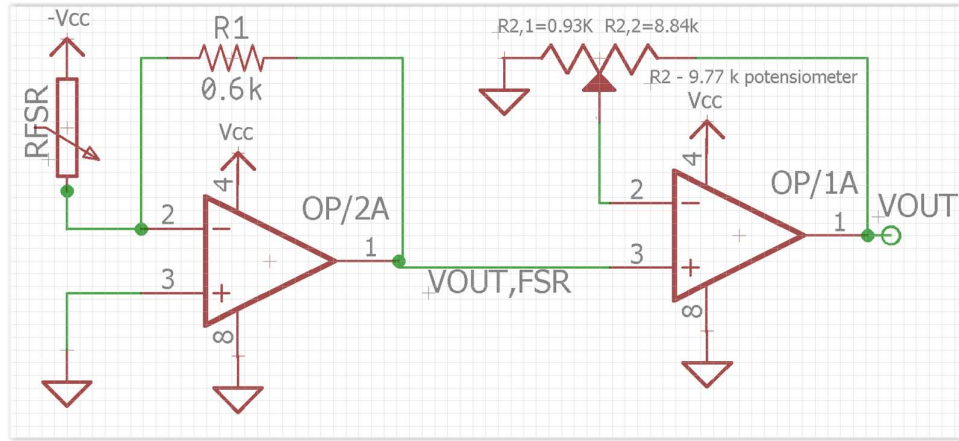


**Figure 3.9. Signal Conditioning Circuit (SCC). Modified from [4].**

The configuration in Figure 3.9 is like a pre-amplifier-amplifier technology. The non-inverting stage of the op-amp OP/1A has a transfer function of:

$$V_{out} = V_{out,fsr} \times \frac{R_{2,1} + R_{2,2}}{R_{2,1}} \quad (3.1)$$

From the inverting stage of the op-amp OP/2A it is conducted that:

$$V_{out,fsr} = -\frac{R_1}{R_{fsr}} \times (-V_{cc}) = \frac{R_1}{R_{fsr}} \times V_{cc} \quad (3.2)$$

By combining Eq. (3.1) and Eq. (3.2), the transfer function of the signal conditioning circuit can be written as:

$$V_{out} = \frac{R_1 \times (R_{2,1} + R_{2,2})}{R_{2,1} \times R_{fsr}} \times V_{cc} \quad (3.3)$$

The output of the circuit must vary from 0 to 5V. The gain of the first stage is:

$$G_1 = -\frac{R_1}{R_{fsr}} \quad (3.4)$$

The aim of this stage is to make the response more proportional and has to be saturated at 0.5V, so G1 must be 0.1 when the maximum force is applied. Muscle cineplasty amputees and exteriorized

tendons amputees can produce a maximum force which varies from 0.6kg for weak amputees to 2.5 kg for strong amputees [4]. Taking the mean value (1.55 kg), we find that the corresponding resistance of the FSR sensor used in the setup is approximately 6k $\Omega$ . Thus, the value of the feedback resistance R1 should be 0.6k $\Omega$ . Depending on the maximum force an amputee can produce, the value of this resistance can be selected respectively and thus the construction of the circuit can be personalized.

The gain of the second stage is:

$$G_2 = \frac{R_{2,1} + R_{2,2}}{R_{2,1}} = 1 + \frac{R_{2,2}}{R_{2,1}} \quad (3.5)$$

G2 must be 10 so as to boost up the output of the first stage to the span 0-5V. This condition is achieved with the usage of a 10k potentiometer. R<sub>2,1</sub> is set to 0.93k $\Omega$  and R<sub>2,2</sub> to 8.84 k $\Omega$ .

### 3.3 Hardware Connectivity

In order to proceed, it is required to connect the previously presented setup with the appropriate hardware, the power supply (see Figure 3.10) and the DS1103 (see Figure 3.11). The setup can be split in three divisions. The first one concerns the prosthesis motor or slave motor for Biomechatronic EPP, the second one the system of the master motors and the third one the FSR sensors.



**Figure 3.10.** Hameg7042-5. Two of these power suppliers (totally five channels) used for the power supply of the whole setup.

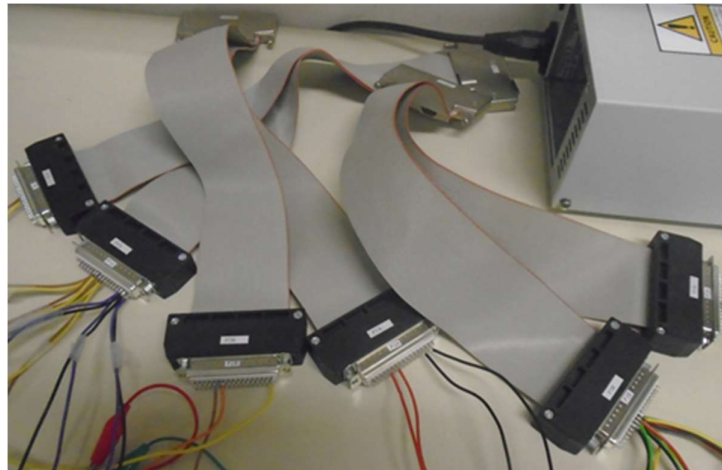


**Figure 3.11.** DS1103 expansion box and the 50 pin D-SUB male connectors cables.

3.3.1 Slave motor subsystem

The slave motor system of the setup consists of the Maxon RE 30 Ø30 mm motor, the Analog Servo Drive AZBDC10A4 (see Figure 3.12), the HEDS 5540 500 Counts per turn encoder (see Figure 3.13), the appropriate ports of DS1103 controller board and of course the power supply.

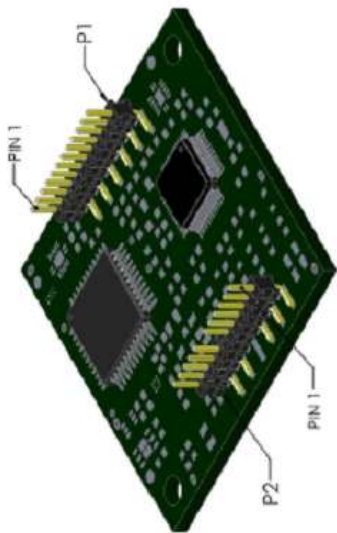


Figure 3.12. AZBDV10A4 analog servo drive.

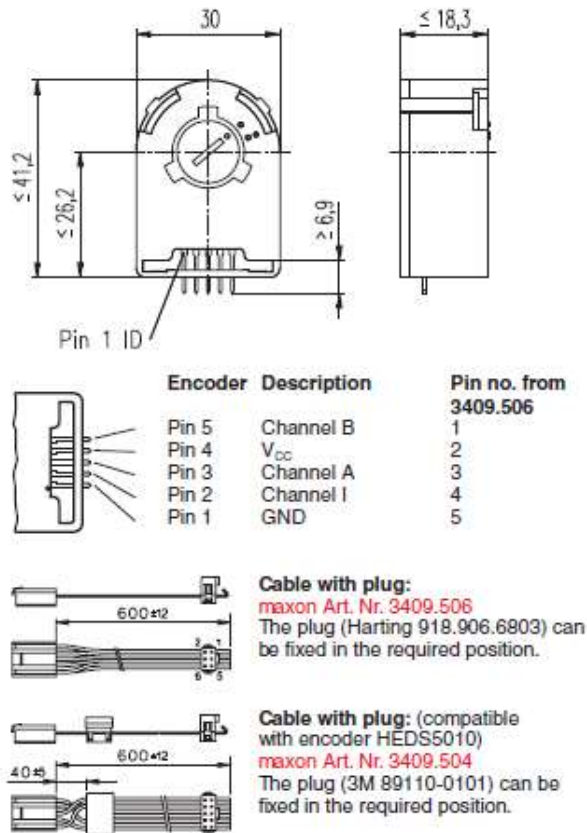


Figure 3.13. HEDS 5540 500 Counts per turn encoder pins mapping.

Table 3.1 and Table 3.2 present the connectivity map of the driver and the encoder, respectively.

Analog Servo Drive AZBDC10A4 Mapping		
a/a	Hardware Pin	DS1103 Pins/Power Supply
1	P1 – Pin 1	P1B25(DACH1)
2	P1 – Pin 2	P2B28(SPWM1)
3	P1 – Pin 6	P1B23(ADCH17)
4	P1 – Pin 8	Signal Ground
5	P1 – Pin 11	Signal Ground
6	P2 – Pin 1	Motor Phase 1 (Red)
7	P2 – Pin 3	Motor Phase 2 (Black)
8	P2 – Pin 8	Power Supply(GND)
9	P2 – Pin 10	Power Supply(+15V)

The Signal Ground is common with Power Ground. Moreover, there is a 100uF decoupling capacitor between Pins 10 and 8. It has to be noted that apart from the three pins of DS1103 showing in Table 3.1, their respective Ground Pins (P1B26, P1B24 and P2B37) are also connected to the ground of the rest setup.

**Table 3.2. ENCODER HEDS5540 500 Counts per turn connectivity map.**

Encoder HEDS 5540		
a/a	Hardware Pin	DS1103 Pins/Power Supply
1	Pin 1- GND	P3B12(GND)/Ground
2	Pin 2-Index	-
3	Pin 3-Channel A	P3B11(PHI0(3))
4	Pin 4- Vcc	Power Supply(+5V)
5	Pin 5 – Channel B	P3B44(PHI90(3))

For completeness and better understanding the schematic design is illustrated in Figure 3.14.

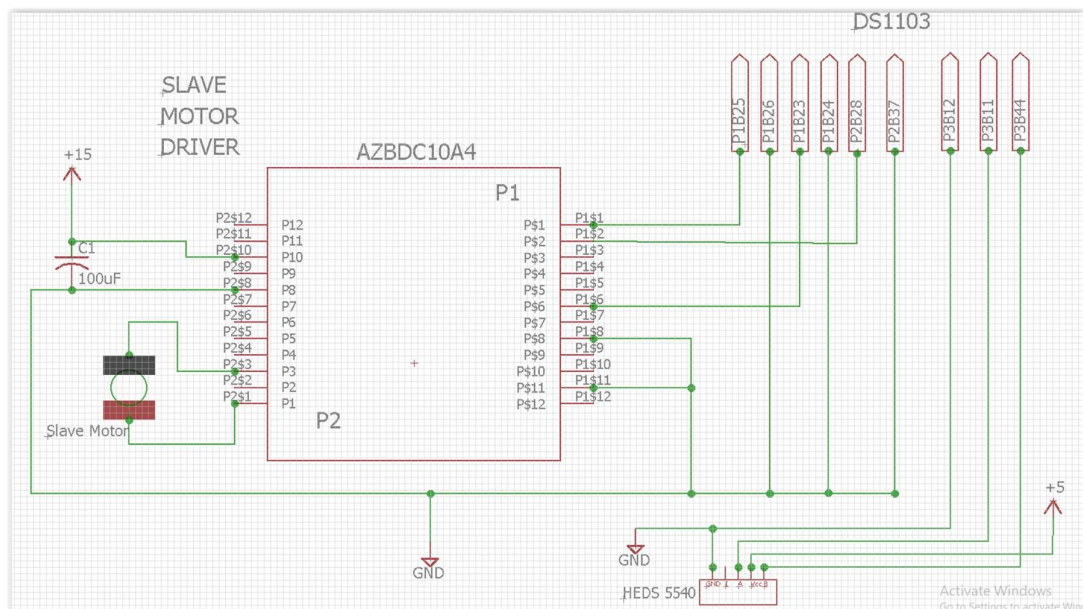


**Figure 3.14. Schematic Design for the Slave Motor Division.**

### 3.3.2 Master motors subsystem

The master motors system division of the setup consists of the two DCX12L EB KL master motors, the DRV8833 Dual Motor Driver Carrier (see Figure 3.15), the encoders Sensor - ENX10 EASY 512IMP of the motors demonstrated in Figure 3.16, the appropriate ports of DS1103 and the power supply.

DRV883 replaced the L293d Quadruple Half-H Driver due to the lack of the last to provide the desirable current to the motors of the setup. More specifically, Texas Instruments' DRV8833 can deliver 1.2A per channel continuously (2A peak) to a pair of DC motors, instead of L293D which can provide only 600mA per channel.

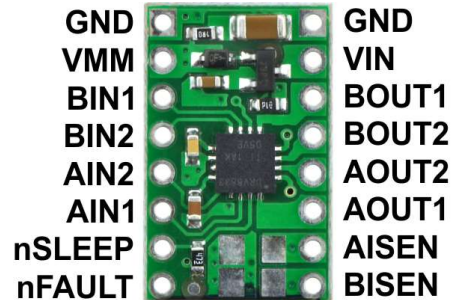


Figure 3.15. DRV8833 motor driver.

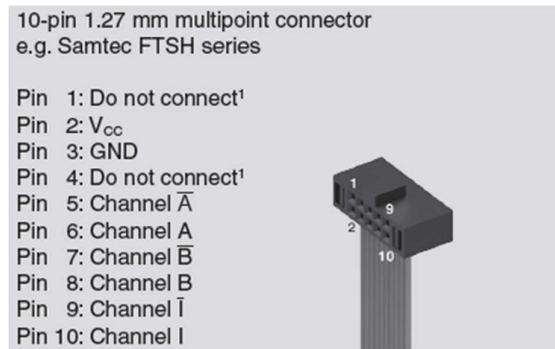


Figure 3.16. The ENX10 EASY 512IMP encoder pins mapping.

Table 3.3, Table 3.4, Table 3.5 present the connectivity map of the motor driver and the encoders.

Table 3.3. DRV8833 Dual Motor Driver Carrier connectivity map.

DRV8833 Dual Motor Driver Carrier		
a/a	Hardware Pin	DS1103/Power Supply
1	Pin 1 – GND	Ground
2	Pin 3 - BIN1	P2B29(SPWM7)
3	Pin 4 - BIN2	P2B13(SPWM9)
4	Pin 5 - AIN2	P2A29(SPWM8)
5	Pin 6 - AIN1	P2A27(ST2PWM)
6	Pin 11 - AOUT1	Master Motor Right(Red)
7	Pin 12- AOUT2	Master Motor Right(Black)
8	Pin 13 - BOUT2	Master Motor Left(Black)
9	Pin 14 - BOUT1	Master Motor Left(Red)
10	Pin 15 - Vin	Power Supply(+6.5V)

The respective Ground Pins (P2A34, P2A35, P2B34 and P2B35) of the DS1103 ports shown on Table 3.3 are connected to the ground of the rest setup.

Table 3.4. Sensor - ENX10 EASY 512IMP connectivity map for Master Motor Right.



Sensor - ENX10 EASY 512IMP (Master Motor Right)		
a/a	Hardware Pin	DS1103 Pins / Power Supply
1	Pin 2 - Vcc	Power Supply (+5V)
2	Pin 3 - GND	P3A27(GND)/P3B27(GND)/Ground
3	Pin 5 - Channel $\bar{A}$	P3A41( $\overline{PHI0(1)}$ )
4	Pin 6 - Channel A	P3B41(PHI0(1))
5	Pin 7 - Channel $\bar{B}$	P3A25 ( $\overline{PHI90(1)}$ )
6	Pin 8 - Channel B	P3B25(PHI90(1))

**Table 3.5. Sensor - ENX10 EASY 512IMP connectivity map for Master Motor Left.**

Sensor - ENX10 EASY 512IMP (Master Motor Left)		
a/a	Hardware Pin	DS1103 Pins / Power Supply
1	Pin 2 - Vcc	Power Supply (+5V)
2	Pin 3 - GND	P3A42(GND)/P3B42(GND)/Ground
3	Pin 5 - Channel $\bar{A}$	P3A26( $\overline{PHIO(2)}$ )
4	Pin 6 - Channel A	P3B26(PHI0(2))
5	Pin 7 - Channel $\bar{B}$	P3A10( $\overline{PHI90(2)}$ )
6	Pin 8 - Channel B	P3B10(PHI90(2))

In Figure 3.17 the schematic design for the master motors division is illustrated.

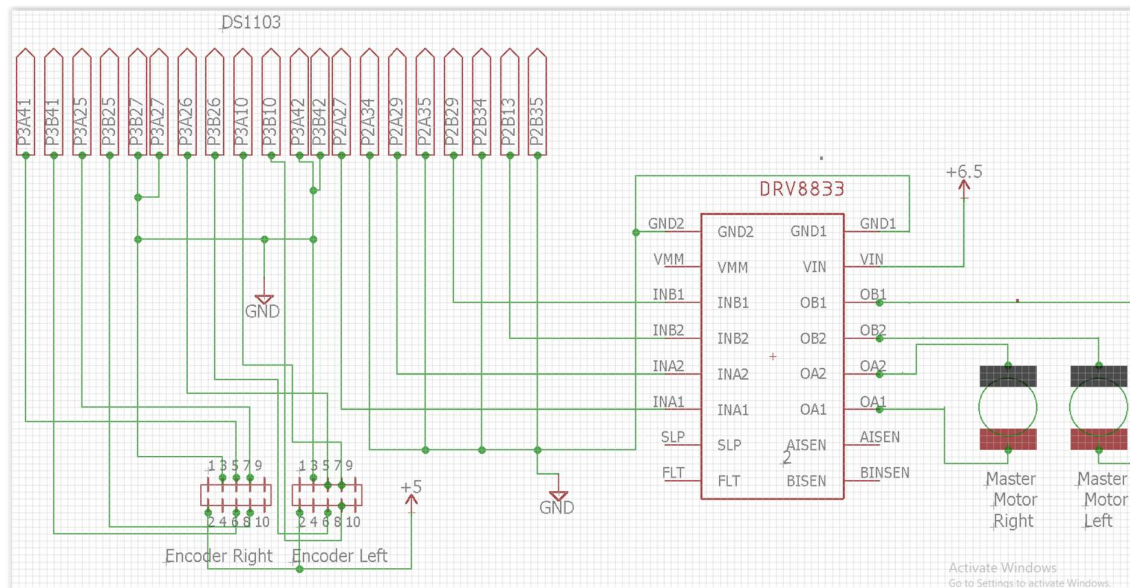


**Figure 3.17. Schematic Design for the Master Motors Subsystem.**

### 3.3.3 FSR Sensors Subsystem

The connection of the FSR Sensors is the least arduous one. It just requires two “analog to digital” channels. Table 3.6 and the Figure 3.18 present the connectivity map and the schematic design for the FSR division, respectively.

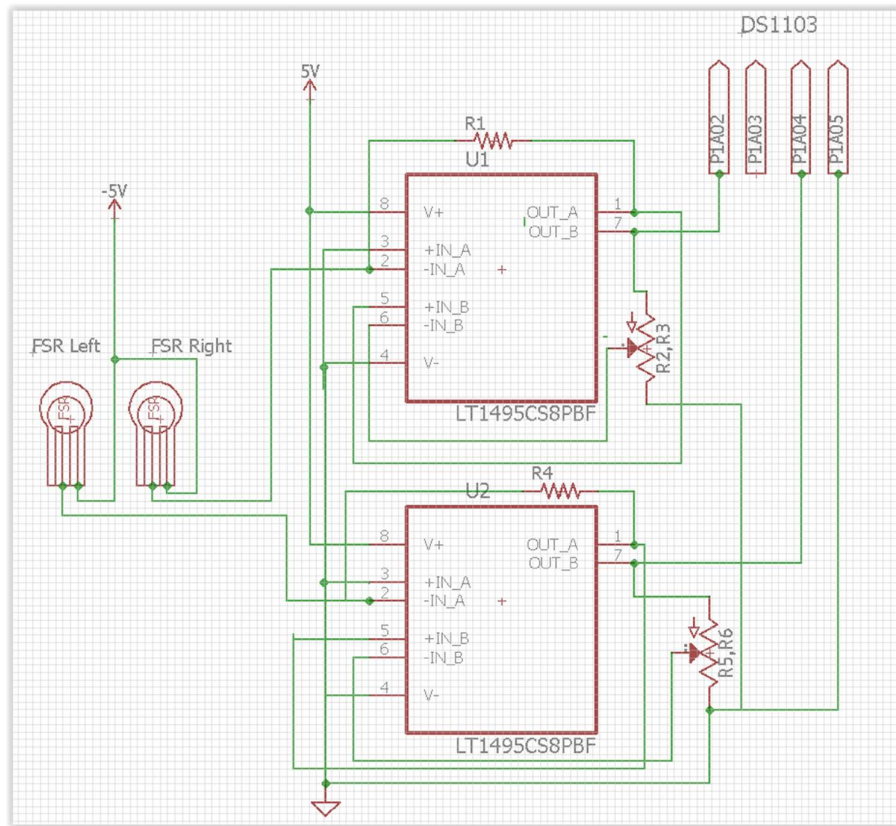


**Figure 3.18. Schematic Design for the FSRs' Subsystem.**

**Table 3.6. FSR Sensors connectivity map.**

FSR Sensors		
a/a	Hardware Pin	DS1103 Pins
1	Sensor Right Output	P1A02(ADCH04)
2	Sensor Left Output	P1A04(ADCH10)

As previously, P1A03 and P1A05 which are the Ground Pins for the DS1103 ports used are connected to the ground of the setup. Moreover, the FSR sensors require two voltage sources: a +5 V and a -5 V.

Concluding, in this chapter the experimental setup, as it was constructed for the experiments to come, was presented. Due to the amount of the required connections, we divided the description of the hardware connectivity in order that the readers and the future users of the setup may be able to understand each subsystem individually.

## 4 Control topologies

The objective of this chapter is to present the control schemes implemented for Classic and Biomechatronic EPP. This notion was already implemented in Simulink and can be found in Chapter 6 of [45]. However, a new version of this program had to be realized in order to include the alterations made in the setup during this thesis. The structure of the program analysis is separated in divisions. At each one, a specific part of the control scheme design is presented.

### 4.1 Classic EPP control topology

A schematic structure of the Classic EPP topology is displayed in Figure 4.1. As it has been mentioned previously, the Classic EPP control is achieved via direct connection of the control muscles to the prosthetic limb, using Bowden cable. In this topology the forces applied by the muscles to the terminals of the Bowden cable are captured by the corresponding sensors and after their processing the controller drives the slave motor.

The relationship between the displacement of the Bowden cable terminals at the points of connection to the muscles and the angular displacement of the slave motor is given by:

$$\begin{cases} x_{ag}^c = r\theta_s \\ x_{ant}^c = -r\theta_s \end{cases} \quad (4.1)$$

Where  $x_{ag}^c$  and  $x_{ant}^c$  in mm are the displacements of the agonistic and antagonistic muscles, respectively,  $r$  is the radius of the slave motor pulley (12mm) and  $\theta_s$  is the angular displacement of the slave motor in rads.

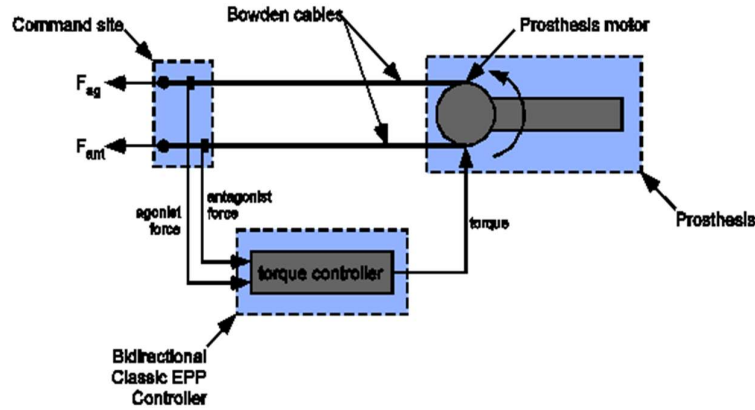


**Figure 4.1. Schematic structure of the Classic EPP topology.**

Figure 4.2 presents the various stages of the controller designed for the evaluation of the Classic EPP topology, which is basically an open loop torque controller. Each one of the stages are described below.



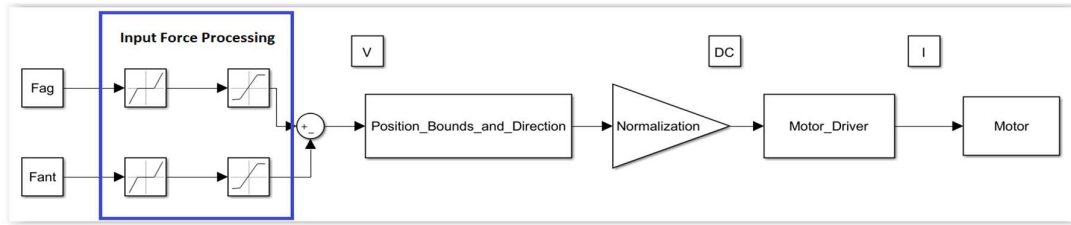
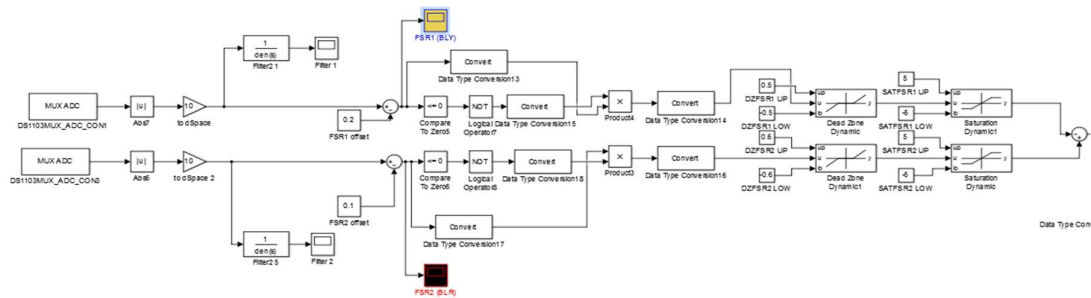


**Figure 4.2.** Schematic diagram of the Classic EPP controller.

#### 4.1.1 Input Force Processing

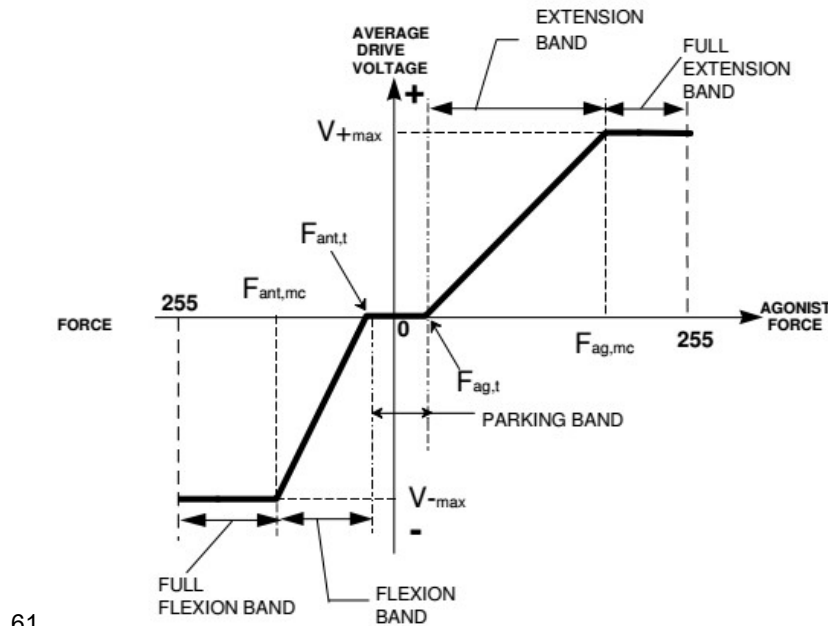
In Section 3.2 the signal conditioning circuit for the FSR sensors was presented. However, the obtained signals need further processing before we can set them as input to the prosthesis motor driver.

Figure 4.3 illustrates the part of the Simulink program which is responsible for the processing of the acquired force signals.



**Figure 4.3.** Processing of the acquired force signals.

The main purpose of this processing is the imitation of the upper limb prosthesis according to the diagram presented in Figure 4.4. A detailed analysis is presented in [45], Section 6.3. The output of this stage is the difference between the force signals in Volts.



**Figure 4.4.** Upper and Lower Bounds of the FSR sensor Output. From [4].

### 4.1.2 Position Bounds Control and Direction

The prosthesis motor is where the mechanical joint is to be placed. Thus, it should not be able to rotate continuously, because in such a situation a mechanical impact would be imminent. Apart from the mechanical stops which will be placed in the setup during the experiments to come. Position bounds must be also set in software. These bounds have to prevent the controller from giving command to the prosthesis motor if the movement limits have been reached.

If  $F$  is the input force and  $\theta_e$ ,  $\theta_f$  are the boundary values of the movement in the extension and flexion bands respectively, then the following equation describes how the controller must command the motor for different combinations of  $F$  and the slave motor angular position,  $\theta_s$ .

$$\begin{aligned}
 F > 0 \text{ and } \begin{cases} \theta_s < \theta_e & \text{clockwise rotation} \\ \theta_e \leq \theta_s \leq \theta_f, & \text{clockwise rotation} \\ \theta_s > \theta_f, & \text{halted} \end{cases} \\
 F < 0 \text{ and } \begin{cases} \theta_s < \theta_e, & \text{halted} \\ \theta_e \leq \theta_s \leq \theta_f, & \text{anticlockwise rotation} \\ \theta_s > \theta_f, & \text{anticlockwise rotation} \end{cases}
 \end{aligned}
 \tag{4.2}$$

Figure 4.5 presents the corresponding Simulink code. It also displays how the direction change is implemented. Depending on the output of the first stage, the D/A converter pin connected to the Analog Servo Drive AZBDC10A4 direction pin is either HIGH or LOW, providing the ability to change direction.

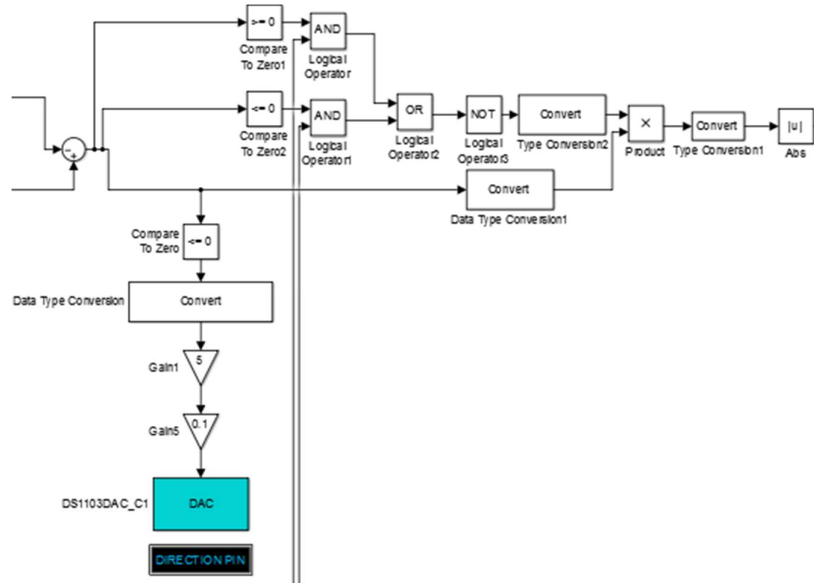


**Figure 4.5. Position limits and direction change**

### 4.1.3 Motor Drive

The output of the driver is current, but its input is PWM pulses. The magnitude of the current depends on the duty cycle of the PWM pulse. Thus, the input of the drive must be normalized to [0 1]. The maximum absolute value of the difference of the two outputs is +5, while the minimum is 0. Ergo, to

normalize it to the desired range the gain  $1/5$  can be used ( $1/V_{max}$  in Figure 4.6). However, if the range of the duty cycle is the  $[0, 1]$ , then even at pretty insignificant forces, the duty cycle will reach the value 1 easily. The “FSR reduce Gain” reduces the range of the duty cycle to a range specified by the user. A range of  $[0, 0.03]$  was used during the realization of the experiments.

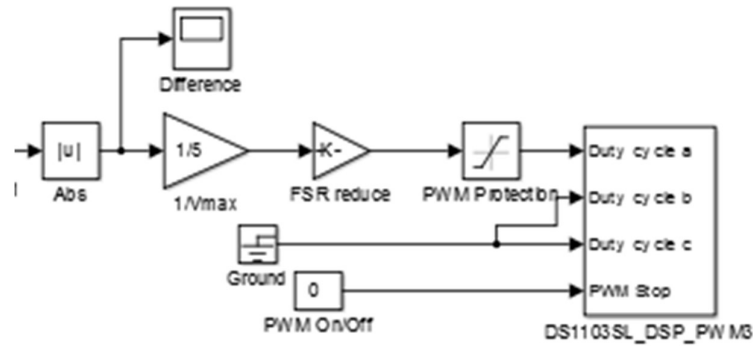
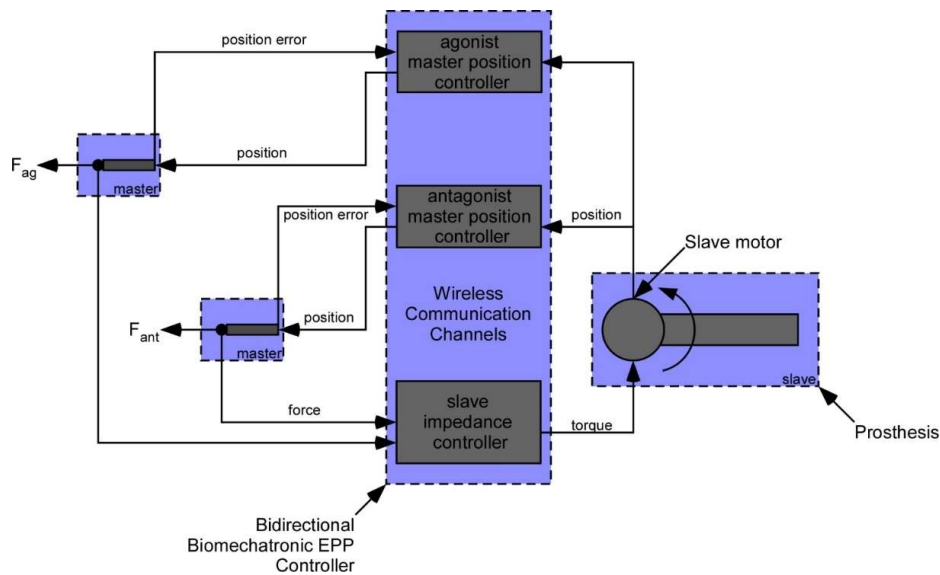


**Figure 4.6.** Normalization of the input for the motor driver.

With the FSR sensors connected to the Bowden Cables or to a fixed pace this part of the Simulink file can be used to conduct experiments either for the Classic EPP or the Unconnected configuration.

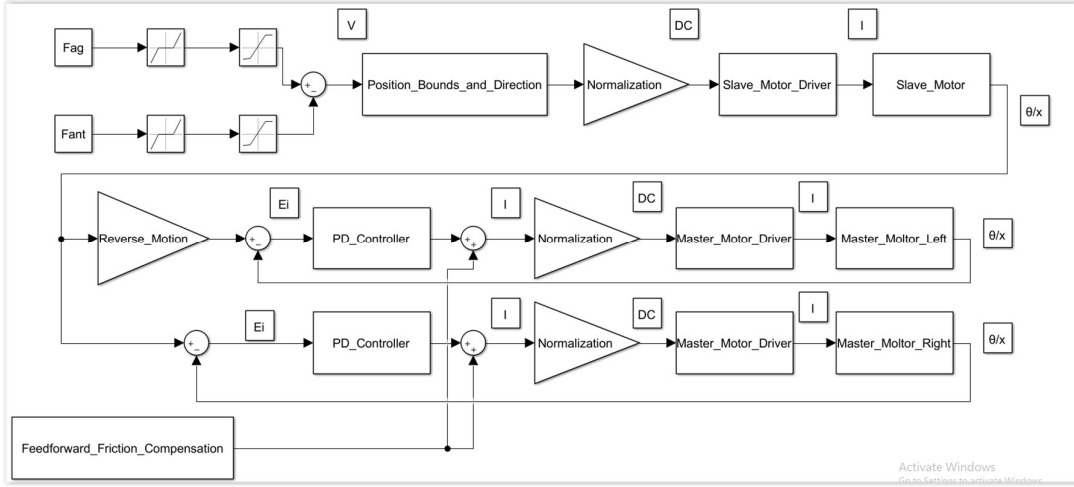
## 4.2 Biomechatronic EPP control topology

Figure 4.7 displays the schematic structure of the proposed Biomechatronic EPP topology. As in Classic EPP configuration the forces applied by the antagonistic pair of muscles are the input of the system. However, in this scheme, the muscle terminals are connected to the master motors of the Biomechatronic EPP topology. The force signals are transmitted to the slave system controller, which sets the torque of the prosthesis motor. Then, each position controller sets the displacement of the corresponding master robot according to the displacement of the slave motor.



**Figure 4.7.** Schematic structure of the Biomechatronic EPP topology.

The Biomechatronic EPP control scheme is illustrated in Figure 4.8. The open loop control of the slave motor is the same as in the Classic EPP configuration. The most important parts are described below.



**Figure 4.8. Biomechatronic EPP control scheme.**

#### 4.2.1 Reference Input

The position response of the slave motor is the reference input for the master motors closed loop controller. The aim of each master robot is to set the length of the corresponding muscle appropriately, according to the response achieved in the Classic EPP configuration. Therefore, according to Eq.(3.6), the desired position of the agonistic ( $x_{ag}^{des}$ ) and antagonistic ( $x_{ant}^{des}$ ) linear actuators can be expressed as:

$$\begin{cases} x_{ag}^{des} = x_{ag}^c = r\theta_s \\ x_{ant}^{des} = x_{ant}^c = -r\theta_s \end{cases} \quad (4.3)$$

The respective desired angular displacement ( $\theta_{ag,ant}^{des}$ ) of the master motors is described by the following equation:

$$\begin{cases} \theta_{ag}^{des} = \frac{2\pi i}{h} r\theta_s \\ \theta_{ant}^{des} = -\frac{2\pi i}{h} r\theta_s \end{cases} \quad (4.4)$$

Where h is the lead of the of the screw used for the construction of the master robots.

#### 4.2.2 PD Controller

It has been already determined from previous works that a PD controller is the appropriate way to implement the closed loop scheme [25] [45]. The system identification of the master motors which is required for the design of the controller, was realized in cooperation with the former MSc student Koukoulas Nikolaos and is presented thoroughly in Section 6.1 of his MSc thesis [23].

The model equation for the system of the master motors and their lead screws is given by Eq. (4.5).

$$\frac{2\pi}{h}J\ddot{x} + \frac{2\pi}{h}b\dot{x} = K_t i - c \operatorname{sgn} \dot{x} \quad (4.5)$$

Where:  $x$  – position of the lead screw

$h$  – lead of the screw

$i$  – armature current

$K_t$  – Torque constant

$J$  – Moment of Inertia of the system

$b$  – Damping of the system

$c$  – Coulomb Friction

In Table 4.1 the values of those parameters are presented for both master motors.

**Table 4.1. The values of the parameters of the system.**

Parameter	Master Motor Right	Master Motor Left
<b>h</b>	1.22 mm	1.22 mm
<b>Kt</b>	6.44 N · mm / A	6.44 N · mm / A
<b>J</b>	$6.061 \cdot 10^{-6}$ N · mm · s <sup>2</sup>	$6.067 \cdot 10^{-6}$ N · mm · s <sup>2</sup>
<b>b</b>	$242.44 \cdot 10^{-6}$ N · mm · s	$242.68 \cdot 10^{-6}$ N · mm · s
<b>c</b>	0.228 N · mm	0.147 N · mm

With these values obtained the open loop transfer function of the plant- $G(s)$  between linear position (mm)- $X(s)$  and input current (A)- $I(s)$  for both right and left master motor is obtained by Eq.(4.6):

$$G(s) = \frac{X(s)}{I(s)} = \frac{3900}{s(0.025s + 1)} = \frac{156000}{s^2 + 40s} \quad (4.6)$$

With the transfer function of the plant obtained, the implementation of the PD controller for position control is the next step. The closed-loop block diagram of the controller is illustrated in Figure 4.9.

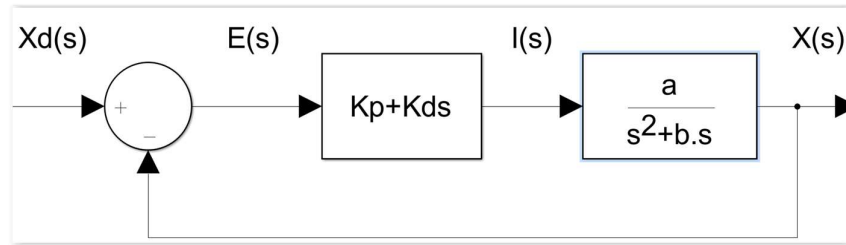


**Figure 4.9. PD Control of DC motor plant.**

The transfer function of such a system can be written as:

$$\frac{X(s)}{X_d(s)} = \frac{aK_d s + aK_p}{s^2 + (b + aK_d)s + aK_p} \quad (4.7)$$

The characteristic equation is:

$$\text{CE: } s^2 + (b + aK_d)s + aK_p \quad (4.8)$$

With two controller parameters, and a 2nd order closed-loop system, the poles can be freely assigned.

Using the  $(\zeta, \omega_n)$  parametrization, we set the characteristic equation to be:

$$s^2 + 2\zeta\omega_n s + \omega_n^2 \quad (4.9)$$

Where:  $\omega_n$  – natural frequency

$\zeta$  – damping ratio ( $0 \leq \zeta \leq 1$ )

Comparing Eq. (4.8) and Eq. (4.9) is derived that:

$$K_p = \frac{\omega_n^2}{a} \quad (4.10)$$

$$K_d = \frac{2\zeta\omega_n - b}{a} \quad (4.11)$$

From Eq. (4.6):  $a = 156000$  and  $b=40$ .

The controller must have fast and “instantaneous” response. Taking into account that the slave encoder has a resolution of 0.68 degrees which increases to 0.0133 degrees due to the “343/17576” reduction rate of the coupling and using Eq. (3.6), it is obtained that the minimum input and therefore the minimum error can be 0.0027mm. It is also known that the maximum current that the master motor driver can provide is 1.2A. Assuming that the controller would provide in its output the maximum current for an error value of 0.06mm and evaluating only proportional control ( $K_d = 0$ ), the value of the gain  $K_p$  obtained is given by Eq. (4.11):

$$0.06 * K_p = 1.2 \Leftrightarrow K_p = 20 \quad (4.12)$$

Then, by Eq. (4.9) natural frequency is computed:

$$\omega_n = 1766.4 \text{ rad / s} \quad (4.13)$$

For minimal overshoot above the desired value the peak time ( $t_p$ ) must be equal to settling time ( $t_s$ ). Peak time and settling time are given by the Eq. (4.13) and Eq. (4.14), respectively.

$$t_p = \frac{\pi}{\omega_n \cdot \sqrt{1 - \zeta^2}} \quad (4.14)$$

$$t_s = \frac{4}{\zeta\omega_n} \quad (4.15)$$

Assuming  $t_p = t_s$ , then the damping ratio  $\zeta$  is computed:

$$\zeta = 0,6 \quad (4.16)$$

With the natural frequency and the damping ratio obtained the gain  $K_d$  can be computed via Eq. (4.10):

$$K_d = 0.0133 \quad (4.17)$$

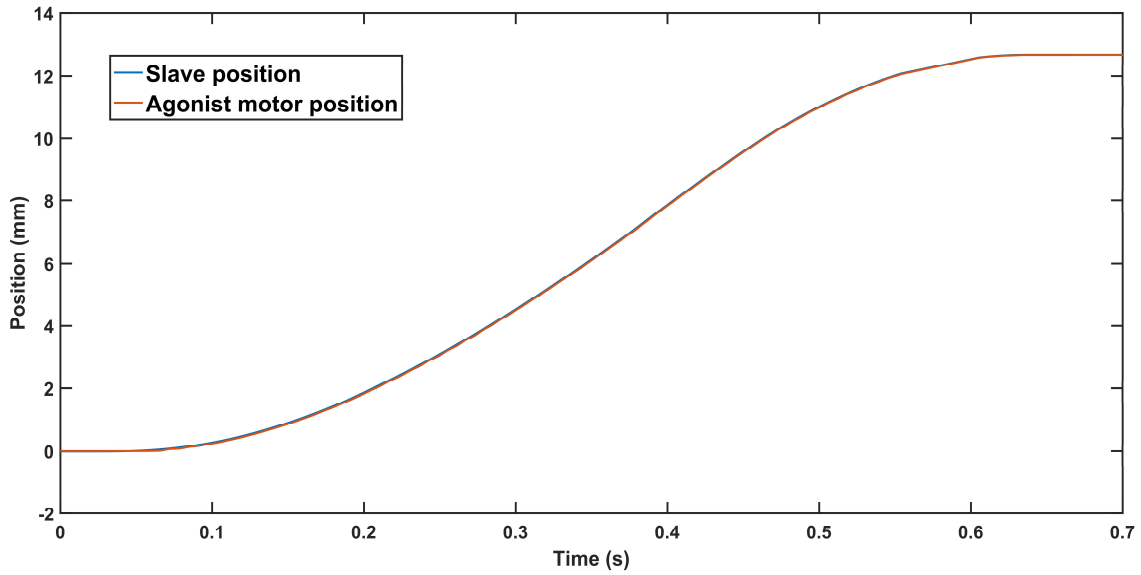


**Figure 4.10.**

### 4.2.3 Feedforward Friction Compensation

Apart from the PD controller, another structure used in order to enhance the tracking performance of the master motors, by means of model based feedforward friction compensation. This structure is illustrated in Figure 4.11 with a block diagram [1].

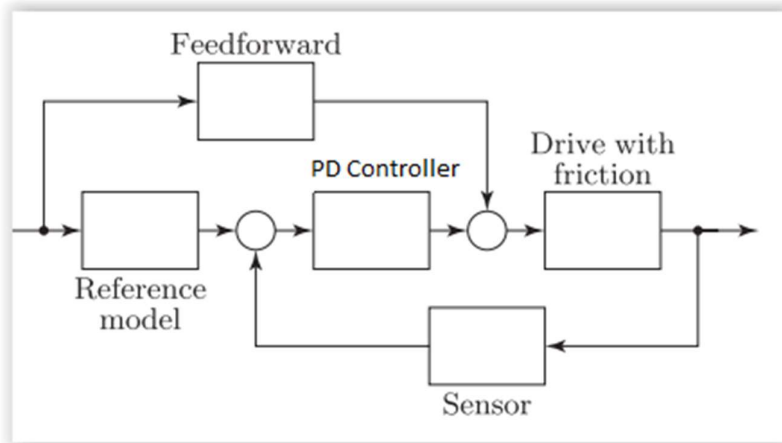


**Figure 4.11. Block diagram of model based feedforward friction compensation.**

The compensation signal is added in the output of the PD controller and is based on the reference signal. Rewriting the Eq. (4.5) we obtain:

$$K_f i = \frac{2\pi}{h} J \ddot{x} + \frac{2\pi}{h} b \dot{x} + c \operatorname{sgn} \dot{x} \quad (4.18)$$

From Eq. (4.17), it is observed that the friction of the motor can be analyzed in three different terms.

- Inertial Friction -  $\frac{2\pi}{h} J \ddot{x}$

- Viscous Friction -  $\frac{2\pi}{h} b\dot{x}$
- Coulomb Friction -  $c \operatorname{sgn} \dot{x}$

The implemented feedforward loop consists of these terms and is illustrated in Figure 4.12.

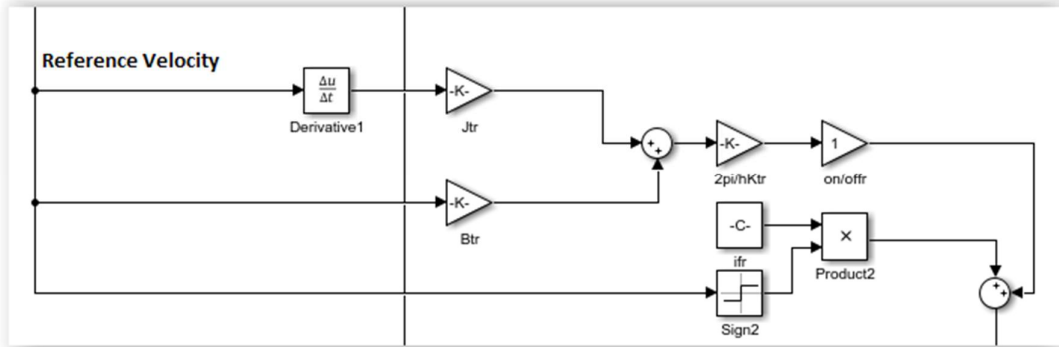


**Figure 4.12. Feedforward loop.**

#### 4.2.4 Motor Drive

The DRV883 which is used as motor driver in the setup can be modeled as a simple gain,  $K_{DC \rightarrow A}$ , which converts the Duty Cycle to Ampere. The way these gains are computed for the two master motors is presented in Section 6.2 of [23]. The gains for the right and the left motor are 1.1208 A/DC and 1.0755A/DC, respectively.

The inverse values of the aforementioned gains are used for the conversion of the controller output, which is current, to the driver input which is PWM as Figure 4.8 illustrates.

The last step is to provide the motor driver with the appropriate input signals. Table 4.2 presents the logic of DRV8833.

**Table 4.2. Logic table of DRV883 Inputs**

xIN1	xIN2	Mode
1	1-DC	Forward, Slow Decay
1-DC	1	Reverse, Slow Decay
DC	0	Forward, Fast Decay
0	DC	Reverse, Fast Decay

The “Slow Decay” mode was used. Looking back to Figure 3.15 there are two input signals for each motor. According to Table 4.2 one of them must be always “1” and the other, the obtained PWM signal subtracted from “1”. The direction in which each motor rotated depends on the signal of the error. For the right motor which moves in the same direction as the slave motor, when the error is positive the “Forward Mode” is activated, while the opposite applies for the left motor.

To summarize, this chapter described the process followed for the design of the required controllers and their implementation using MATLAB/Simulink. Due to the size of the written Simulink program, we were not able to present it as a complete entity. However, it is available in the CD-ROM provided with this thesis.



## 5 EMG Setup and Controller

The aim of this chapter is to present the setup used for the realization of the EMG control topology along with the way the EMG signals acquired and processed in order to drive the prosthesis. However, before the acquisition of the EMG signals the placement of the muscle sensors had to be identified. As the experiments to come concern the wrist movement, the part of the upper limb which had to be examined was the forearm.

### 5.1 Anatomy of the Forearm

Forearm is split into two compartments, the posterior and the anterior. Generally, the muscles in these two parts are split into three categories: superficial, intermediate and deep. Nevertheless, the surface electromyography concerns the superficial muscles (see Figure 5.1 and Figure 5.2) so the following sections describe those and only.

#### 5.1.1 Anterior compartment of the forearm

The superficial muscles in the anterior compartment are *the flexor carpi ulnaris*, *palmaris longus*, *flexor carpi radialis* and *pronator teres*. They all originate from a common tendon, which arises from *the medial epicondyle of the humerus*.

##### Flexor Carpi Ulnaris

- Attachments: Originates from the medial epicondyle with the other superficial flexors. It also has a long origin from the ulna. It passes into the wrist, and attaches to the pisiform carpal bone.
- Actions: Flexion and adduction at the wrist.
- Innervation: Ulnar nerve.

##### Palmaris Longus

This muscle is absent in about 15% of the population.

- Attachments: Originates from the medial epicondyle, attaches to the flexor retinaculum of the wrist.
- Actions: Flexion at the wrist.
- Innervation: Median nerve.

##### Flexor Carpi Radialis

- Attachments: Originates from the medial epicondyle, attaches to the base of metacarpals II and III.
- Actions: Flexion and abduction at the wrist.
- Innervation: Median nerve.

##### Pronator Teres

The lateral border of the pronator teres forms the medial border of the cubital fossa, an anatomical triangle located over the elbow.

- Attachments: It has two origins, one from the medial epicondyle, and the other from the coronoid process of the ulna. It attaches laterally to the mid-shaft of the radius.
- Actions: Pronation of the forearm.
- Innervation: Median nerve.

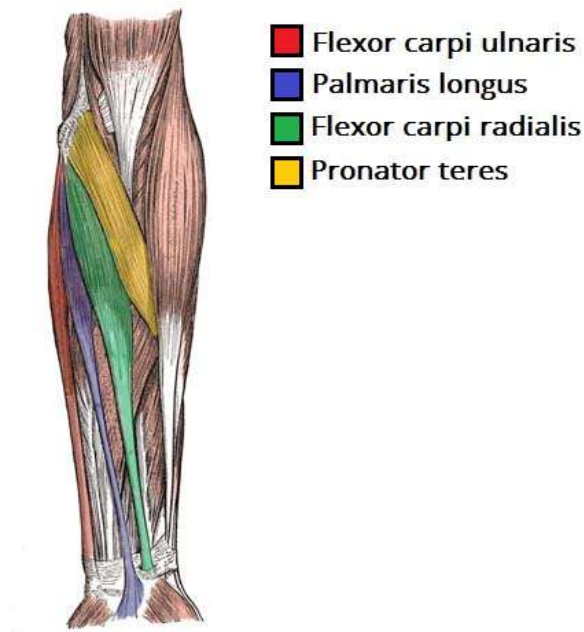


**Figure 5.1. The superficial muscles of the anterior forearm**

### **5.1.2 Posterior compartment of the forearm**

The superficial layer of the posterior forearm contains seven muscles. Four of these muscles – *extensor carpi radialis brevis*, *extensor digitorum*, *extensor carpi ulnaris* and *extensor digiti minimi* share a common *tendinous* origin at the *lateral epicondyle*.

#### **Brachioradialis**

- Attachments: Originates from the proximal aspect of the lateral supracondylar ridge of humerus, and attaches to the distal end of the radius, just before the radial styloid process.
- Actions: Flexes at the elbow.
- Innervation: Radial nerve.

#### **Extensor Carpi Radialis Longus and Brevis**

The extensor carpi radialis muscles are situated on the lateral aspect of the posterior forearm. Due to their position, they are able to produce abduction as well as extension at the wrist.

- Attachments: The ECRL originates from the supracondylar ridge, while the ECRB originates from the lateral epicondyle. Their tendons attach to metacarpal bones II and III.
- Actions: Extends and abducts the wrist.
- Innervation: Radial nerve.

#### **Extensor Digitorum**

The extensor digitorum is the main extensor of the fingers. To test the function of the muscle, the forearm is pronated, and the fingers extended against resistance.

- Attachments: Originates from the lateral epicondyle. The tendon continues into the distal part of the forearm, where it splits into four, and inserts into the extensor hood of each finger.
- Actions: Extends medial four fingers at the MCP and IP joints.
- Innervation: Radial nerve (deep branch).

### **Extensor Digiti Minimi**

The extensor digiti minimi is thought to originate from the extensor digitorum muscle. In some people, these two muscles are fused together. Anatomically, the extensor digiti minimi lies medially to the extensor digitorum.

- Attachments: Originates from the lateral epicondyle of the humerus. It attaches, with the extensor digitorum tendon, into the extensor hood of the little finger.
- Actions: Extends the little finger, and contributes to extension at the wrist.
- Innervation: Radial nerve (deep branch).

### **Extensor Carpi Ulnaris**

The extensor carpi ulnaris is located on the medial aspect of the posterior forearm. Due to its position, it is able to produce adduction as well as extension at the wrist.

- Attachments: Originates from the lateral epicondyle of the humerus, and attaches to the base of metacarpal V.
- Actions: Extension and adduction of wrist.
- Innervation: Radial nerve (deep branch).

### **Anconeus**

The anconeus is situated medially and superiorly in the extensor compartment of the forearm. It is blended with the fibers of the triceps brachii, and the two muscles can be indistinguishable.

- Attachments: Originates from the lateral epicondyle, and attaches to the posterior and lateral part of the olecranon.
- Actions: Extends and stabilizes the elbow joint. Abducts the ulna during pronation of the forearm.
- Innervation: Radial nerve.

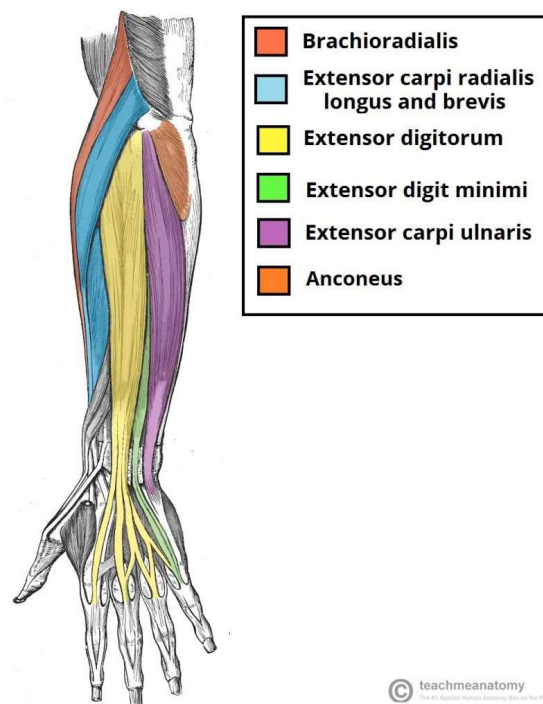


**Figure 5.2. The muscles in the superficial layer of the posterior forearm.**

## 5.2 EMG Sensors

The bioelectrical activity inside the muscle of a human body is detected with the help of EMG electrodes. There are two main types of EMG electrodes: surface (sEMG) and inserted electrodes. Application of inserted electrodes requires strict medical supervision and certification. Surface EMG electrodes require no such formalities. Surface EMG electrodes have found their use in motor behavior studies, neuromuscular recordings and sports medical evaluations [29]. Apart from all this, surface EMG is being increasingly used to detect muscle activity in order to control device extensions to achieve prosthesis for physically disabled and amputated population.

### 5.2.1 Myo Armband

For the needs of this thesis the Myo Armband (see Figure 5.3), developed by Thalmic Labs, was employed. It is a commercial EMG-based sensor band for estimating hand gestures. It provides high quality EMG measurements with an 8-bit resolution, and a sample rate of 200 Hz. It consists of 8 pods that are placed evenly around the wearers forearm, each containing a surface EMG sensor. The pods are connected to one another with an expandable band, assuring a comfortable and secure grip around the arm. It also has a built in gyroscope and accelerometer, which can be sampled at 50 Hz.

The finish and ease of use of the Myo Band, along with the fact that is made for use for the forearm makes it a compelling choice for this thesis.



**Figure 5.3.** The Thalmic Labs Myo Armband.

### 5.2.2 Placement

Myo Armband has to be placed in such way so that we can capture the activity of the muscles which control the wrist flexion and extension. From Sections 5.1.1 and 5.1.2 it is derived that the muscles of interest are Flexor Carpi Radialis and Extensor Carpi Radialis for wrist flexion and extension respectively. This consideration can also be verified from other works in this field [14] [17]. In order to acquire the best possible signal, the Myo Armband must be placed so that its EMG sensors are attached on the belly of the muscle, as there, the target muscle fiber density is the highest [42]. Figure 5.4.b

demonstrates the exact way the Myo Armband is placed. The sensor pod number 4 is attached on the Extensor Carpi Radialis, while sensor pod number 7 is on the top of Flexor Carpi Radialis. The numbering of the sensor pods is shown in Figure 5.4.a.



**Figure 5.4.** (a) Numbering of sensor pods. (b) The Myo Armband mounted on the forearm.

### 5.3 EMG Signal Acquisition and Configuration

With the Myo Armband properly placed, the EMG signals acquisition and configuration are the next steps. The data is transmitted by Myo Armband over a Bluetooth Low Energy (BLE) protocol to the computer in which its USB connector is adapted. To establish this connection, the application *Myo Connect* must be installed.

#### 5.3.1 Acquisition

The raw EMG data provided by MYO should be available on the platform which controls the prosthesis motor. As it has been previously mentioned in Chapter 3, this platform consists of the DS1103 controller board and MATLAB. Myo Connect and other programs provided in Myo Market (e.g Myo Data Capture) were not sufficient to create this communication. After extensive research, Myo SDK MATLAB MEX Wrapper, created by Mark Tomaszewski was finally used (<https://github.com/mark-toma/MyoMex>). On the surface, this package contains a simplified m-code class, MyoMex, that enables MATLAB users to stream data from one or two Myo devices at 50Hz (IMU and meta data) and 200Hz (EMG) [44].

The digitization process of the analog EMG signals is carried out with the Analog to Digital Converters (ADC) of MYO. The range of potentials provided by the Myo armband is between -128 and 128 in units of activation and is not translated to volts (V) or millivolts (mV). MyoMex normalizes the EMG data to the span [-1,1].

#### 5.3.2 Configuration

With the EMG data being streamed in MATLAB in real-time, it has to be processed so that it can be used as input for the motor driver. Figure 5.5 illustrates the various processing stages.

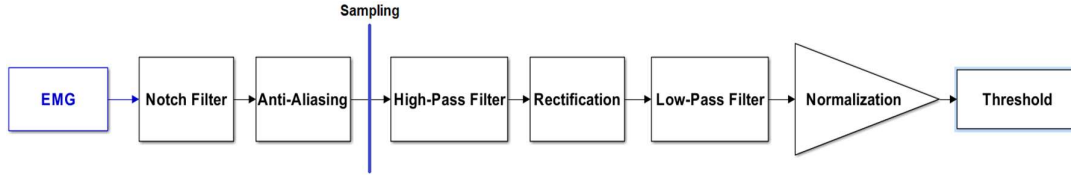


**Figure 5.5. EMG configuration stages.**

The notch filter removes 50 Hz noise which is present anywhere in the vicinity of electrical installations. This, along with an anti-aliasing filter is implemented by Thalmic Labs on the Myo Armband. The high-pass filter removes any DC offset. The rectification along with the low-pass filter functions as an implementation of a linear envelope. Both the high pass and the low pass filters used are fourth order Butterworth filters with cut-off frequencies of 30Hz and 6Hz respectively. The filters have been designed according to [24]. Then, the EMG data are normalized using the method of Maximum Voluntary Isometric Contraction (MVIC) and thresholds are applied [31]. The resulting signal represents the activation level of the corresponding muscle. The mean absolute values (MAVs) of the EMG signals are calculated from 100ms sliding windows, with a frame increment of 50ms. Following, the processing stages are discussed thoroughly.

### High-Pass Filter

The raw EMG signals provided by MYO are firstly high-pass filtered using a fourth-order Butterworth filter with a cut-off frequency at 30Hz (Figure 5.6) to remove movement artifact. The filter was designed in MATLAB.

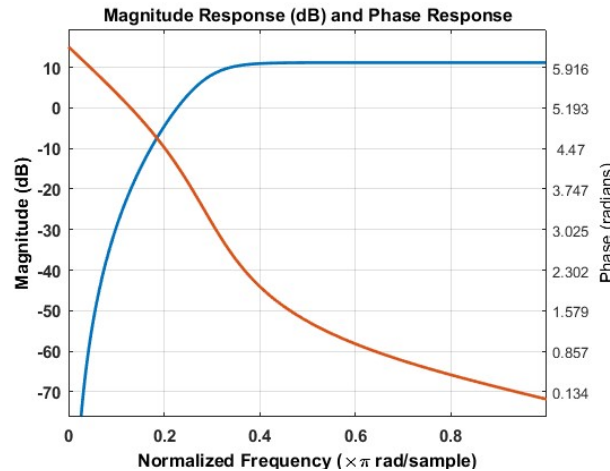


**Figure 5.6. High-Pass filter magnitude and phase responses.**

### Rectification and Low-Pass Filter

After high pass filtering, the signals are rectified and low-pass filtered using a fourth-order Butterworth filter with a cut-off frequency at 6Hz (Figure 5.7). The full wave rectification before low-pass filtering is obligatory for the EMG signal as it is naturally zero-mean, with fast oscillations. Smoothing it without firstly rectifying it would result to an almost “zero” signal.

The combination of rectification and low pass filtering is also called finding the “linear envelope” of the signal, since the filtering operation meets the mathematical definition of linearity, and because it is low pass, it captures the “envelope” of the signal.

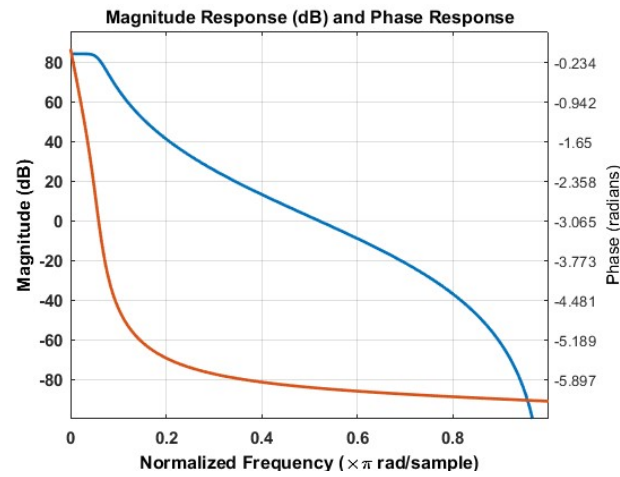


**Figure 5.7. Low-Pass filter magnitude and phase responses.**

Figure 5.8 illustrates how the high-pass filtering and the “linear envelope” stages influence on the form of an excerpt of EMG signal taken from Extensor Carpi Radialis during extension exercise.

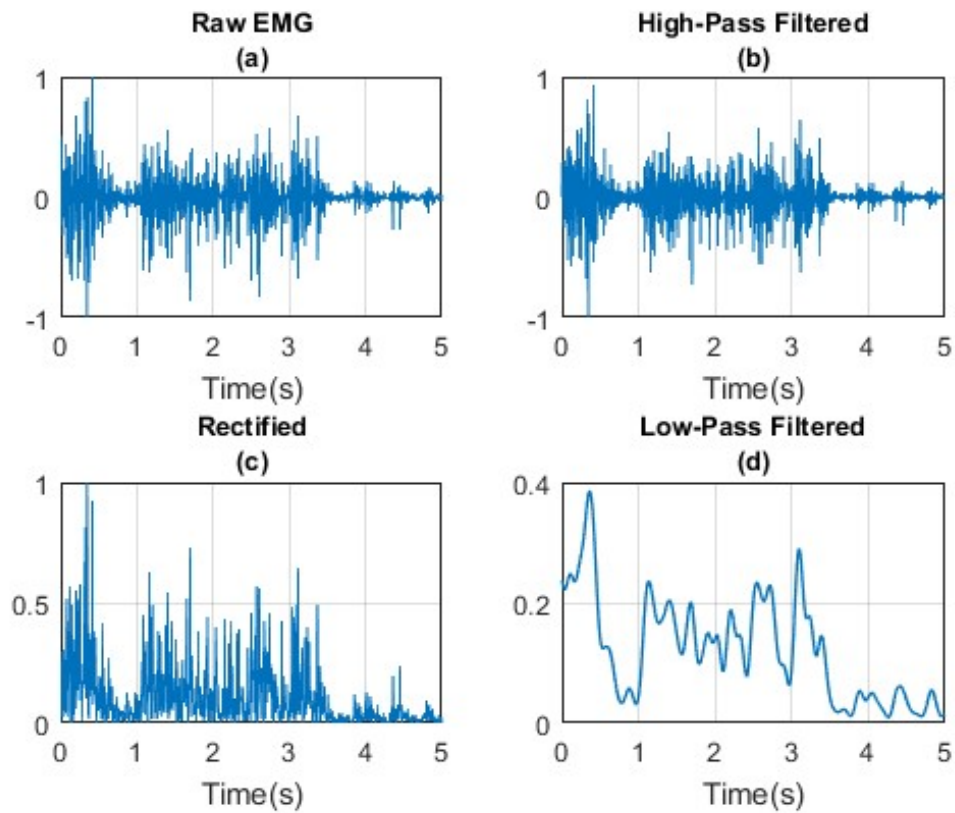


**Figure 5.8. EMG signal excerpt from Extensor Carpi Radialis during configuration. (a) Raw EMG signal, (b) High-Pass Filtered, (c) Rectified and (d) Low-Pass Filtered.**

## Normalization

For the normalization of the acquired EMG signals, the method of Maximum Voluntary Isometric Contraction (MVIC) was selected. The process of normalization using MVICs is that a reference test (usually a manual muscle test) is identified which produces a maximum contraction in the muscle of interest [15]. Three repetitions of the test were performed, separated by two minutes to reduce any fatigue effects, so as to preserve the repeatability between test measures. MVIC EMG data were processed the same way as described above. For all trials, the processed EMG data from each muscle were divided by the single greatest value of the processed EMG data from all that muscle's corresponding MVIC trials. Figure 5.9 presents the EMG signal excerpt after the stage of normalization. The normalized signal is an assessment of the level of the activity of the muscle compared to the maximal neural activation of the muscle.

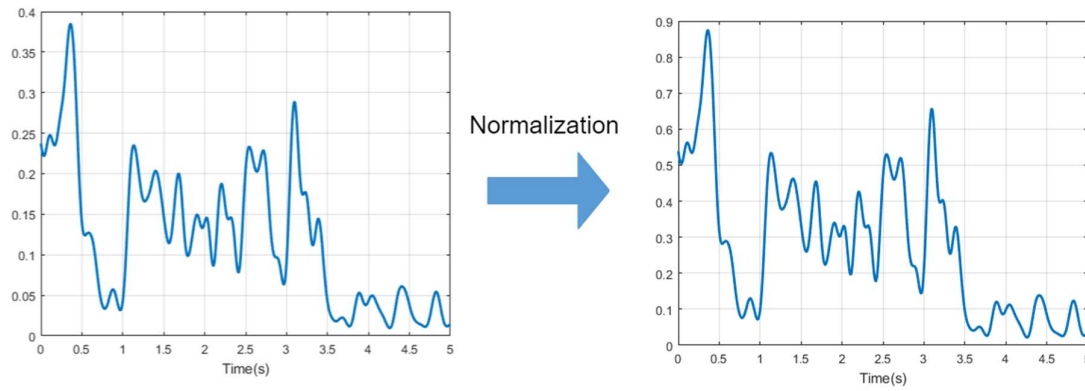


**Figure 5.9. Normalization of EMG signal.**

## Threshold

The control of the prosthesis motor is provided through the threshold technique. The idea behind that technique is that there is an activation level below which the muscle does not trigger movement on the corresponding limb. The thresholds are applied in the normalized MAVs of the antagonistic pair of muscles. The difference in signal amplitude is used to set the %DC of the motor driver. More explicitly:

$$\%DC = \left| \left[ \frac{M_1}{G_1} - T_1 \right] - \left[ \frac{M_2}{G_2} - T_2 \right] \right| \times 100\% \quad (5.1)$$

where M1 is the MAV of the first muscle in the antagonistic pair, G1 is the respective value obtained during MVIC and T1, is the threshold applied. Similarly, M2, G2, and T2 represent the MAV, MVIC value and threshold for the second muscle. Thresholds are manually set to minimize unintended activity. Figure 5.10 demonstrates processed excerpts from Extensor Carpi Radialis and Flexor Carpi Radialis along with a common applied threshold.

Thereupon, the position bounds of the prosthesis motor are set exactly the same way as in the situation of Classic EPP (Section 4.1.2).



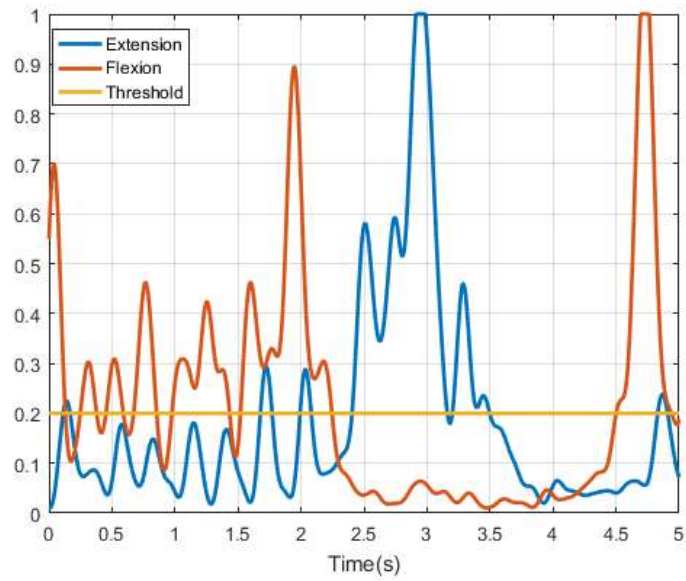


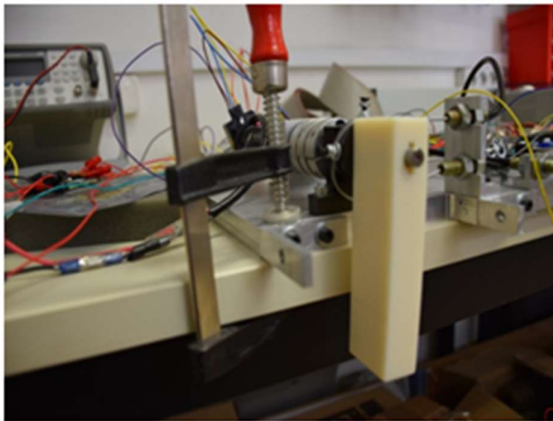
**Figure 5.10. Threshold of the input signals.**

As a conclusion, the presented EMG control scheme will be used in the experiments to come where its performance will be evaluated. It is worth mentioning the usefulness of the Myo Armband as its compact form facilitated the implementation of the EMG control topology.

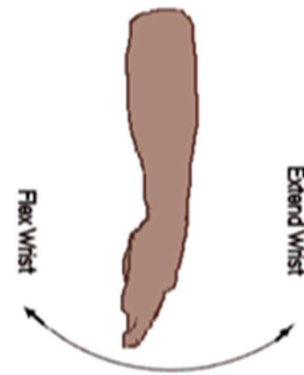
## 6 Target experiment

In this experiment, a rectangular shaft was added in the gearhead of the slave motor, see Figure 6.1.a. As the motor rotates, the shaft moves similarly to the movement a hand makes during wrist flexion and extension, see Figure 6.1.b. We also added two mechanical stops, one 90 degrees in clockwise direction and one 75 degrees in counterclockwise direction, modeling the wrist flexion and extension bounds, respectively. This way, the shaft served the role of the prosthetic hand and the slave motor of its movement actuator.

The aim of the experiment was to compare the ability of the subjects to control the rotational displacement of the slave motor, therefore the position of the prosthesis, using four different control methods, the Classic EPP, the Biomechatronic EPP, the “Unconnected” method and the EMG control.



(a)



(b)

**Figure 6.1. (a) Shaft added to imitate wrist movement. (b) Extension and flexion of the wrist.**

### 6.1 Protocol

In Fitts' original experiment, subjects moved a stylus back and forth between two targets and tapped on them as quickly and accurately as possible, see Figure 6.2. In the Human Computer Interaction research area, many works have mimicked Fitts' paradigm with the difference that the subjects had manipulated an input device to move a cursor between two targets displayed on a monitor display (see Figure 6.3), in order to exclude results for the efficiency of the input device. In our experiment, the position of the shaft was displayed on a computer monitor as the position of the cursor. Subjects manipulated the shaft, to move the cursor between targets displayed on the monitor. The graphical interface was constructed in the environment of MATLAB, using the Psychophysics Toolbox Version 3 (PTB-3), a free set of Matlab functions for vision and neuroscience research [20].

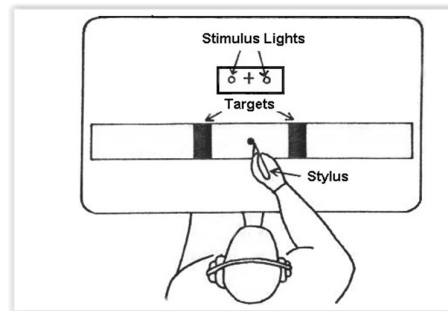


**Figure 6.2. Fitts' Paradigm.**

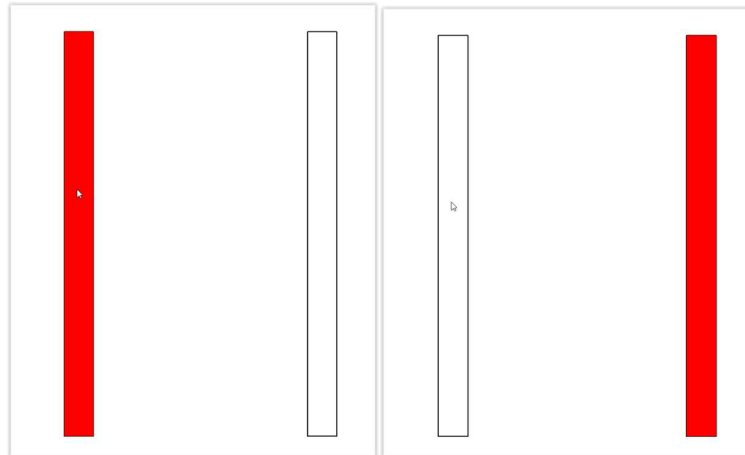


**Figure 6.3. Fitts' Law application in Human Computer Interaction.**

### 6.1.1 Subjects

Twelve male and two female subjects took part in the experiment as volunteers, see Figure 6.4.

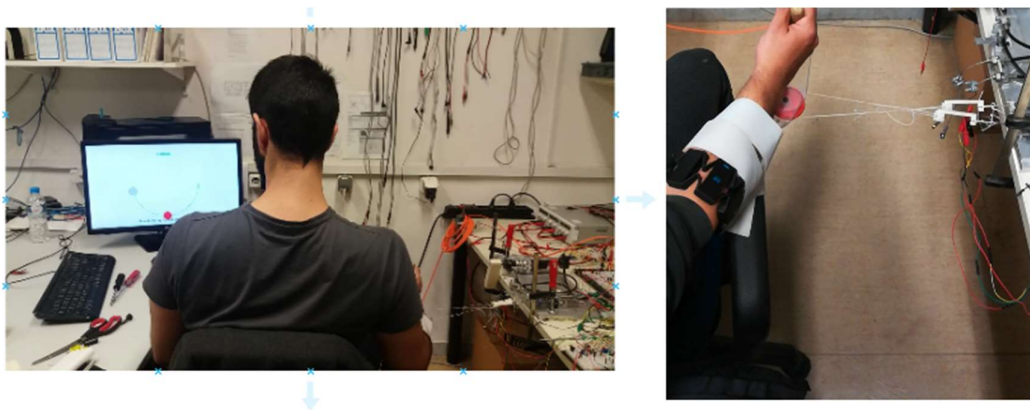


**Figure 6.4. Subjects during the experiments.**

### 6.1.2 Procedure

Subjects performed multiple trials on a simple task using the four aforementioned control topologies. The operation of the experimental setups and the requirements of the task were explained and demonstrated to each subject before the beginning of the experiments. One warm-up block of trials was given prior to data collection.

The task which had been constructed was proportional to Fitts' serial task. The subjects did reciprocal pointing on a pair of circular targets (see Figure 6.5). The targets appeared on the periphery of a semicircle, which corresponded to the shaft orbit. Their position was determined as the angle in which their center lied upon the semicircle. One target was the starting point (GREY COLOR) and the other was the target point (RED COLOR). The subjects tried to reach the target and remain inside it for 1 second (dwell time), otherwise if they were reaching it and then overshooting it, the attempt was considered a failure. After each iteration, the targets switched colors, guiding subjects through the block of trials. Subjects were instructed to balance speed and accuracy. They were told that if too many errors were made, they were moving too fast, and if they never (or rarely) made an error, they weren't moving fast enough.

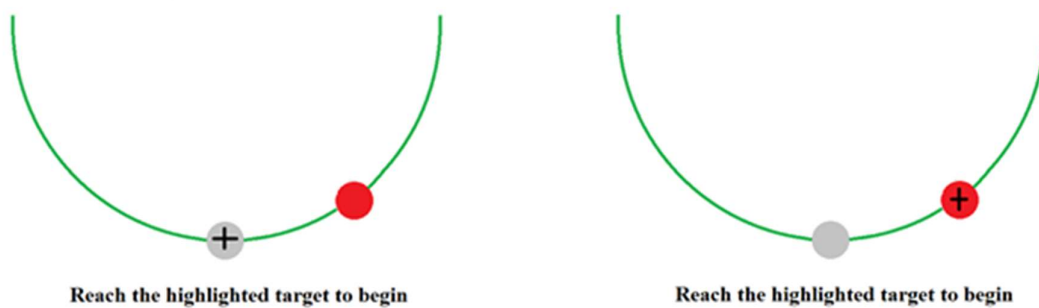


**Figure 6.5, Monitor display during experiments.**

### 6.1.3 Design

A fully within-subjects repeated measures design was used. Controlled variables were the control method (four levels), the task (one level), the target distance (five levels) and the target width (five levels). Dependent variables were the movement time ( $MT$ ), the error rate (calculated from the reaching angle), and the throughput ( $TP = MT/ID$ ). The movement time was measured from the beginning of a move to the reaching of a target (Dwell time and Reaction Time excluded from the measurement of Movement time). The beginning of a move occurred with the first cursor position change after the end of the previous move.

The experiment was sequenced by trials, blocks and sessions. Each trial was a single target-select task. each block was a series of 15 trials for the same target-select task; each session was a series of 25 blocks covering, in descending target width, the 25 combinations of target distance and target width. Sessions were conducted on four separate days for each subject, using a different control method. The order of administering control topologies was counterbalanced by 2 groups of 3 subjects and two groups of 4 subjects. After one session for all control methods, a subject had completed a total of  $15 \times 5 \times 5 \times 4 = 1500$  trials.

The width ( $W$ ) of the targets and the center-to-center distances ( $D$ ) between the circles were set at  $W = 2, 3, 5, 10$  and  $15$  degrees and  $D = 27.5, 67.5, 80, 95$  and  $135$  degrees (see Table 6.1), resulting in IDs from 1.5025 to 6.0298 bits.

**Table 6.1** Possible widths and distances

Possible widths (degrees)	Possible distances (degrees)
2	27.5
3	67.5
5	80
10	95
15	135

## 6.2 Results

This section presents and discusses the results of the previous experiment. The plan for analysis is as follows. First, adjustments to the data are introduced to perform the adjustment of accuracy and to eliminate outliers. Then, summary measures and tests for main effects are presented on movement time, error rate and throughput across levels of experimental factors.

### 6.2.1 Adjustment of Data

A measure of the scatter of subjects' movement end-points have been gathered, both by determining the error rate and by recording the physical end-points of each movement task. Movement time (MT) data was also collected. Movement time refers to the time subjects spent from the beginning of their movement until the time the cursor reached the target position.

This data was used to remove outliers. The outliers were of two different types, *spatial* and *timing*. Spatial outliers were considered trials in which the subject lost accidentally the control of the setup, or was hurried and started the next movement before dwell time was completed, even if he or she had reached the previous target successfully (registering an error for the following trial). An example of the latter is presented in Figure 6.6.

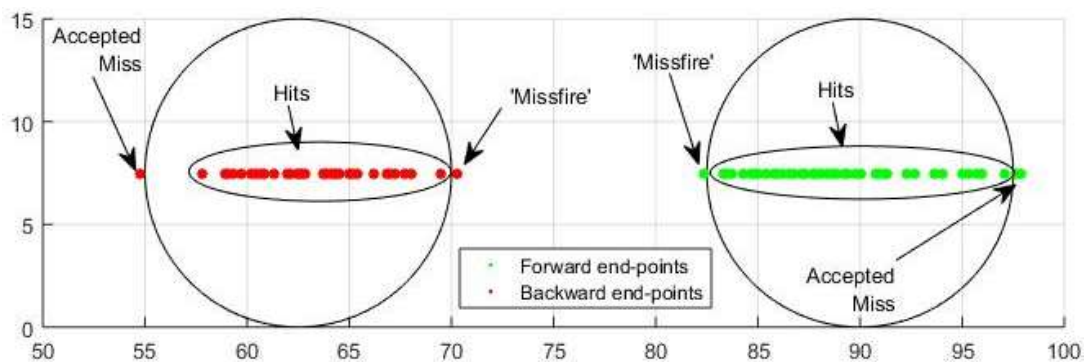


**Figure 6.6** The distribution of end-points for a pair of targets with  $W=15$  and  $D=27.5$ . With green color the end-points for forward movement and with red color for backward. The end-points that lie on the right side of the left circle and on the left side of the right circle are considered as outliers.

For the first situation any trial in which the movement distance was 3 standard deviations away from the average was removed. For the second one we removed any trial in which the total displacement was less than the target distance and an error had been registered. Timing outliers were considered those trials where the subject paused mid-trial violating the rules that the movements had to be rapid. A simple rule was followed in order to remove these trials from further analysis. Any trial with final movement time more than 5 s was considered a 'misfire' and was deleted.

Of the 21000 trials 1036(4.9%) were considered outliers and removed from further analysis. Total trials removed for Biomechatronic, Classic, Unconnected and EMG respectively were 188, 248, 216 and 384.

The end-point scatter data was used to perform the adjustment of accuracy for each subject, for each target width-distance condition. Adjustment of accuracy needs effective target width( $W_e$ ) and effective distance( $D_e$ ) to be calculated.  $W_e$  was calculated by using the following equation

$$W_e = 4.133\sigma \quad (6.1)$$

Where  $\sigma$  refers to the standard deviation of end-point positions.

This method is commonly known as the standard deviation method (SD) and is considered to be superior to the discrete error method (DE) which has been mentioned in Chapter 1.

$D_e$  was calculated as the mean movement distance from the start-of-movement position to the end points.

These adjusted parameters were used to define the effective index of difficulty  $ID_e$ :

$$ID_e = \log_2\left(\frac{D_e}{W_e} + 1\right) \quad (6.2)$$

Table 6.2 shows the data before and after adjustment for one specific subject.

**Table 6.2. Target widths and distances before and after adjustment.**

Unadjusted Data			Adjusted Data		
Width (Degrees)	Distance (Degrees)	ID (bits)	$W_e$ (Degrees)	$D_e$ (Degrees)	$ID_e$ (bits)
2	27.5	3.883	2.866	28.23	1.78
2	67.5	5.119	2.872	67.84	1.84
2	80	5.358	2.975	79.78	1.65
2	95	5.6	3.953	96.28	1.88
2	135	6.098	3.332	135.8	1.73
3	27.5	3.346	3.492	27.59	1.93
3	67.5	4.555	2.645	67.11	2.22
3	80	4.79	3.924	79.93	1.61
3	95	5.03	4.081	94.78	2.05
3	135	5.524	4.09	134.6	1.76
5	27.5	2.7	4.57	26.69	2.3
5	67.5	3.858	3.699	66.83	2.27
5	80	4.087	4.997	78.59	1.85
5	95	4.322	6.052	94.78	2
5	135	4.807	5.303	133.8	1.73
10	27.5	1.907	9.996	25.88	2.64
10	67.5	2.954	8.049	67.95	2.94
10	80	3.17	11.35	76.02	2.24
10	95	3.392	9.258	94.84	2.63
10	135	3.858	7.936	133.4	2.41
15	27.5	1.503	15.52	24.56	2.9
15	67.5	2.459	12.13	64.1	3.21
15	80	2.663	14.04	76.72	2.5
15	95	2.874	9.014	92.56	2.73
15	135	3.322	11.01	135.7	2.21

## 6.2.2 Summary Tables

The organization of the data follows its adjustment. Since the experimental design specifically mimicked Fitts' original tapping experiments, tables similar to Table 2.1 form the basis for subsequent analyses.

Table 6.3 to Table 6.6 demonstrate the means for movement time, error rate and throughput across levels of W and D, for all the four different control methods used in the experiment. These tables also include both the specified values of target width and distance and their effective ones. The same applies also for index of difficulty, as it is computed before (ID) and after (IDe) the adjustment of data. The number of outliers detected for each W-D condition can be obtained by subtracting the entry on the last column from 210.

**Table 6.3. Summary Data for Biomechatronic EPP.**

Width (Deg.)	Distance (Deg.)	We (Deg.)	De (Deg.)	Id (bits)	Id <sub>e</sub> (bits)	Mt (ms)	Error Rate (%)	TP (bits/s)	Trials #
2	27.5	2.869	27.89	3.883	3.443	1628.3	24.3	2.164	207
2	67.5	3.331	67.90	5.119	4.500	2034.3	27.6	2.262	205
2	80	2.938	80.22	5.358	4.846	2302.7	21.9	2.243	201
2	95	3.082	95.47	5.600	5.029	2312.4	28.1	2.256	194
2	135	3.002	135.40	6.098	5.555	2638.5	27.1	2.182	189
3	27.5	3.684	27.75	3.346	3.132	1346.8	17.1	2.535	208
3	67.5	3.433	67.41	4.555	4.400	1825.8	11.4	2.619	205
3	80	3.697	80.07	4.790	4.515	2071.0	13.8	2.321	201
3	95	3.934	95.33	5.030	4.682	2134.5	22.9	2.270	196
3	135	3.706	135.20	5.524	5.270	2354.9	18.6	2.353	197
5	27.5	5.861	27.46	2.700	2.545	1049.3	12.4	2.551	209
5	67.5	5.603	67.60	3.858	3.752	1470.0	10.5	2.754	206
5	80	5.427	79.85	4.087	3.997	1658.4	10.0	2.559	204
5	95	5.550	94.85	4.322	4.190	1806.0	10.5	2.422	204
5	135	5.764	134.80	4.807	4.628	2112.5	11.0	2.366	198
10	27.5	10.910	25.70	1.907	1.769	809.4	7.6	2.458	206
10	67.5	9.711	66.36	2.954	3.013	1117.2	7.1	2.829	207
10	80	9.495	78.60	3.170	3.291	1364.2	7.6	2.518	200
10	95	10.020	93.81	3.392	3.396	1369.5	5.7	2.617	205
10	135	9.774	133.10	3.858	3.909	1713.4	6.7	2.344	203
15	27.5	15.480	24.34	1.503	1.385	468.3	4.3	3.056	206
15	67.5	13.800	65.12	2.459	2.566	934.9	5.2	2.926	207
15	80	16.740	77.32	2.663	2.522	1521.7	7.1	1.952	200
15	95	14.470	91.77	2.874	2.918	1184.4	7.1	2.551	204
15	135	14.080	131.90	3.322	3.437	1474.0	3.3	2.413	200
Mean						1628.1	13.2	2.461	
SD						538.8	7.9	0.252	

**Table 6.4. Summary data for Classic EPP.**

<b>Width (Deg.)</b>	<b>Distance (Deg.)</b>	<b>We (Deg.)</b>	<b>De (Deg.)</b>	<b>Id (bits)</b>	<b>Ide (bits)</b>	<b>MT (ms)</b>	<b>Error Rate (%)</b>	<b>TP (bits/s)</b>	<b>Trials #</b>
2	27.5	3.09	28.09	3.883	3.361	1609.5	26.7	2.216	204
2	67.5	3.57	68.21	5.119	4.375	2036.1	38.6	2.240	200
2	80	3.60	80.75	5.358	4.589	2358.7	39.0	1.995	199
2	95	3.32	95.86	5.600	4.955	2351.9	37.1	2.155	192
2	135	3.47	135.79	6.098	5.358	2738.8	35.7	2.008	187
3	27.5	4.15	28.31	3.346	2.997	1465.4	26.7	2.257	200
3	67.5	4.64	68.51	4.555	4.028	1978.3	31.4	2.204	198
3	80	4.39	80.60	4.790	4.306	2138.4	28.6	2.143	195
3	95	4.58	95.75	5.030	4.476	2155.7	30.0	2.185	198
3	135	4.06	135.71	5.524	5.148	2386.3	24.3	2.246	189
5	27.5	5.35	27.47	2.700	2.657	1093.1	11.4	2.826	203
5	67.5	6.14	67.93	3.858	3.653	1569.1	17.1	2.493	204
5	80	6.35	80.85	4.087	3.858	1852.2	22.9	2.263	200
5	95	6.13	95.20	4.322	4.082	1903.1	17.6	2.287	202
5	135	6.03	135.20	4.807	4.610	2186.3	20.5	2.223	191
10	27.5	9.93	26.53	1.907	1.896	794.5	7.6	2.879	205
10	67.5	10.01	67.31	2.954	3.001	1220.2	8.6	2.894	206
10	80	10.34	78.97	3.170	3.151	1427.3	6.2	2.437	207
10	95	9.19	94.85	3.392	3.549	1480.6	9.5	2.599	202
10	135	9.56	134.67	3.858	3.967	1752.1	6.7	2.423	205
15	27.5	13.36	27.17	1.503	1.713	631.3	8.1	3.327	208
15	67.5	13.48	65.85	2.459	2.611	1051.0	4.8	2.819	205
15	80	15.18	80.18	2.663	2.702	1242.8	10.0	2.267	198
15	95	12.78	93.19	2.874	3.130	1389.2	4.8	2.544	205
15	135	14.48	133.74	3.322	3.442	1746.3	9.0	2.109	199
<b>Mean</b>						1702.3	19.3	2.402	
<b>SD</b>						532.1	11.8	0.327	



**Table 6.5. Summary data for Unconnected method.**

<b>Width (Deg.)</b>	<b>Distance (Deg.)</b>	<b>We (Deg.)</b>	<b>De (Deg.)</b>	<b>Id (bits)</b>	<b>Ide (bits)</b>	<b>Mt (ms)</b>	<b>Error Rate (%)</b>	<b>TP (bits/s)</b>	<b>Trials #</b>
2	27.5	4.81	29.21	3.883	2.836	1700.8	64.8	1.738	207
2	67.5	4.48	68.91	5.119	4.068	2093.2	58.6	2.002	196
2	80	4.46	81.32	5.358	4.304	2133.1	61.4	2.167	197
2	95	5.04	96.70	5.600	4.365	2328.5	64.8	1.936	194
2	135	5.20	136.76	6.098	4.795	2340.5	68.6	2.150	186
3	27.5	6.29	29.64	3.346	2.543	1492.9	60.0	1.840	206
3	67.5	6.20	69.50	4.555	3.628	1944.8	58.1	1.949	203
3	80	6.49	82.14	4.790	3.790	1974.9	63.8	2.084	195
3	95	6.10	96.67	5.030	4.109	2045.8	51.4	2.069	190
3	135	6.05	136.77	5.524	4.576	2383.0	54.8	2.002	194
5	27.5	8.71	29.67	2.700	2.168	1274.1	42.9	1.821	206
5	67.5	8.50	69.68	3.858	3.222	1630.9	44.3	2.098	203
5	80	8.75	81.96	4.087	3.432	1767.2	46.7	2.065	198
5	95	9.09	97.37	4.322	3.578	1819.9	47.6	2.058	203
5	135	8.81	137.08	4.807	4.075	2171.1	44.3	1.990	202
10	27.5	15.65	29.81	1.907	1.550	936.9	35.7	1.862	202
10	67.5	15.61	69.15	2.954	2.453	1330.8	31.0	1.989	206
10	80	15.89	82.18	3.170	2.640	1451.2	34.3	1.990	206
10	95	14.74	96.34	3.392	2.932	1552.8	26.2	2.044	205
10	135	14.32	136.07	3.858	3.422	1759.6	27.6	2.097	206
15	27.5	21.38	30.08	1.503	1.275	698.0	24.8	2.023	209
15	67.5	20.76	68.65	2.459	2.131	1019.8	20.5	2.184	207
15	80	23.28	83.25	2.663	2.207	1373.2	34.3	1.728	201
15	95	21.45	95.86	2.874	2.464	1252.1	24.3	2.071	204
15	135	20.29	135.26	3.322	2.965	1521.6	17.6	2.148	208
<b>Mean</b>						1679.9	44.3	2.004	
<b>SD</b>						453.7	15.9	0.125	

**Table 6.6. Summary data for EMG.**

<b>Width (Deg.)</b>	<b>Distance (Deg.)</b>	<b>We (Deg.)</b>	<b>De (Deg.)</b>	<b>Id (bits)</b>	<b>Ide (bits)</b>	<b>Mt (ms)</b>	<b>Error Rate (%)</b>	<b>TP (bits/s)</b>	<b>Trials #</b>
2	27.5	8.35	30.27	3.883	2.295	1833.4	80.0	1.310	185
2	67.5	8.48	69.82	5.119	3.357	2128.1	74.8	1.619	166
2	80	7.58	82.32	5.358	3.656	2206.4	72.4	1.764	174
2	95	8.40	97.39	5.600	3.737	2335.3	76.2	1.667	162
2	135	7.34	137.18	6.098	4.364	2489.3	71.9	1.809	170
3	27.5	10.09	31.11	3.346	2.100	1799.6	74.3	1.307	197
3	67.5	8.80	70.60	4.555	3.213	2166.4	68.6	1.569	198
3	80	9.43	83.20	4.790	3.352	2133.6	74.8	1.679	183
3	95	8.79	98.02	5.030	3.655	2203.0	67.1	1.750	193
3	135	8.43	137.76	5.524	4.174	2255.3	65.2	1.910	188
5	27.5	11.87	31.28	2.700	1.902	1610.9	56.7	1.288	203
5	67.5	11.92	71.22	3.858	2.841	1846.2	60.0	1.621	200
5	80	11.56	83.35	4.087	3.060	1843.7	60.0	1.772	201
5	95	12.92	99.35	4.322	3.162	2103.7	64.3	1.569	203
5	135	11.27	138.41	4.807	3.756	2203.6	58.1	1.786	199
10	27.5	17.60	31.07	1.907	1.473	1207.4	40.5	1.395	208
10	67.5	18.21	71.84	2.954	2.318	1659.3	44.3	1.535	207
10	80	17.82	83.59	3.170	2.525	1732.6	42.4	1.585	205
10	95	17.75	97.85	3.392	2.725	1898.0	39.5	1.536	197
10	135	17.22	139.08	3.858	3.213	2109.0	41.4	1.598	202
15	27.5	24.44	31.77	1.503	1.211	994.1	35.2	1.355	208
15	67.5	23.42	71.12	2.459	2.027	1410.4	30.0	1.563	208
15	80	24.27	84.17	2.663	2.169	1582.7	38.6	1.470	197
15	95	24.31	98.42	2.874	2.345	1691.1	33.3	1.539	207
15	135	23.07	138.10	3.322	2.825	1728.3	30.0	1.739	205
<b>Mean</b>						1886.9	56.0	1.589	
<b>SD</b>						359.6	16.7	0.169	

### 6.2.3 Statistical analysis

Tests for main effects of the control method factor on three dependent variables; movement time(MT), error rate and throughput (TP) were conducted using one-way analysis of variance (one-way ANOVA) to determine whether there were any statistically significant differences between the means of the four independent control methods (groups). However, ANOVA is an omnibus test statistic that cannot tell which specific groups are statistically different from each other [41]. To determine which specific groups differed from each other, the *Bonferroni* procedure, a post hoc comparison test, was used. It must be mentioned that the statistical analysis was applied as long as the data was rearranged to represent the performance across all subjects, for all the four different control methods used.

#### Statistical Tools

##### 1. One – Way ANOVA

Mathematically, ANOVA can be written as:

$$x_{ij} = \mu_i + e_{ij} \quad (6.3)$$

where  $x_{ij}$  are the individual points ( $i$  and  $j$  denote the group and individual observation),  $\epsilon$  is the unexplained variation and the parameters of the model ( $\mu$ ) are the population means for each group. Thus, each data point ( $x_{ij}$ ) is its group mean plus error.

The one-way ANOVA is used to calculate a test statistic (F-value) with which the probability (p-value) of obtaining the data assuming the null hypothesis (6.4) can be obtained. A significant p-value (usually taken as  $p < 0.05$ ) suggests that at least one group mean is significantly different from the others.

$$H_0 : \mu_1 = \mu_2 = \mu_3 = \dots = \mu_k \quad (6.4)$$

Where  $\mu$  = group mean and  $k$  = number of groups. If, however, the one-way ANOVA returns a statistically significant result, then the alternative hypothesis ( $H_1$ ) is accepted, which is that there are at least two group means that are statistically significantly different from each other.

For the calculation of the F-value the ANOVA table, as presented in Table 6.7, is used.

**Table 6.7. ANOVA table.**

Source	SS	DF	Mean Square	F value	p value
<b>Error(Within group)</b>	$SS_{\text{error}}$	$N-k$	$SS_{\text{error}}/(N-a)$		
<b>Between groups</b>	$SS_{\text{group}}$	$k-1$	$SS_{\text{group}}/(a-1)$	$MS_{\text{group}}/MSE$	$1-P(F,a-1,N-a)$
<b>Total</b>	$SS_{\text{total}}$	$N-1$			

- The first column contains the source of variation. It divides the sources of variation into two major categories: within group (error) and between group. The objective is to determine if there are any differences between groups. This is done by comparing the between groups sum of square (variance) to the error sum of square (variance). If the variance between groups can be explained by the within group variance, there are no differences between the groups. If the variance between groups cannot be explained by the within group variance, then there are differences between the groups.
- The second column in the table contains the sum of squares.

- The third column is the degrees of freedom. The number of levels is given by k. N is the total number of experimental runs.
- The fourth column is the mean square. The mean square is obtained by dividing the sum of squares for the source by the degrees of freedom for the source. Thus,  $MSE = SS_{\text{error}}/(N-a)$ .
- The fifth column is the F value. This is determined by dividing the mean square for the groups by the mean square error. It is this value that determines if there are any significant differences between the group means.
- The final column is the p value which is associated with the F value. This is the probability of obtaining the calculated F value if there were in fact no difference between the group levels. If p is less than 0.05, there is a significant difference.  $P(F, a-1, N-a)$  is the value of the lower-cumulative distribution function of the F distribution for  $x = F$ .

## 2. **Bonferroni Post-Hoc Test**

Bonferroni procedure answers the question: "Which group means are significantly different from each other?"

This method provides a pairwise comparison of means. If k is the number of groups, there are  $k(k-1)/2$  possible pairs. The idea is to divide the selected confidence level (usually  $\alpha=0.05$ ) among all the pairwise comparisons.

According to the Bonferroni post-hoc test a pairwise difference is significant if:

$$T_{ij} = \frac{|\bar{y}_i - \bar{y}_j|}{s_p \sqrt{\frac{1}{n_i} + \frac{1}{n_j}}} > t_{v, \alpha/2k} \quad (6.5)$$

where  $t_{v, \alpha/2k}$  is the value from the t distribution for v degrees of freedom at the  $\alpha/2k$  confidence level,  $\bar{y}$  is the mean and n the sample size. The i and j represent two different groups.  $s_p$  is the pooled standard deviation which is computed as:

$$s_p = \sqrt{\frac{\sum (n_i - 1) s_i^2}{\sum (n_i - 1)}} \quad (6.6)$$

Eq. (5.5) can be rewritten as:

$$|\bar{y}_i - \bar{y}_j| > t_{v, \alpha/2k} s_p \sqrt{\frac{1}{n_i} + \frac{1}{n_j}} \quad (6.7)$$

The right-hand side of this equation is the critical value. Any difference in pair of means that is larger than this will be significant.

The p-value for each pairwise comparison can be obtained using the following equation:

$$P_{i,j} = [1 - P(T_{i,j}, v)] \times 2 \times k \quad (6.8)$$

where  $P(T_{i,j}, v)$  is the value of the lower-cumulative distribution function of the student's t distribution for  $x = T_{i,j}$

## Tests for main effects

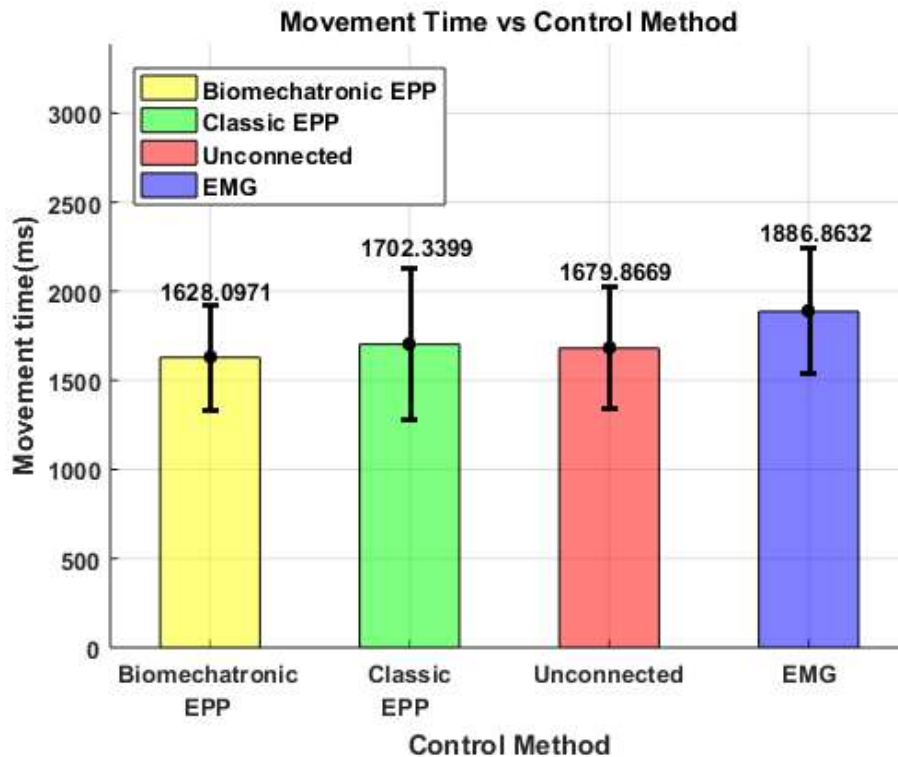
### 1. Movement Time

Table 6.8 demonstrates the data collected for movement time and Figure 6.7 illustrates it in a bar plot.

The grand mean for movement time was 1724.3 ms. Across the control method factor, means for Biomechatronic, Classic, Unconnected and EMG were 1628.1, 1702.3, 1679.9, and 1886.9 ms. The ANOVA results are presented in Table 6.9.

**Table 6.8. Data for Movement Time.**

Subjects	Movement Time(ms) Control Method				
	Bio	Classic	Unconnected	EMG	
S1	1845.9	1752.2	2039.6	2699.5	
S2	1768.7	1789.9	1921.2	1948.8	
S3	1482.5	1385.1	1416.0	1871.5	
S4	1450.5	1333.5	1573.2	1824.5	
S5	1384.7	1384.7	1590.0	1737.3	
S6	1343.1	1343.1	1682.9	1719.8	
S7	1585.7	1546.6	1307.2	1879.0	
S8	1827.1	2930.1	1627.8	2275.4	
S9	1361.3	1509.6	2143.6	2098.5	
S10	1152.3	1469.0	1330.7	1856.1	
S11	1603.4	1795.6	1373.6	1307.2	
S12	2030.9	2030.9	1414.9	2143.6	
S13	1733.4	1503.4	1638.8	1638.8	
S14	2223.9	2059.1	2458.6	1416.0	
Mean	1628.1	1702.3	1679.9	1886.9	1724.3
SD	294.6	428.2	342.8	350.9	



**Figure 6.7. Movement time by control method**

**Table 6.9. ANOVA table for Movement Time.**

	Sum of Sares	DF	Mean Square	F-Value	P-Value
<b>Subject</b>	6639582.046	52	127684.270		
<b>Control Method</b>	5668109.955	3	177978.903	1.3939	0.255
<b>Total</b>	7173518.754	55			

The p-value corresponding to the F-statistic of one-way ANOVA is higher than 0.05(  $F_{3,52} = 1.399, p > .05$  ), suggesting that there was not significant effect of control method on movement time, see Table 6.10.

**Table 6.10. Bonferroni's Method for Movement Time.**

<b>Bonferroni's Method</b>					
<b>Family Conf. Int.=95%, Individual Conf.Int. = 97.58%</b>					
<b>Comparisons</b>	<b>Mean Difference</b>	<b>Critical Difference</b>	<b>L CON</b>	<b>U CON</b>	<b>P-Value</b>
<b>Bio-Classic</b>	-74.2	370.5	-444.7	296.2	3.5092
<b>Bio-Unconnected</b>	-51.8	370.5	-422.2	318.7	4.2183
<b>Bio-EMG</b>	-258.8	370.5	-629.2	111.7	0.3652
<b>Classic-Unconnected</b>	22.5	370.5	-348.0	392.9	5.2109
<b>Classic-EMG</b>	-184.5	370.5	-555.0	185.9	1.0664
<b>Unconnected-EMG</b>	-207.0	370.5	-577.5	163.5	0.7885

The result of one-way ANOVA is also confirmed using Bonferroni's Method as the pairwise comparison does not reveal any significant difference between the means of movement time (red color for insignificant and green for significant differences).

The confidence intervals can also be plotted as shown in Figure 6.8. This shows that all the intervals include 0. All the means are not significantly different from one another.

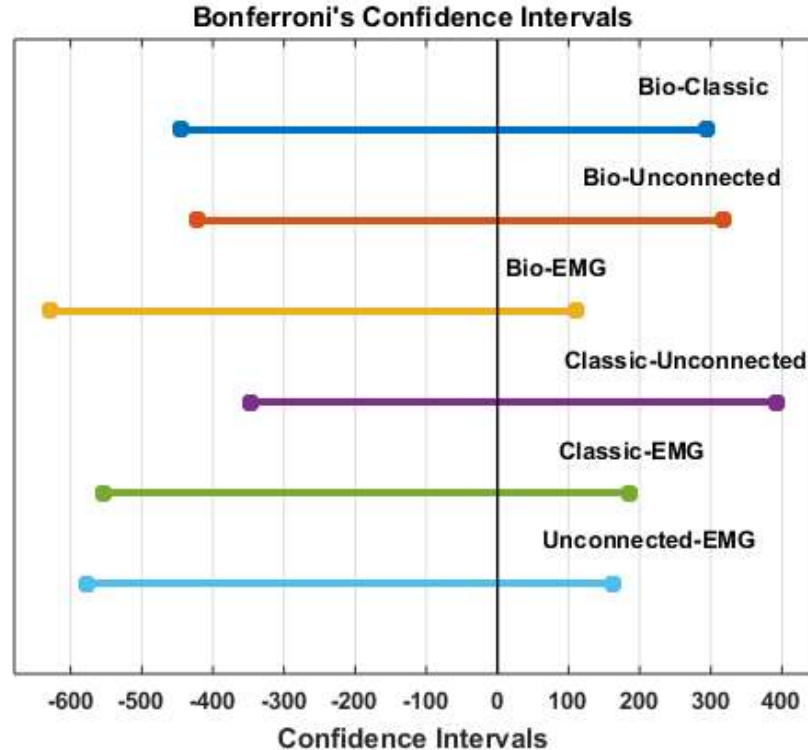


**Figure 6.8. Bonferroni's Confidence Intervals for Movement Time.**

## 2. Error Rate

An error was defined as overshooting the target. The grand mean of error rate was 33.2%. Error rates were 13.2%, 19.3%, 44.3% and 56.0% for Biomechatronic, Classic, Unconnected and EMG, respectively (Figure 6.9 and Table 6.11. Results for Error Rate.). The ANOVA results are presented in Table 6.12.

**Table 6.11. Results for Error Rate.**

Subjects	Error Rate(%) Control Method				
	Bio	Classic	Unconnected	EMG	
S1	11.2	9.3	24.0	44.8	
S2	5.3	17.1	51.2	58.7	
S3	18.4	23.7	38.9	61.1	
S4	17.9	30.7	45.6	52.5	
S5	8.0	8.0	48.5	56.8	
S6	15.5	15.5	47.5	57.3	
S7	21.1	14.9	39.2	60.8	
S8	8.0	11.7	46.7	56.0	
S9	12.3	10.1	70.4	60.5	
S10	29.6	46.9	52.8	59.7	
S11	1.3	18.9	25.3	39.2	
S12	8.8	8.8	33.3	70.4	
S13	21.1	21.1	66.9	66.9	
S14	5.9	33.6	30.1	38.9	
Mean	13.2	19.3	44.3	56.0	Grand Mean
SD	7.8	11.2	13.9	9.3	33.2

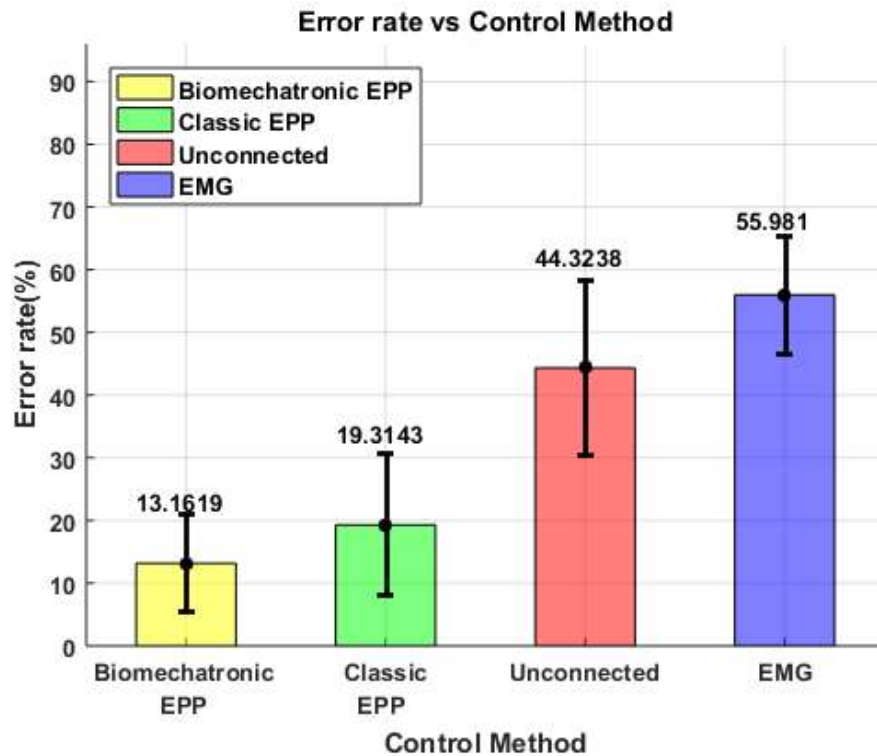


**Figure 6.9. Error rate by control method.**

**Table 6.12. ANOVA table for Error Rate.**

	Sum of Squares	DF	Mean Square	F-Value	P-Value
<b>Subject</b>	6045.719	52	116.264		
<b>Control Method</b>	17318.688	3	5772.896	49.6534	2.75E-15
<b>Total</b>	23364.408	55			

The p-value corresponding to the F-statistic of one-way ANOVA is lower than 0.05(  $F_{3,52} = 49.6534, p < .05$  ). Thus, there was a significant main effect of control method on error rate.

**Table 6.13. Bonferroni's Method for Error Rate.**

Bonferroni's Method					
Family Conf. Int.=95%, Individual Conf.Int. = 97.58%					
Comparisons	Mean Difference	Critical Difference	L CON	U CON	P-Value
<b>Bio-Classic</b>	-6.2	11.2	-17.3	5.0	0.8231
<b>Bio-Unconnected</b>	-31.2	11.2	-42.3	-20.0	0.0000
<b>Bio-EMG</b>	-42.8	11.2	-54.0	-31.6	0.0000
<b>Classic-Unconnected</b>	-25.0	11.2	-36.2	-13.8	0.0000
<b>Classic-EMG</b>	-36.7	11.2	-47.8	-25.5	0.0000
<b>Unconnected-EMG</b>	-11.7	11.2	-22.8	-0.5	0.0365

Using Bonferroni's post-hoc test, the pairs of control methods that were significantly different from each other are identified. As Table 6.13 indicates and Figure 6.10 illustrates, there was a statistically significant difference on the means of error rate for all the pairwise compared control methods, apart from the Bio-Classic pair in which the p-value is greater than 0.05. More specifically, the error rate was greater for Unconnected and EMG compared to Bio and Classic, while Unconnected presented lower error rate compared to EMG.

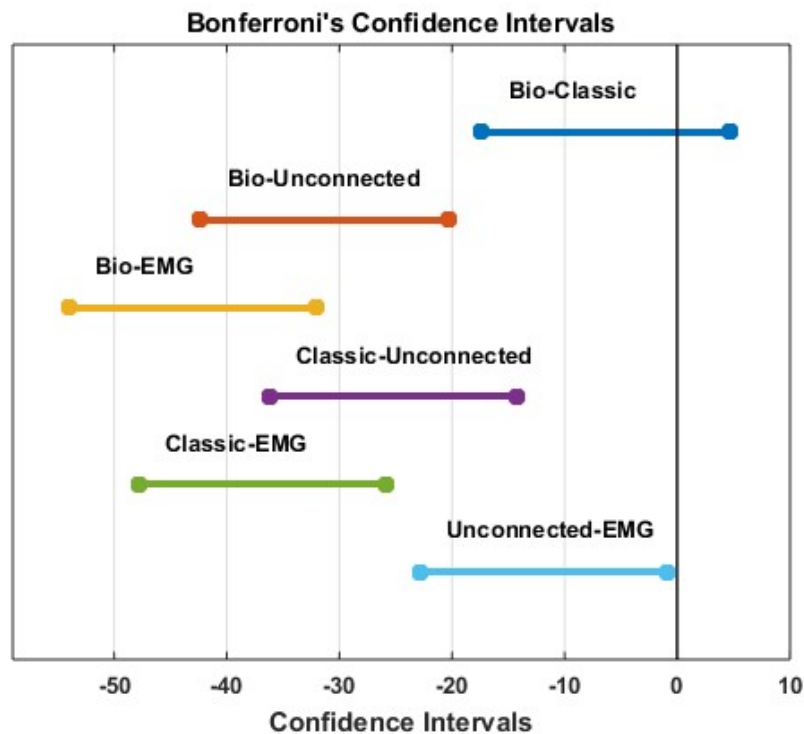


**Figure 6.10. Bonferroni's Confidence Intervals for Error Rate.**



### 3. Throughput

The grand mean for throughput was 2.114 bits/s, with means for Biomechatronic, Classic and Unconnected respectively of 2.461, 2.402, 2.004 and 1,589 bits/s (Table 6.14 and Figure 6.11). The ANOVA results are presented in Table 6.15.

**Table 6.14. Results for Throughput.**

Throughput(bits/s)					
Control Method					
Subjects	Bio	Classic	Unconnected	EMG	
S1	2.200	2.274	1.731	1.074	
S2	2.236	2.005	1.720	1.400	
S3	2.646	2.894	2.343	1.502	
S4	2.577	2.794	2.018	1.503	
S5	2.800	2.800	2.046	1.592	
S6	2.817	2.817	1.909	1.621	
S7	2.442	2.951	2.573	1.502	
S8	2.237	1.273	1.921	1.151	
S9	3.021	3.059	1.362	1.290	
S10	3.140	2.472	2.441	1.485	
S11	2.371	1.965	2.427	2.573	
S12	1.875	1.875	2.358	1.362	
S13	2.299	2.693	1.855	1.855	Grand Mean
S14	1.792	1.747	1.356	2.343	
Mean	2.461	2.402	2.004	1.589	2.114
SD	0.398	0.547	0.388	0.419	

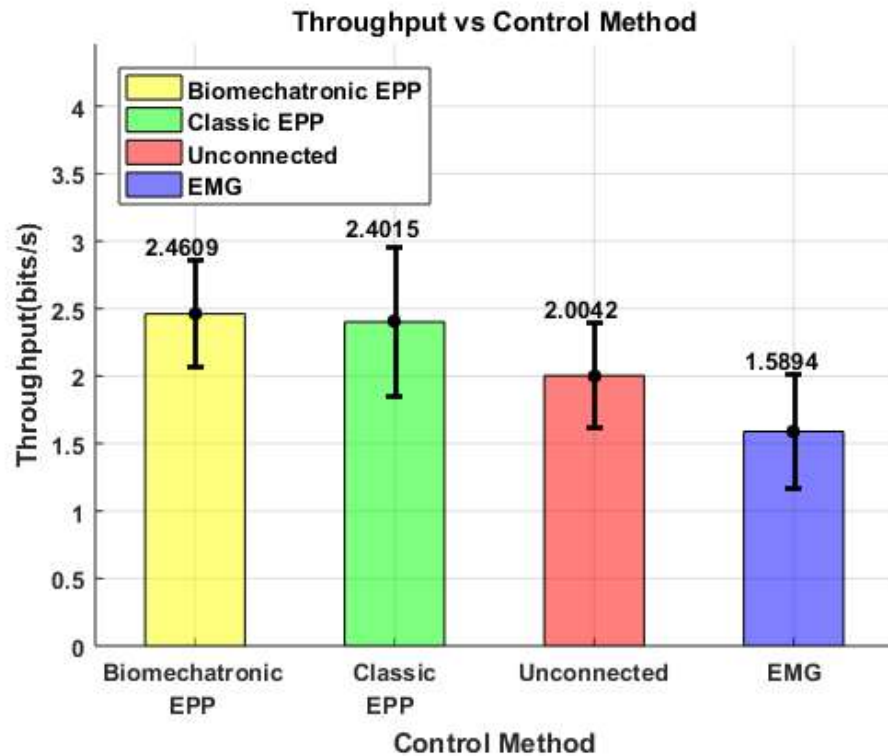


**Figure 6.11. Throughput by control method.**

**Table 6.15. ANOVA table for Throughput.**

	Sum of Squares	DF	Mean Square	F-Value	P-Value
<b>Subject</b>	10.190	52	0.196		
<b>Control Method</b>	6.864	3	2.288	11.6751	5.82E-06
<b>Total</b>	17.053	55			

The p-value corresponding to the F-statistic of one-way ANOVA is lower than 0.05(  $F_{3,52} = 11.6751, p < .05$  ). Thus, there was a significant main effect of control method on throughput.

**Table 6.16. Bonferroni's Method for Throughput.**

Bonferroni's Method					
Family Conf. Int.=95%, Individual Conf.Int. = 97.58%					
Comparisons	Mean Difference	Critical Difference	L CON	U CON	P-Value
<b>Bio-Classic</b>	0.059	0.459	-0.400	0.518	4.3455
<b>Bio-Unconnected</b>	0.457	0.459	-0.002	0.916	0.0049
<b>Bio-EMG</b>	0.871	0.459	0.413	1.330	0.0000
<b>Classic-Unconnected</b>	0.397	0.459	-0.062	0.856	0.1278
<b>Classic-EMG</b>	0.812	0.459	0.353	1.271	0.0001
<b>Unconnected-EMG</b>	0.415	0.459	-0.044	0.874	0.0986

Using Bonferroni's post-hoc test, the pairs of control methods that were significantly different from each other are identified. As Table 6.16 indicates, there was a statistically significant difference on the means of throughput for the pairs Bio-Unconnected, Bio-EMG and Classic-EMG ( $p < 0.05$ ). Users had better performance using Bio over Unconnected and EMG. The same applied also for the performance using Classic compared to EMG. These are also demonstrated graphically in Figure 6.12.

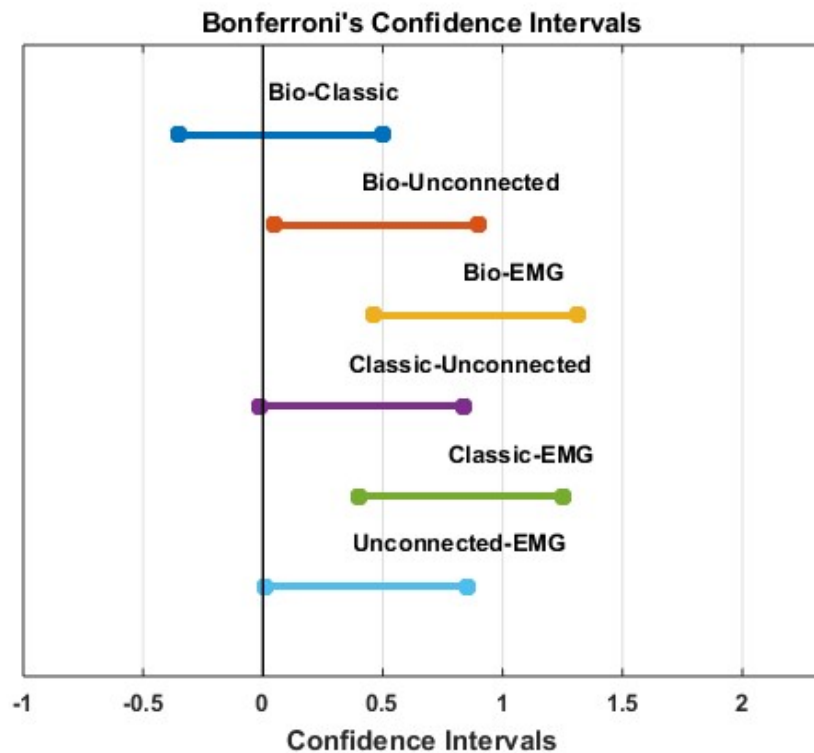


**Figure 6.12. Bonferroni's Confidence Intervals for Throughput.**

## 6.2.4 Fit of the model

Least-squares linear regression was used to find the intercept (a) and slope (b) parameters of the Fitts' law equation (or coefficients of linear regression model) for all the four different control methods used in the experiment as the standard presented in section 2.5 indicates. These parameters are presented below in the coefficient tables along with their standard errors and the t statistic with its p value. The value of the t statistic serves as an indicator of significance for the corresponding coefficient and can be computed as follows:

$$t - statistic = \frac{\beta - coefficient}{Std.Error} \quad (6.9)$$

$$p - value = \Pr(>|t|)$$

The higher the t statistic the lower the p value. When p value is less than significance level ( $< 0.05$ ), the null hypothesis that the co-efficient  $\beta$  is zero can be safely rejected.

Figure 6.13 to Figure 6.16 demonstrate the linear regression relationship between movement time and effective index of difficulty along with a scatter plot of the actual data obtained during experiments (see Table 6.3 to Table 6.6).

Having built the linear models ANOVA tests were conducted in order to test their statistical significance. The results are presented in the ANOVA tables below. The F statistic of ANOVA along with linear regression diagnostics as the coefficient of determination (R square), adjusted and not and the Standard Error of the estimate were computed using the following formulas:

$$F - statistic = \frac{MSR}{MSE} \quad (6.10)$$

$$R^2 = 1 - \frac{SSE}{SST} \quad (6.11)$$

Where SSR- Sum of squared errors and SST- Sum of squared total.

$$R_{adj}^2 = 1 - \frac{MSE}{MST} \quad (6.12)$$

Where MSE- Mean squared error and MST- Mean squared total.

$$Std.Error = \sqrt{MSR} \quad (6.13)$$

R square determines the proportion of variation in the dependent (response) variable that has been explained by the built model. Both standard error and F-statistic are measures of goodness of fit.

The error in the above equations is determined as the difference between an observed value and the fitted one.

The results for the goodness of fit are presented analytically below for all the four different control methods.

## Biomechatronic EPP

A simple linear regression was calculated to fit movement time based on effective index of difficulty. A significant regression equation was found ( $F_{1,23} = 354.3895$ ,  $p < .000$ ), with an  $R^2$  of .939, see Table 6.17 to 6.19. Fitts' law equation for Biomechatronic EPP was:

$$MT = -168.043 + 484.445IDe \quad (6.14)$$

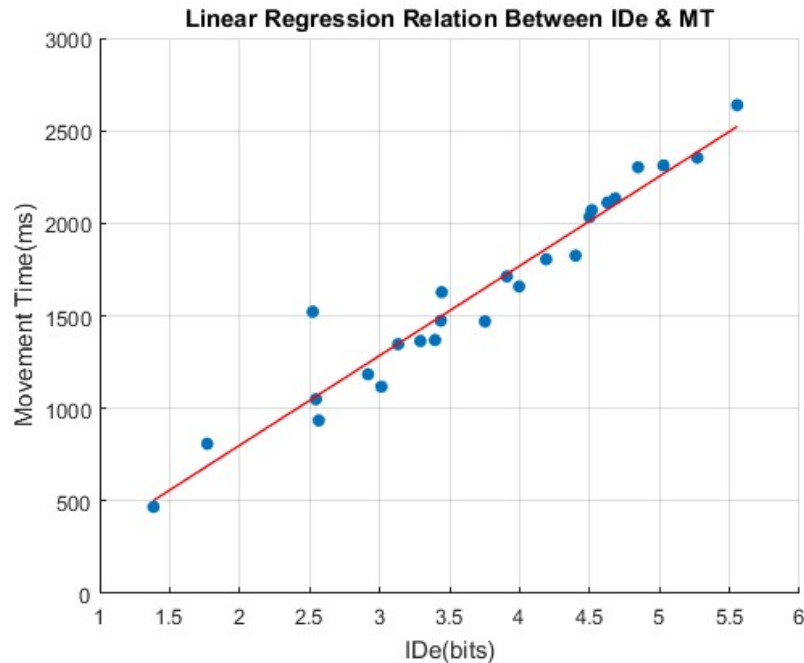


Figure 6.13. Linear regression model for Biomechatronic EPP

Table 6.17. Summary of the Model for Biomechatronic EPP.

Model	R	R Square	Adjusted R Square	Standard Error of the estimate
Regression	0.969	0.939	0.936	135.882

Table 6.18. ANOVA table for Biomechatronic EPP.

Model	Sum of Squares	df	Mean Square	F	p-value
Regression	6543386.431	1	6543386.431	354.3895	1.80E-15
Error	424668.069	23	18463.829		
Total	6968054.501	24	290335.604		

Table 6.19. Coefficients of model for Biomechatronic EPP.

Model	Estimate	Standard Error	tStat	p -Value
Intercept	-168.043	99.206	-1.694	0.103790129
Slope	484.445	25.734	18.825	1.80E-15

### Classic EPP

A simple linear regression was calculated to fit movement time based on effective index of difficulty. A significant regression equation was found ( $F_{1,23} = 720.9423$ ,  $p < .000$ ), with an  $R^2$  of .984, see Table 6.20 to 6.22. Fitts' law equation for Classic EPP was:

$$MT = -299.489 + 546.256IDe \quad (6.15)$$

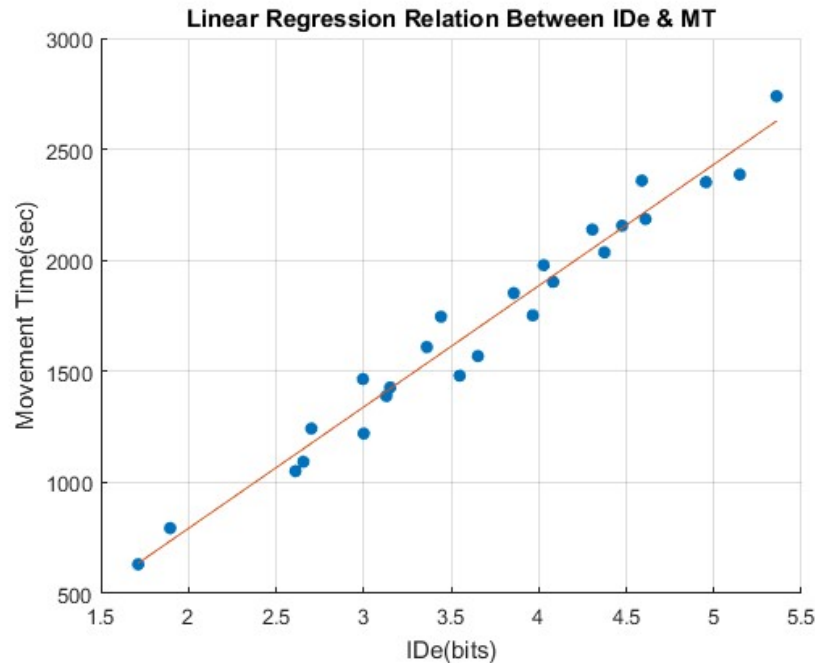


Figure 6.14. Linear regression model for Classic EPP

Table 6.20. Summary of the Model for Classic EPP.

Model	R	R Square	Adjusted R Square	Standard Error of the estimate
Regression	0.984	0.969	0.968	95.752

Table 6.21. ANOVA table for Classicc EPP.

Model	Sum of Squares	df	Mean Squares	F	p-value
Regression	6585114.979	1	6585114.979	720.9423	7.24E-19
Error	210082.884	23	9134.038		
Total	6795197.863	24	283133.244		

Table 6.22. Coefficients of model for Classic EPP.

Model	Estimate	Standard Error	tStat	p -Value
Intercept	-299.489	76.966	-3.891	0.000736828
Slope	546.256	20.344	26.850	7.24E-19

## Unconnected

A simple linear regression was calculated to fit movement time based on effective index of difficulty. A significant regression equation was found ( $F_{1,23} = 646.7148, p < .000$ ), with an  $R^2$  of .939, see Table 6.23 to 6.25. Fitts' law equation for Unconnected was:

$$MT = 193.489 + 467.261 \quad (6.16)$$

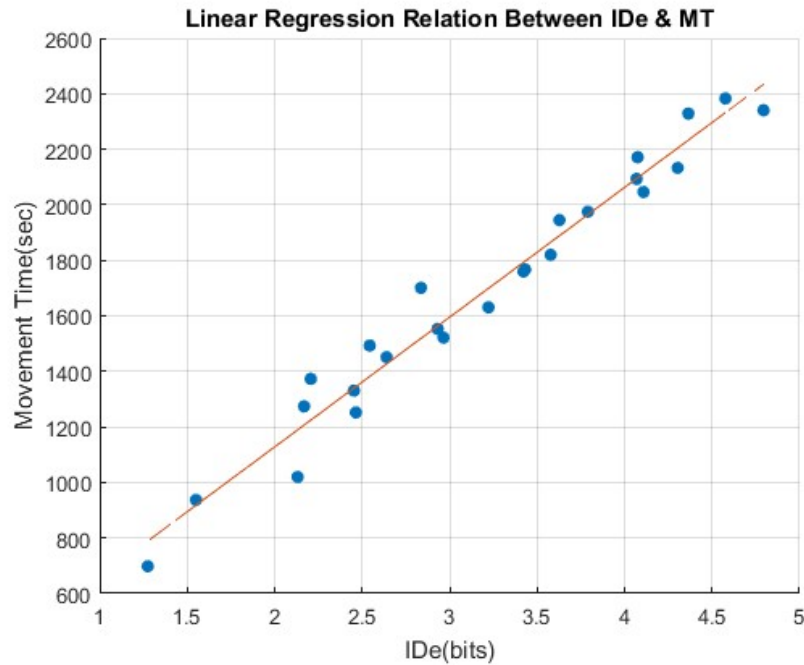


Figure 6.15. Linear regression model for Unconnected method.

Table 6.23. Summary of the Model for Unconnected.

Model	R	R Square	Adjusted R Square	Standard Error of the estimate
Regression	0.983	0.966	0.964	85.888

Table 6.24. ANOVA table for Unconnected.

Model	Sum of Squares	df	Mean Squares	F	p-value
Regression	4770627.630	1	4770627.630	646.7148	2.43E-18
Error	169664.330	23	7376.710		
Total	4940291.960	24	205845.498		

Table 6.25. Coefficients of model for Unconnected.

Model	Estimate	Standard Error	tStat	p -Value
Intercept	193.489	60.920	3.176	4.21E-03
Slope	467.261	18.374	25.431	2.43E-18

## EMG

A simple linear regression was calculated to fit movement time based on effective index of difficulty. A significant regression equation was found(  $F_{1,23} = 222.4156, p < .000$  ), with an  $R^2$  of .939, see Table 6.26 to 6.28. Fitts' law equation for Unconnected was:

$$MT = 689.020 + 419.078IDe \quad (6.17)$$

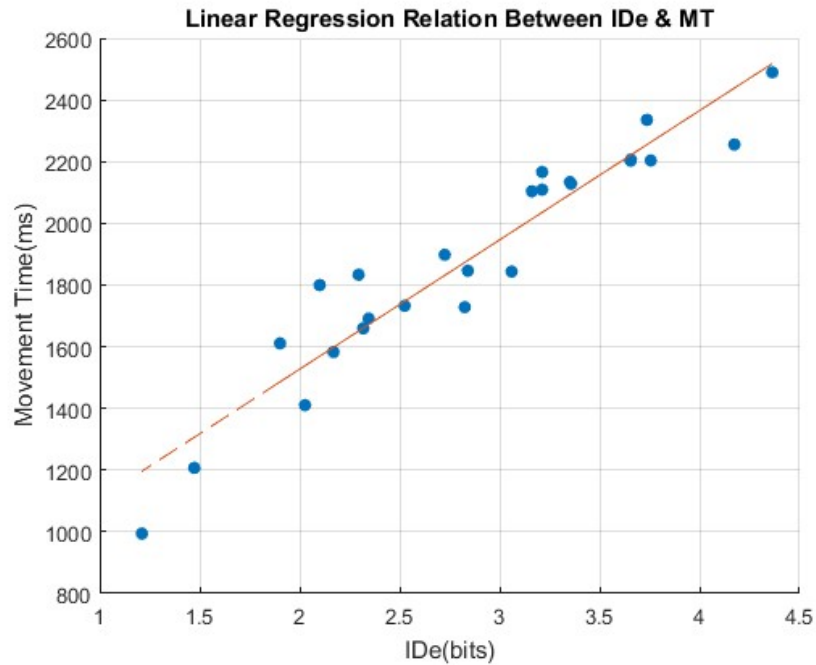


Figure 6.16. Linear regression model for EMG method.

Table 6.26. Summary of the Model for EMG.

Model	R	R Square	Adjusted R Square	Standard Error of the estimate
Regression	0.952	0.906	0.902	112.451

Table 6.27. ANOVA table for EMG.

Model	Sum of Squares	df	Mean Squares	F	p-value
Regression	2812490.036	1	2812490.036	222.4156	2.58E-13
Error	290839.580	23	12645.199		
Total	3103329.616	24	129305.401		

Table 6.28. Coefficients of model for EMG.

Model	Estimate	Standard Error	tStat	p -Value
Intercept	689.020	83.408	8.261	2.46E-08
Slope	419.078	28.100	14.914	2.58E-13

## 7 Experimental Data Evaluation

### 7.1 Transparency-Equivalency Test

The objective of this section is the assessment of the quality of the control provided by Biomechatronic EPP. Transparency is the most common measure to evaluate the performance of a master-slave system [28].

The Biomechatronic EPP intends to replicate the relation between the power variables (velocity and force) of the muscles and the prosthesis that is mechanically achieved with the use of cables in Classic EPP. The degree in which this goal is achieved also determines the degree of the system transparency.

The following figures demonstrate the responses of the system variables as they were measured during the experiment conducted to evaluate the system transparency. It is noted that the experiment was realized in free space, therefore there was no external force applied to the prosthetic joint of the setup.

Figure 7.1.a presents the output of the agonist and antagonist FSR sensors. The difference of these signals (Figure 7.1.b) served as input for the controller of the slave motor. The output (current command) of the Classic EPP controller for the same time range was monitored and is demonstrated in Figure 7.2 .a. The corresponding torque (Figure 7.2.b) of the slave motor can be then calculated via:

$$T_s = I_s G K t_s \quad (7.1)$$

where  $K t_s$  is the torque constant of the slave motor,  $G$  is the gearbox ratio and  $I_s$  is the current of the slave motor.

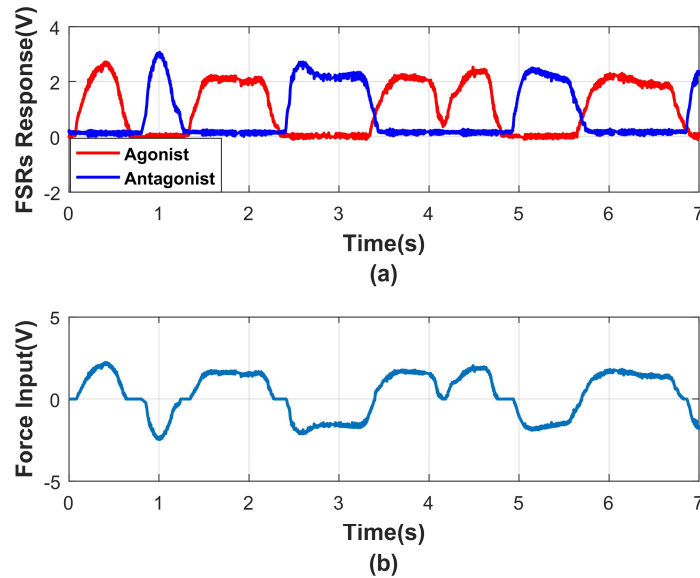


**Figure 7.1.** (a) Responses of the FSR sensors connected to the agonist (red line) and the antagonist muscle (blue line) (b) Difference ( $F_{ag}-F_{ant}$ ) between the FSR responses of the antagonistic muscle pair.



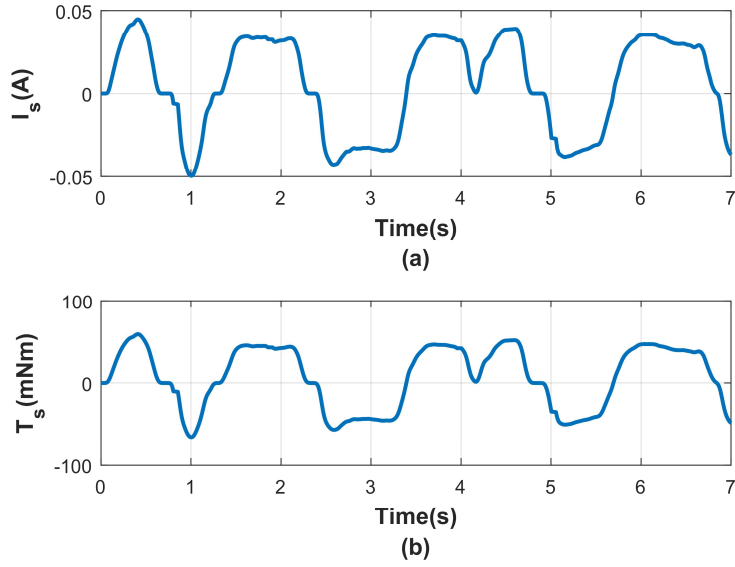


**Figure 7.2. (a) Current and (b) torque of the slave motor.**

The current commands given to the agonistic and the antagonistic master motors and the corresponding torque responses are plotted in Figure 7.3 and Figure 7.4, respectively, for the same time range. The torque of the master motors is computed via:

$$T_m = Kt_m I_m \quad (7.2)$$

where  $Kt_m$  is the torque constant of the master motors and  $I_m$  is the current provided even on the agonistic or antagonistic master motor.

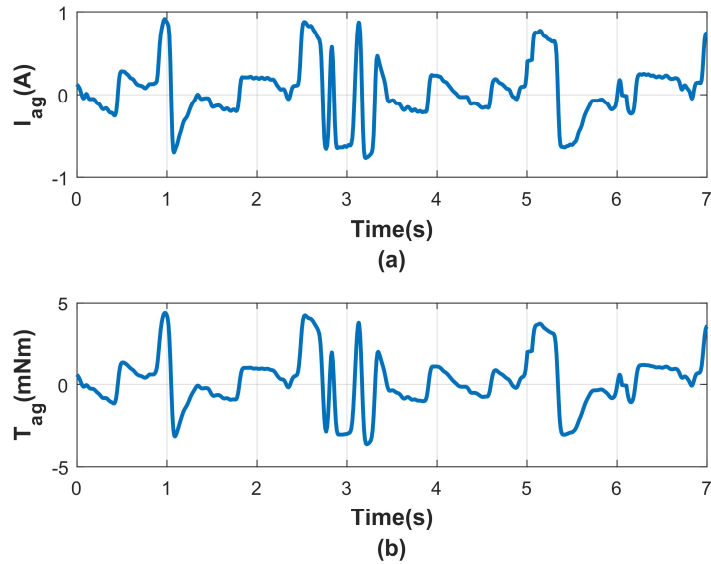


**Figure 7.3. (a) Current and (b) torque of the agonistic master motor.**

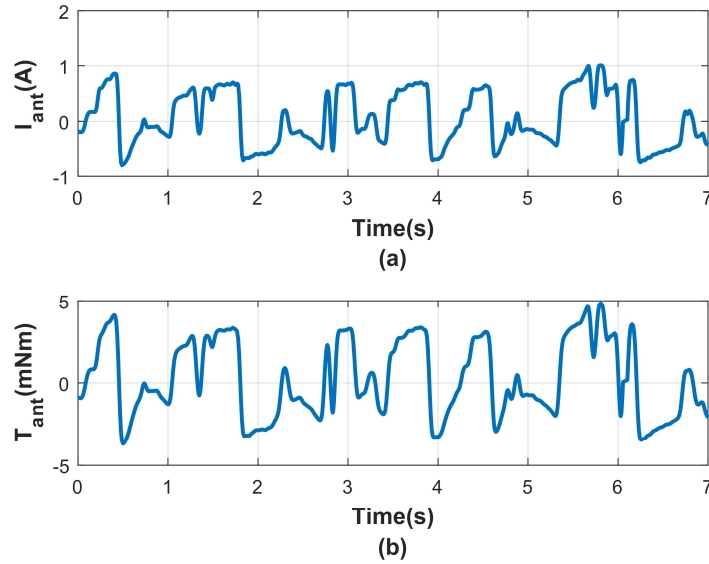


**Figure 7.4. (a) Current and (b) torque of the antagonistic master motor.**

In light of what was mentioned in Section 4.2, the current provided to the master motors fulfils the requirement of reaching close to the maximum value of 1.2 A.

In Figure 7.5 the total torque developed by the system of the master motors in Biomechatronic EPP (red line) configuration is compared to the torque response of the slave motor (blue line). The difference between the two (yellow dotted line) is also plotted in the same Figure so as to construct an overview of their relationship.

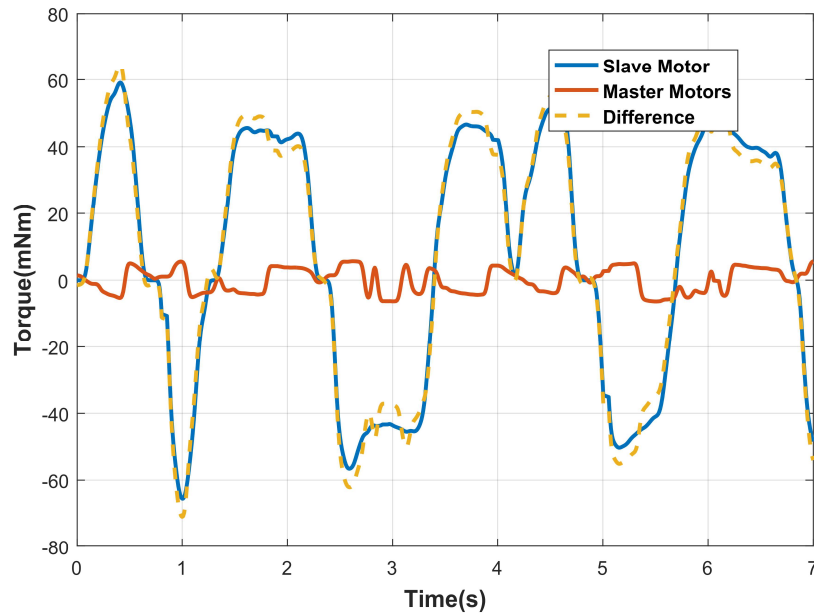


**Figure 7.5. Torque response of the slave motor (blue line), master motors (red line) and the difference between them (yellow dotted line).**

It is important to notice that the slave motor develops much higher torque than the master motors. This is reasonable as the slave motor is connected to the prosthetic limb and consequently interacts with

the external environment where high torque is of great importance. Also, it is apparent from the difference of the two waveforms that the torque developed by the slave motor is proportional to the one developed by the system of the master motors. A time-delay estimation was made by computing the cross-correlation of the slave motor torque and the total torque of the master motors. Using the “xcorr” function in Matlab, the maximum lag was computed to be 2 ms.

Figure 7.6 shows the position and the velocity of the slave motor, for the same time range. Having obtained the angular displacement of the prosthesis, the displacement of the Bowden cable terminals varied in time as Figure 7.7 presents according to 4.1.

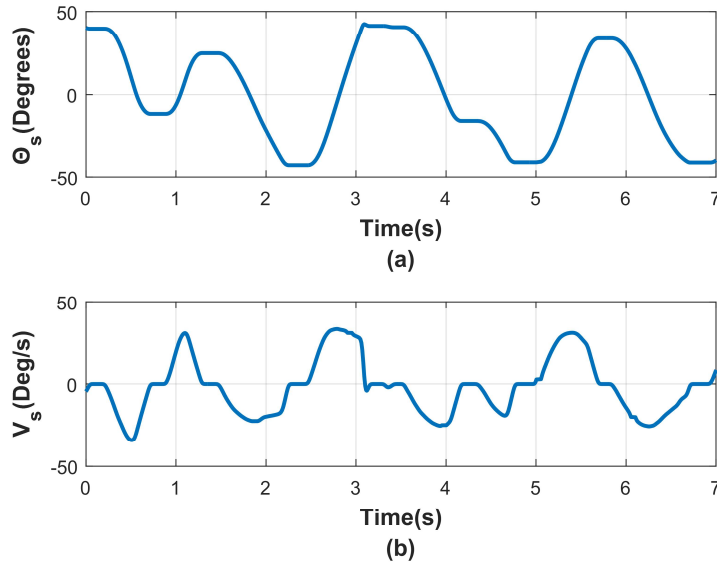


**Figure 7.6. (a) Angular position and (b) velocity of the slave motor.**

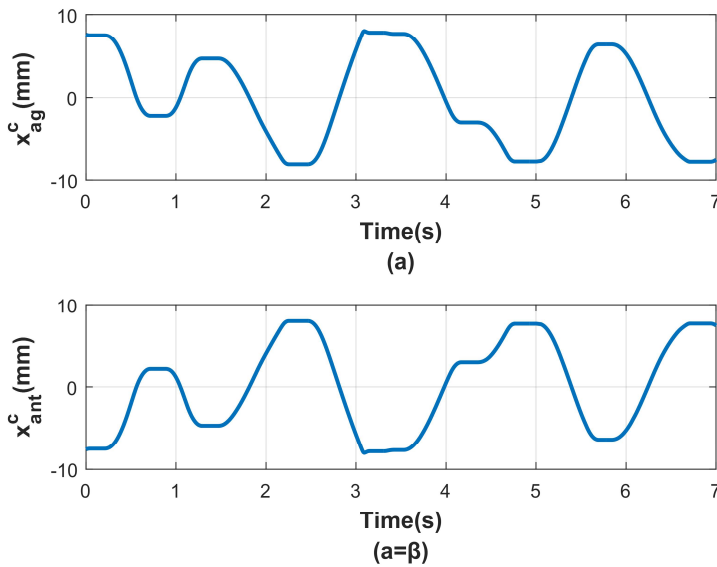


**Figure 7.7. Displacement of the Bowden cable terminals in Classic EPP topology: Terminal connected to the (a) Agonistic (b) Antagonistic muscle.**

Figure 7.8 and Figure 7.9 illustrate the displacement and velocity responses of the linear actuators connected to the agonistic and the antagonistic muscles during the Biomechatronic EPP configuration, respectively.

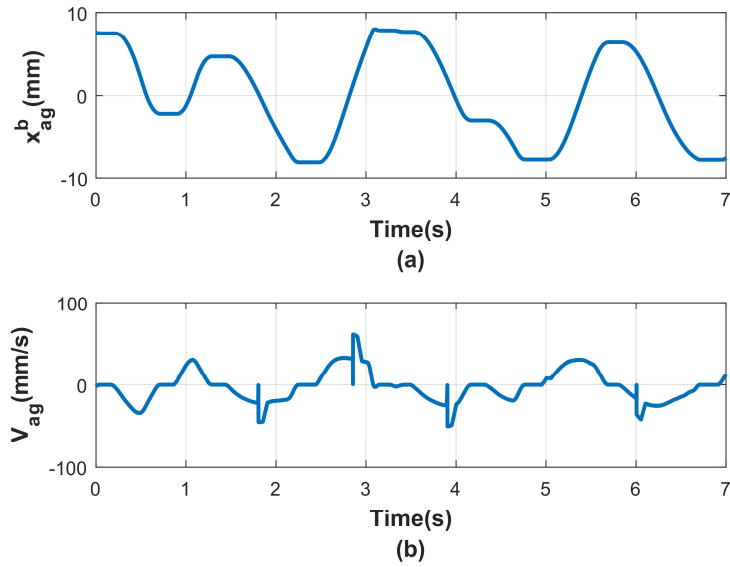


**Figure 7.8. (a) Displacement and (b) velocity responses of the agonistic linear actuator in Biomechatronic EPP topology**

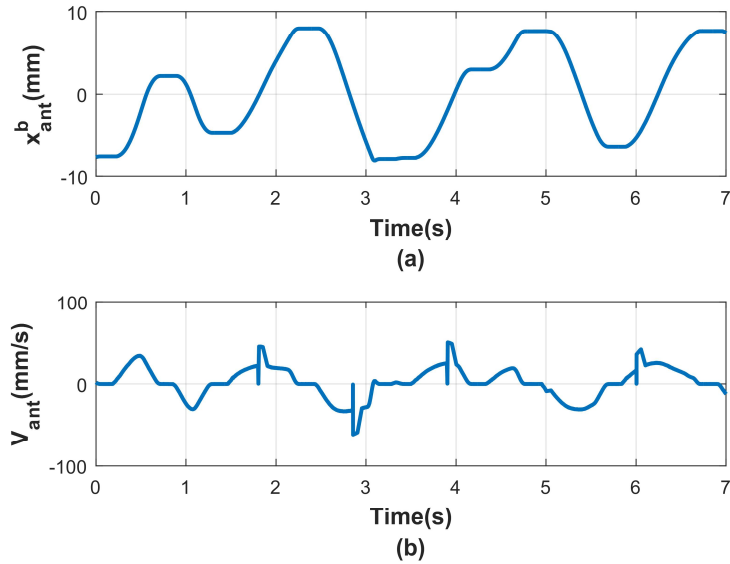


**Figure 7.9. (a) Displacement and (b) velocity responses of the antagonistic linear actuator in Biomechatronic EPP topology**

Having obtained the responses of the above system variables for both Classic and Biomechatronic EPP configurations, it was possible to compare them (Figure 7.10 and Figure 7.11).

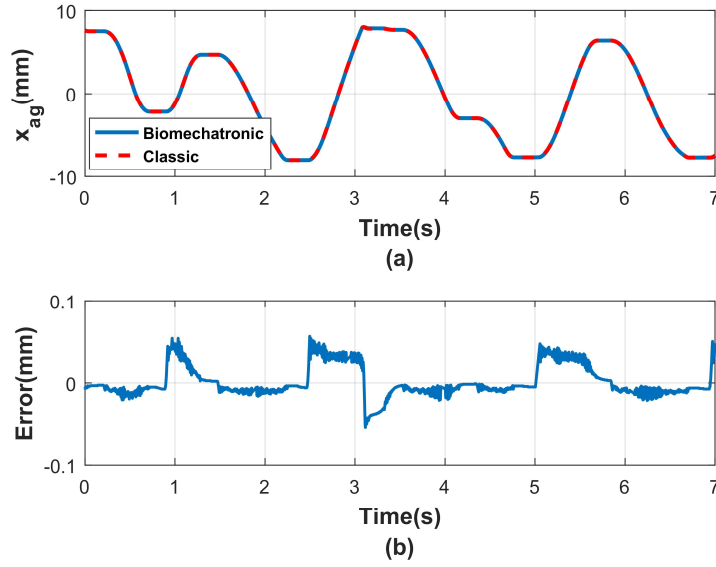


**Figure 7.10. (a) Comparison of the agonistic terminal displacement responses during Biomechatronic (blue line) and Classic EPP (red dotted line) and (b) their respective error**

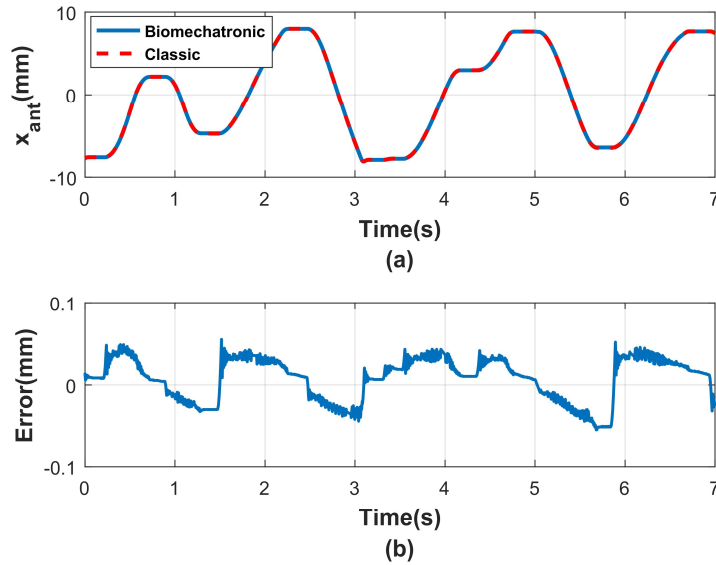


**Figure 7.11. (a) Comparison of the antagonistic terminal displacement responses during Biomechatronic (blue line) and Classic EPP (red dotted line) and (b) their respective error**

Considering as ideal the responses obtained during the operation of Classic EPP, the percentage RMS value of the error can be calculated as follows:

$$e_{length}^{rms} = \frac{rms(x^{classic} - x^{bio})}{rms(x^{classic})} \times 100\% \quad (7.3)$$

Where  $x^{classic}$  and  $x^{bio}$  the displacement even of the agonistic or the antagonistic terminals during Classic and Biomechatronic EPP, respectively. The error turned to be too small for both the agonistic (0.35%) and the antagonistic (0.49%) muscle. Apart from the RMS error, a time-delay estimation was made by

computing the cross-correlation of the slave motor displacement and the respective displacements of the master motors. Using the “xcorr” function in Matlab, the maximum lag was computed and it turned out to be practically zero (less than sampling period of 1ms) for both the agonist and the antagonist master motor.

After that, the delay of the system depends only on the delay between applying the force and the displacement of the prosthesis motor. As shown in Figure 7.12, for our experimental setup, this is approximately 78ms.

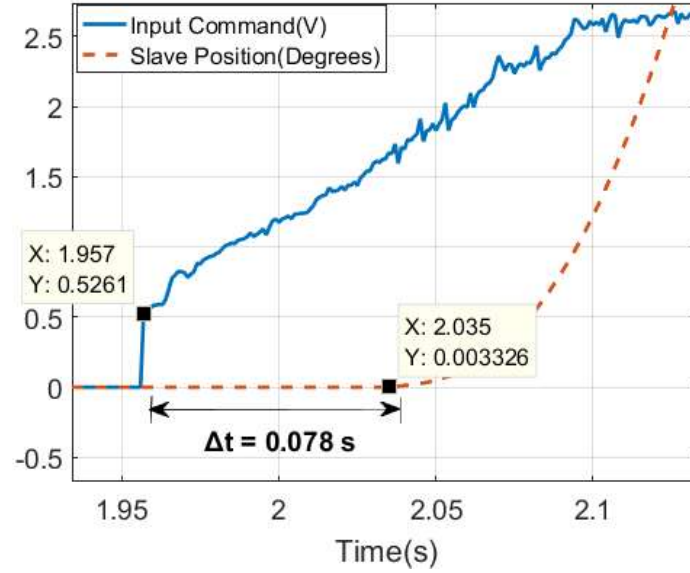


**Figure 7.12. Measurement of the delay between the applying force and the displacement of the prosthesis motor.**

According to the results presented above for the responses of the power variables of the system and observing their differences between the Classic and Biomechatronic EPP configurations, the transparency of the system is considered sufficient.

Finally, an estimation of each master robot power losses was made by subtracting the mechanical ( $P_{mechanical}$ ) from the electrical power ( $P_{electrical}$ ) of the motor:

$$P_{loss} = P_{electrical} - P_{mechanical} \Leftrightarrow P_{loss} = I^2 R_t - T \omega \quad (7.4)$$

where  $I$  is the armature current,  $R_t$  is the terminal resistance of the dc motor,  $T$  is the torque and  $\omega$  is the angular velocity. The results presented in Figure 7.13 demonstrate the power losses of the master robots which are released inside the human tissue in the form of thermal power. In a former related work [32] the power losses for each master robot were estimated to be 0.76W. However, the power rating of the motors used was 0.5W while the motors of our experimental setup have a powering rate of 2.5W. This justifies the higher losses recorded in this work. The presented results are nothing more than a first experimental estimation of the thermal losses. A more detailed thermal analysis along with the realization of experiments in a human tissue-like environment will reveal the effects of the setup in the human body and may also reveal weaknesses.

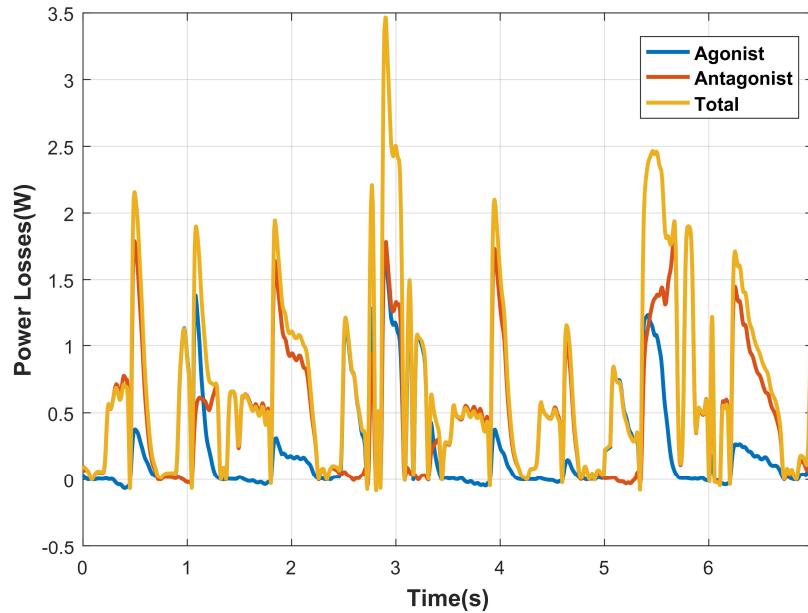


**Figure 7.13.** Power losses of the agonist (blue line) and antagonist (red line) master motors. Yellow line represents the total power losses.

## 7.2 Force Application Test

This test was realized in order to examine how changes on the load applied to the joint of the slave motor affect the user who operates the Biomechatronic EPP configuration. The experiment conducted is divided in two parts. In both of them, the user had no visual contact with the setup.

In the first one, a weight of 1,17 kg held by a rope was attached to the shaft of the slave motor, see Figure 7.14. During this phase, we compared the output of the FSR sensors, thus the force applied by the user, with the weight attached and not attached, see Figure 7.15. The RMS values of the FSRs output calculated for both situations. They computed to be 1.47V and 2.56V with the weight not attached and attached respectively. The difference between the two situations is about 42.5 % indicating that the user had been capable to feel the extra load applied to the joint of the slave motor and therefore increased the force.

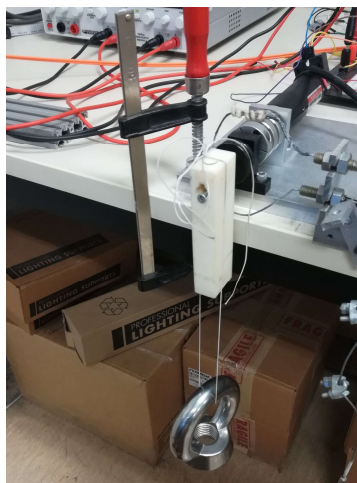


**Figure 7.14.** The weight attached to the shaft of the slave motor.

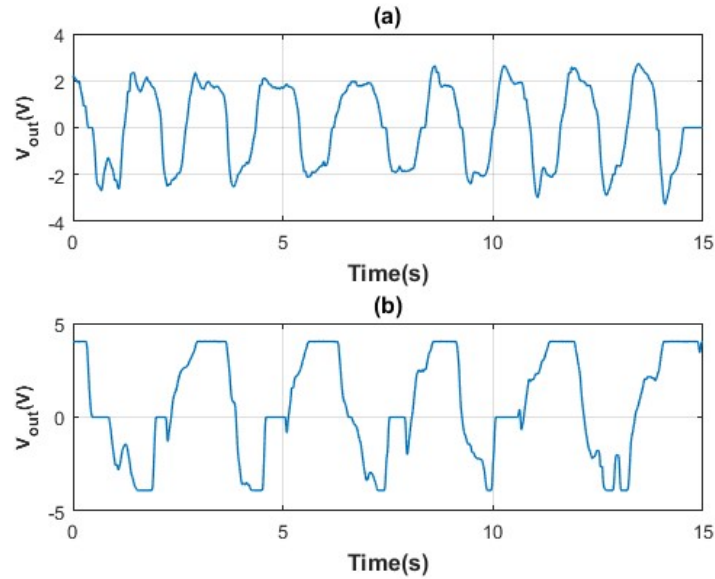


**Figure 7.15. FSRs output with the weight (a) not attached and (b) attached to the shaft of the slave motor.**

For the second part of the experiment we made use of the two mechanical stops of the experimental setup. We set the stops in such positions so as a collision could occur between the shaft of the slave motor and them. The aim of this experiment was to determine if the user was able to feel the impulse imparted to the shaft during the collision and it was realized for both Classic and Biomechatronic EPP. Five of the subjects who took part in the target experiment were selected to participate in this experimental phase. The subjects did not know the position of the stops. They were instructed to apply reciprocal steep forces to the FSR sensors and were asked to indicate whenever they felt resistance. Each experiment was terminated after a total of 20 collisions for each control method. Thus, we had 200 trials, totally, for each subject. As it was foreseen, during Classic EPP the resistance that the subjects felt was obvious. Table 7.1 summarizes the answers given by the subjects through the experiment, while using the Biomechatronic EPP setup.

The results are proved particularly encouraging, as the number of positive answers is obviously greater than that of the negative ones. More specifically, the subjects managed to feel the impact imparted during the collision the 82% of the times, while for the 18% of the trials they did not give an affirmative answer.

In order to establish an overall picture of the subjects' performance, we also measured their reaction time. The reaction time was defined as the time interval between the collision and the moment the subjects started moving the prosthesis to the opposite direction. The unsuccessful trials were excluded from this analysis. Figure 7.16 and Figure 7.17 present the mean reaction time for each subject along with the standard deviation of the measurements, for Biomechatronic and Classic EPP respectively. The mean reaction time of the subjects during Classic EPP was  $0.27 \pm 0.10s$ , while during Biomechatronic EPP was  $0.46 \pm 0.13s$ .



The high rate of positive answers along with the comparable reaction times indicate that Biomechatronic EPP achieved to transmit to the users the disturbances occurred to the environment of the prosthesis motor in a satisfactory level.

**Table 7.1.** Answers given by the five subjects through the experiment. Each cell corresponds to a collision. With green color are the positive answers and with red color are the negative ones.

Subject Collision	S1	S2	S3	S4	S5	
C1	P	N	P	P	P	
C2	P	N	N	P	P	
C3	N	P	P	P	P	
C4	N	P	P	P	P	
C5	P	P	P	P	N	
C6	P	P	P	P	P	
C7	P	P	P	N	N	
C8	P	P	N	P	P	
C9	P	P	P	N	P	
C10	P	P	P	N	N	
C11	P	P	P	P	P	
C12	P	P	P	P	P	
C13	P	P	P	N	P	
C14	P	P	P	P	N	
C15	P	P	N	P	P	
C16	P	P	P	P	P	
C17	N	P	P	N	P	
C18	P	P	P	P	P	
C19	P	P	P	P	P	
C20	N	P	P	P	P	TOTAL
Positive	16	18	17	15	16	82
Negative	4	2	3	5	4	18

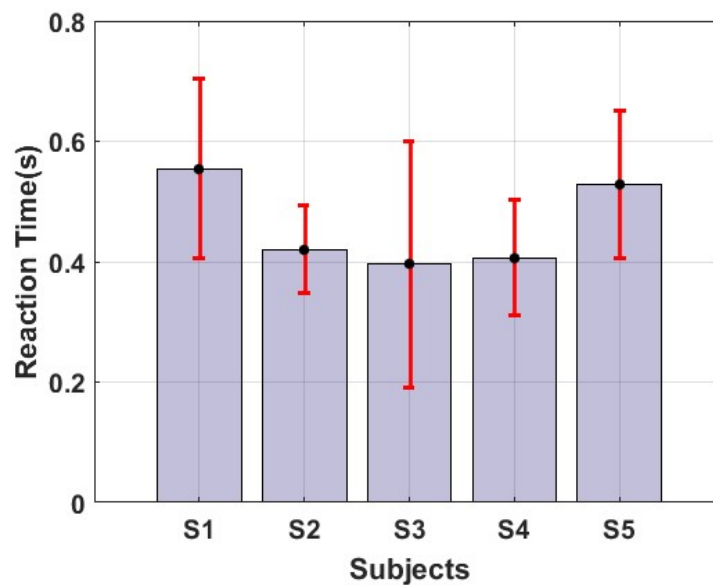


**Figure 7.16.** Reaction time among subjects for Biomechatronic EPP.

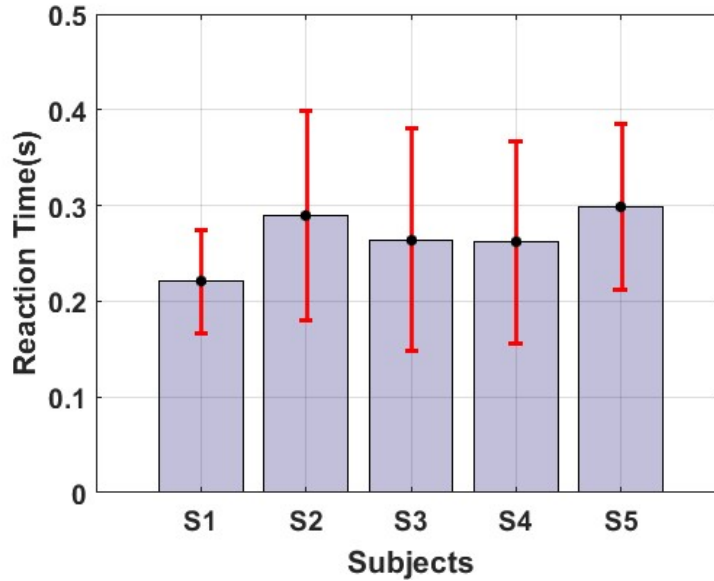


**Figure 7.17. Reaction time among subjects for Classic EPP.**

### 7.3 EMG signals comparison

In Chapter 5, we demonstrated the basic steps for the configuration of an EMG signal. As it has been mentioned, after its processing, the EMG data, represents the activation level (AL) of the corresponding muscle. This information can be proved very useful in the assessment of the muscle fatigue during an exercise. When speaking for a specific exercise then, the greater the level of activation of a muscle, the greater the fatigue [6]. We made use of this simple rule in order to evaluate the fatigue caused to Extensor Carpi Radialis and Flexor Carpi Radialis of a subject during the target experiments. The aim of this evaluation is to compare the level of fatigue caused to the muscles of interest while using the four different control methods presented previously.

The EMG data from the muscles of interest were collected from a subject during the target experiment and for all the four different control topologies. The data were processed according to Section 5.3.2 and then were divided in five sections, each one of them corresponding to a single target width task (see Section 6.1.3). This division was chosen as a different target width demands different precision and therefore the EMG response may differ from width to width. Figure 7.18 and Figure 7.19 demonstrate the electrical activity of Extensor Carpi Radialis and Flexor Carpi Radialis respectively during the experiments. The sections of the EMG data have been separated. The mean duration time of each section was  $210 \pm 25s$ . Observing the following figures, the highest peaks for both the extensor and the flexor muscle are recorded during the EMG sessions, while the activation level of the muscles is less during Classic and Biomechatronic EPP. The mean values of the activation level, shown in Table 7.2 Table 7.3, confirm these observations. However, the fatigue analysis could be more accurate and completed if the EMG data had been recorded for more subjects. This may be part of future work.

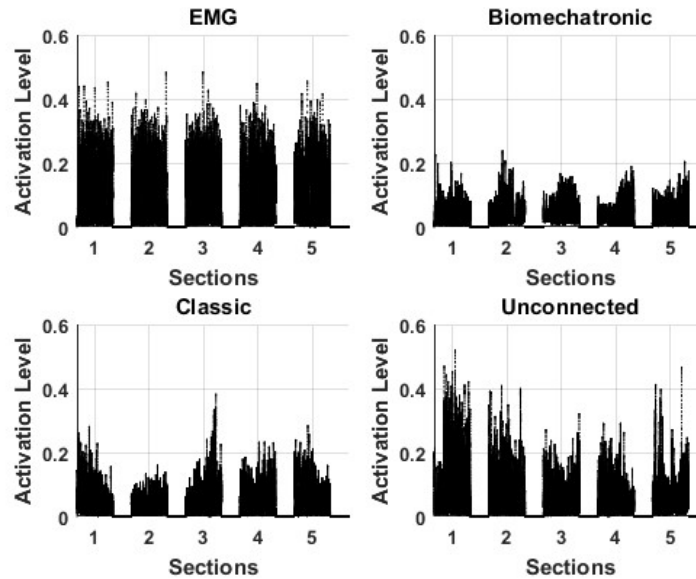


Figure 7.18. Five sections of the Activation Level (AL) of Extensor Carpi Radialis recorded during the realization of the target experiments.

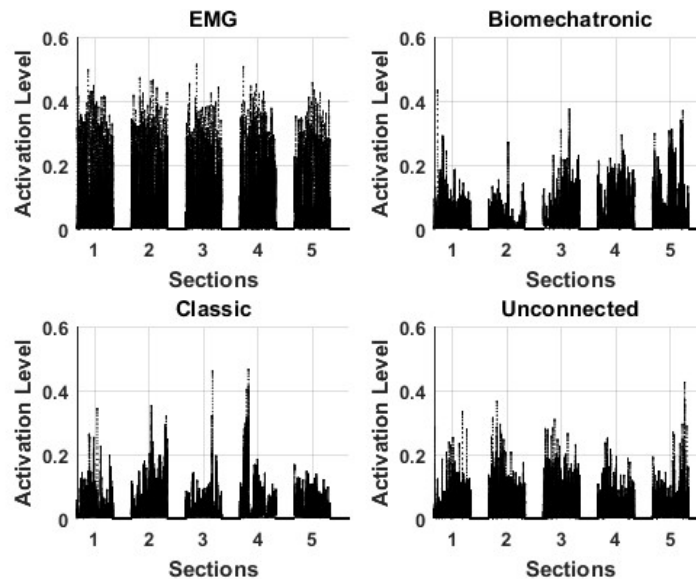


Figure 7.19. Five sections of the Activation Level (AL) of Flexor Carpi Rasdialis recorded during the realization of the target experiments.

Table 7.2. Mean activation levels of the flexor muscle.

FLEXOR CARPI RADIALIS						
Control Method	Sections					Grand Mean
	1	2	3	4	5	
Biomechatronic	3.25%	2.18%	4.28%	3.96%	5.28%	3.79%
Classic	3.01%	4.54%	2.88%	4.00%	3.06%	3.50%
Unconnected	3.13%	3.65%	3.41%	2.91%	3.38%	3.30%
EMG	6.18%	6.97%	7.22%	6.97%	6.81%	6.83%

**Table 7.3. Mean activation levels of the extensor muscle.**

EXTENSOR CARPI RADIALIS						
Control Method	Sections					Grand Mean
	1	2	3	4	5	
Biomechatronic	3.33%	3.76%	4.50%	3.55%	3.53%	3.73%
	Classic	4.59%	3.29%	4.82%	4.64%	4.79%
Unconnected	8.75%	6.35%	5.04%	5.13%	6.10%	6.27%
	EMG	7.49%	8.08%	8.74%	7.66%	9.04%

## 8 Conclusion and Future Work

### 8.1 Conclusion

In this thesis we investigated the performance of the Biomechatronic EPP, a novel upper-limb control topology, to three other traditional control topologies. We used a computer-based target acquisition test, built according to Fitts' law.

The data collected from the fourteen able-bodied subjects which took part in the experiment suggests that the proposed method is able to compete with commonly used upper-limb control methods and even surpass them.

No statistical differences were observed in any performance metric between Biomechatronic and Classic EPP, but subjects generally moved slower and made much more mistakes during the sessions of the other two control topologies. These results indicate that the feedback information provided to the users while controlling the prosthesis with Biomechatronic EPP and Classic EPP helped them to perform better than when using the "Unconnected" and EMG configurations. Also it is worth mentioning the usefulness and the fitness of Fitts' Law analysis in the conducting of this study.

From the experiments realized, we also proved the transparency of the Biomechatronic EPP controller, as well as its equivalency to the Classic EPP. In addition, the operation of the proposed prosthesis system with the occurrence of disturbances in the environment of the prosthesis motor is judged at least satisfactory. The results of the fatigue analysis can be considered as an in principle proof that Biomechatronic EPP would not handicap the proper functioning of the antagonistic pair of muscles.

The proposed topology manages everything described above without the drawbacks of cineplasty and Bowden cables, which render the EPP unaesthetic for the user, while at the same moment achieves the adequate sensory feedback and activates the proprioception of the user, elements that the extensively studied myoelectric control is unable to offer.

Concluding, the proposed EPP topology restores the idea of the user proprioception in the field of upper-limb prosthetics. We truly believe that Biomechatronic EPP is a promising and novel topology and has the potential to ameliorate the life of perspective users.

### 8.2 Future Work

First of all, the realization of the experiments inside a human muscle-like environment for thermal losses analysis along with the migration to the wireless setup would give an aggregate picture for the potential of the proposed control topology and might also reveal weaknesses. Moreover, improvements on the experimental setup are always feasible. A change that can be implemented in the near future is the design of FSRs circuitry on a PCB board. This would eliminate unintended disconnections of the FSR sensors from the rest of the setup and would also reduce the electrical noise. In addition, part of a future work could be the implementation of a more complicated EMG control strategy. In this thesis is a simple proportional myoelectric control was implemented. However, pattern recognition algorithms have recently overtaken this method. A comparison of our proposal with an, more up-to-date, EMG topology would have a more significant impact in the scientific society. Furthermore, a more detailed and

accurate fatigue analysis can be achieved if the EMG data is recorded for more subjects. This will allow us to statistically prove the results presented in Section 7.3.

To sum up, the results presented in this study are encouraging and lead us to invest more in this control topology, which in future can become the core of many DOFs prosthetic systems. A physically implemented bio-compatible Biomechatronic EPP prototype is the next ultimate objective.

## 9 References

- [1] Altpeter, F., *Friction Modeling, Identification and Compensation*. 1999, p. 74.
- [2] Beamish, D., Bhatti, S.A., MacKenzie, I.S., and Wu, J., "Fifty years later: a neurodynamic explanation of Fitts' law," *Journal of the Royal Society Interface*, vol. 3, no. 10, pp. 649-654,.
- [3] Beggs, W.D.A. and Howarth, C.I., "Movement Control in a Repetitive Motor Task," *Nature*, vol. 225, p. 752.
- [4] Bertos, Y.A., "A Microprocessor-based E.P.P. position controller for electric-powered upper-limb prostheses," *Master of Science*, Electrical & Computer Engineering, Northwestern University, Evanston, IL, USA, 1999.
- [5] Biddiss, E.A. and Chau, T.T., "Upper limb prosthesis use and abandonment: a survey of the last 25 years," *Prosthet Orthot Int*, vol. 31, no. 3, Sep 2007, pp. 236-57.
- [6] Cao, L. *et al.*, "Effects of Force Load, Muscle Fatigue, and Magnetic Stimulation on Surface Electromyography during Side Arm Lateral Raise Task: A Preliminary Study with Healthy Subjects," *BioMed Research International*, vol. 2017, p. 8943850, 04/11
- [7] Childress, D.S., "Control of Limb Prostheses," in *Atlas of Limb Prosthetics, Surgical, Prosthetic, and Rehabilitation Principles*, J. W. Bowker and J. W. Michael, Eds. St. Louis MO: Mosby-Year Book, Inc., 1992, pp. 175-199.
- [8] Crossman, E.R.F.W., "A theory of the acquisition of speed-skill\*," *Ergonomics*, vol. 2, no. 2, pp. 153-166.
- [9] Crossman, E.R.F.W., "The information-capacity of the human motor-system in pursuit tracking," *The Quarterly Journal of Experimental Psychology*, vol. 12, 1960, pp. 1-16.
- [10] Enderle, J. and Bronzino, J., *Introduction to Biomedical Engineering*, 3rd ed. Elsevier, 2011, p. 1272.
- [11] Fitts, P.M., "The information capacity of the human motor system in controlling the amplitude of movement," *Journal of Experimental Psychology*, vol. 47, no. 6, 1954, pp. 381-391.
- [12] Fitts, P.M. and Peterson, J.R., "Information capacity of discrete motor responses," (in eng), *J Exp Psychol*, vol. 67, Feb 1964, pp. 103-12.
- [13] Gan, K.C. and Hoffmann, E.R., "Geometrical conditions for ballistic and visually controlled movements," (in eng), *Ergonomics*, vol. 31, no. 5, May 1988, pp. 829-39.
- [14] Ghapanchizadeh, H., Ahmad, S.A., and Ishak, A.J., "Recommended surface EMG electrode position for wrist extension and flexion," in *2015 IEEE Student Symposium in Biomedical Engineering & Sciences (ISSBES)*, 2015, pp. 108-112.
- [15] Halaki, M. and Ginn, K., *Normalization of EMG Signals: To Normalize or Not to Normalize and What to Normalize to?* 2012, pp. 175-194.
- [16] Hashim, N.A., Abd Razak, N.A., Abu Osman, N.A., and Gholizadeh, H., "Improvement on upper limb body-powered prostheses (1921–2016): A systematic review," *Proceedings of the Institution of Mechanical Engineers, Part H: Journal of Engineering in Medicine*, vol. 232, no. 1, 2018, pp. 3-11.
- [17] Jung, P., Lim, G., Kim, S., and Kong, K., "A Wearable Gesture Recognition Device for Detecting Muscular Activities Based on Air-Pressure Sensors," *IEEE Transactions on Industrial Informatics*, vol. 11, no. 2, 2015, pp. 485-494.
- [18] Keates, S., Hwang, F., Langdon, P., Clarkson, P.J., and Robinson, P., "Cursor measures for motion-impaired computer users," presented at the Proceedings of the fifth international ACM conference on Assistive technologies, Edinburgh, Scotland, 2002.
- [19] Kerr, B.A. and Langolf, G.D., "Speed of aiming movements," *Quarterly Journal of Experimental Psychology*, vol. 29, no. 3, 1977/08/01 1977, pp. 475-481.
- [20] Kleiner, M., Brainard, D.H., Pelli, D., Ingling, A., Murray, R., and Broussard, C., *What's new in Psychtoolbox-3*. 2007, pp. 1-16.
- [21] Klopsteg, P.E. and Wilson, P.D., *Human Limbs and their substitutes*, 2nd Edition ed. New York: McGraw-Hill, 1954.
- [22] Knight, A.A. and Dagnall, P.R., "Precision in Movements," *Ergonomics*, vol. 10, no. 3, , 1967/05/01 1967 pp. 321-330.
- [23] Koukoulas, N., "Ασύρματος Βιομηχανοτρονικός Έλεγχος Προσθετικού Άνω Άκρου," School of Mechanical Engineering, National Technical University of Athens, Athens, 2017.
- [24] Lloyd, D.G. and Besier, T.F., "An EMG-driven musculoskeletal model to estimate muscle forces and knee joint moments in vivo," (in eng), *J Biomech*, vol. 36, no. 6, Jun 2003, pp. 765-76.

- [25] Mablekos-Alexiou, A., "Design and Simulation of a Master Slave Architecture Biomechatronic EPP upper-limb prosthesis (Σχεδιασμός και προσομοίωση συστήματος τηλεχειρισμού προσθετικού άκρου με ιδιοδεκτική αίσθηση)," B.Sc., Mechanical Engineering, National Technical University of Athens, Athens, Greece, 2016.
- [26] MacKenzie, I.S. and Jusoh, S., "An Evaluation of Two Input Devices for Remote Pointing," in *Engineering for Human-Computer Interaction*, Berlin, Heidelberg, 2001: Springer Berlin Heidelberg, pp. 235-250.
- [27] MacKenzie, I.S. and Oniszczak, A., "A comparison of three selection techniques for touchpads," presented at the Proceedings of the SIGCHI Conference on Human Factors in Computing Systems, Los Angeles, California, USA, 1998.
- [28] Mahvash, M. and Okamura, A.M., "Enhancing Transparency of a Position-Exchange Teleoperator," in *Second Joint EuroHaptics Conference and Symposium on Haptic Interfaces for Virtual Environment and Teleoperator Systems (WHC'07)*, 2007, pp. 470-475.
- [29] Massó, N., Rey, F., Romero, D., and Gual, G., *Surface electromyography applications in the sport*. 2010.
- [30] McKenzie, I.S., "Fitts' Law as a Performance Model in Human-Computer Interaction," University of Toronto, Toronto, 1991.
- [31] Meldrum, D., Cahalane, E., Conroy, R., Fitzgerald, D., and Hardiman, O., "Maximum voluntary isometric contraction: reference values and clinical application," (in eng), *Amyotroph Lateral Scler*, vol. 8, no. 1, Feb 2007, pp. 47-55.
- [32] Moutopoulou, E., Bertos, G.A., Mablekos-Alexiou, A., and Papadopoulos, E.G., "Feasibility of a biomechatronic EPP Upper Limb Prosthesis Controller," in *2015 37th Annual International Conference of the IEEE Engineering in Medicine and Biology Society (EMBC)*, 2015, pp. 2454-2457.
- [33] Poupyrev, I., Okabe, M., and Maruyama, S., *Haptic feedback for pen computing: directions and strategies*. 2004, pp. 1309-1312.
- [34] Proctor, R.W. and Schneider, D.W., "Hick's law for choice reaction time: A review," *Quarterly Journal of Experimental Psychology*, vol. 71, no. 6, 2018, pp. 1281-1299.
- [35] Scott, R., "Myoelectric control of prostheses: A brief history," 1992: Myoelectric Symposium.
- [36] Shannon, C.E. and Weaver, W., *The mathematical theory of communication*. Urbana: University of Illinois Press, 1949, pp. 100-103.
- [37] Sheridan, M.R., "A Reappraisal of Fitts' Law," *Journal of Motor Behavior*, vol. 11, no. 3, , 1979/09/01 1979 pp. 179-188.
- [38] Simpson, D.C., "The choice of control system for the multimovement prosthesis: extended physiological proprioception (EPP)," in *The Control of Upper-Extremity Prostheses and Orthoses*, e. a. Herberts, Ed.: Springfield, IL: Thomas, 1974, pp. 146-150.
- [39] Soukoreff, R.W. and MacKenzie, I.S., "Towards a standard for pointing device evaluation, perspectives on 27 years of Fitts' law research in HCI," *Int. J. Hum.-Comput. Stud.*, vol. 61, no. 6, 2004, pp. 751-789.
- [40] ISO, 2002. *Reference Number: ISO 9241-9:2000(E). Ergonomic requirements for office work with visual display terminals (VDTs)—Part 9—Requirements for non-keyboard input devices (ISO 9241-9) (Vol. February 15, 2002): International Organisation for Standardisation*.
- [41] Statistics, L. (2018, 02 September). *One-way ANOVA - An introduction to when you should run this test and the test hypothesis* Available: <https://statistics.laerd.com/statistical-guides/one-way-anova-statistical-guide.php>
- [42] Takala, E.P. and Toivonen, R., "Placement of forearm surface EMG electrodes in the assessment of hand loading in manual tasks," (in eng), *Ergonomics*, vol. 56, no. 7, 2013, pp. 1159-66.
- [43] Tavakoli, M., Lourenco, J., and de Almeida, A.T., "3D Printed endoskeleton with a soft skin for upper-limb body actuated prosthesis," (in English), *2017 IEEE 5th Portuguese Meeting on Bioengineering (Enbeng)*, 2017.
- [44] Tomaszewski, M. (2018, 2 September). *Myo SDK MATLAB MEX Wrapper* Available: <https://www.mathworks.com/matlabcentral/fileexchange/55817-myo-sdk-matlab-mex-wrapper>
- [45] Vangelatos, Z., "Design of Upper limb prosthesis: Experimental Comparison of the Classic and Biomechatronic Extended Physiological Proprioception," School of Mechanical Engineering, National technical University of Athens, Athens, 2017.
- [46] Vanghetti, G., "Plastica dei Monconi a Scopo di Protesi Cinematica," *Arch. d. Ortop.*, vol. 16, no. 5, 1899, pp. 305-324..



- [47] Welford, A.T., "The measurement of sensory-motor performance : Survey and reappraisal of twelve years' progress" *Ergonomics*, vol. 3, no. 3, , 1960/07/01 1960 pp. 189-230.
- [48] Welford, A.T., *Fundamentals of skill* (Fundamentals of skill.). New York, NY, US: Methuen, 1968.
- [49] Yokokohji, Y. and Yoshikawa, T., "Bilateral Control of Master-Slave Manipulators for Ideal Kinesthetic Coupling - Formulation and Experiment," (in English), *Ieee Transactions on Robotics and Automation*, vol. 10, no. 5, Oct 1994, pp. 605-620.

## 10 Appendix A

In this appendix, the MATLAB code written for the realization of the target experiment is presented. The detailed programs written for the processing of the data along with the Simulink codes can be found in the CD-ROM attached with this thesis. In order for the reader to fully comprehend the cited code we will make a brief reference to three software tools used alongside MATLAB; Psychtoolbox for the construction of the experimental user interface, Myo Mex SDK MATAB Wrapper for the streaming of the EMG Data from Myo Armband and XIL API for the interface between the software(MATLAB) and the test hardware (dSPACE DS1103 controller board).

### 10.1 Psychophysics Toolbox Version 3 (PTB-3)

Psychophysics Toolbox Version 3 (PTB-3) is a free set of Matlab and GNU Octave functions for vision and neuroscience research. It makes it easy to synthesize and show accurately controlled visual and auditory stimuli and interact with the observer.

Psychtoolbox interfaces between MATLAB and the computer hardware. The routines at the core of Psychtoolbox provide access to the display frame buffer and color lookup table, allow synchronization with the vertical retrace, support sub-millisecond timing, expose raw OpenGL commands, support video playback and capture as well as low-latency audio or hardware triggers, and facilitate the collection of observer responses through regular and specialized input devices. Ancillary routines support common needs like color space transformations and the QUEST threshold seeking algorithm.

Every Psychtoolbox function has its own documentation available through the MATLAB “help” command, and, in the case of MEX files, through the function itself. The most important and generally useful functions, especially Screen, are in PsychBasic. A list of these functions is easily accessible in MATLAB just by typing “help Psychbasic” in the command line. The results of this command are demonstrated below. Furthermore, many demonstration scripts are provided with the toolbox. These scripts are available in the directory ‘PsychDemos’ located in the installation directory of the Psychtoolbox. These demo scripts are a good basis for the establishment of customized experiments. They show the implementation of the key functionality of the Psychtoolbox.

Detailed information, installation instructions and the system requirements can be found in the official web page of Psychtoolbox: <http://psychtoolbox.org/>, while the developers who want to contribute to this project can visit the main Git repository for development of Psychtoolbox-3 in GitHub: <https://github.com/Psychtoolbox-3/Psychtoolbox-3>.

```
>> help PsychBasic
```

```
    Beeper                - Play a nice beep tone of selectable
duration, frequency and volume.

    CharAvail              - Is a keypress available for GetChar?

    DisableKeysForKbCheck - Tell KbCheck and KbWait to ignore
specific keys.
```

DoNothing overhead.	- Does nothing. Used to time Matlab's
DrawFormattedText	- Drawing of formatted text into windows.
DrawFormattedText2 with more formatting options.	- Drawing of formatted text into windows,
FlushEvents	- Flush any unprocessed events.
FontInfo installed fonts.	- Return a struct array describing
Gestalt X.	- Query system configuration on OS 9 and OS
GetBusTicks	- Number of system bus ticks since startup.
GetBusTicksTick clock.	- Duration of one tick of the GetBusTicks
GetChar it.	- Wait for keyboard character and return
GetPID	- Get the process ID of the MATLAB process.
GetMouse	- Get mouse position.
GetMouseWheel mouse.	- Get mouse wheel position delta on a wheel
GetSecs	- Time since startup with high precision.
GetSecsTick clock.	- Duration of one tick of the GetSecs
GetTicks	- Number of 60.15 Hz ticks since startup.
GetTicksTick clock.	- Duration of one tick of the GetTicks
HideCursor	- Hide cursor.
IOPort	- A I/O driver for access to serial ports.
KbCheck	- Get instantaneous keyboard state.
KbEventAvail in ringbuffer.	- Return number of pending keyboard events
KbEventFlush ringbuffer.	- Remove all pending keyboard events in
KbEventGet ringbuffer.	- Get oldest pending keyboard event in
KbKeysAction value, depending on keys pressed.	- Return an incremented or decremented

KbName	- Convert keycode to key name and vice versa.
KbPressWait	- Wait for key press, make sure no keys pressed before.
KbQueueCreate	- Create keyboard queue.
KbQueueRelease	- Destroy keyboard queue.
KbQueueFlush	- Empty keyboard queue.
KbQueueStart	- Start recording of key presses into queue.
KbQueueStop	- Stop recording of key presses into queue.
KbQueueCheck	- Check keyboard queue for key presses/releases.
KbReleaseWait	- Wait until all keys on keyboard are released.
KbStrokeWait	- Wait for single, isolated key stroke.
KbTriggerWait	- Wait for trigger keys on keyboard.
KbWait	- Wait until at least one key is pressed and return its time.
ListenChar	- Start GetChar queue.
LoadPsychHID	- Helper function for loading PsychHID on MS-Windows.
MachAbsoluteTimeClockFrequency	- Mach Kernel time measurement.
PredictVisualOnsetForTime	- Predict stimulus onset for given Screen('Flip') 'when' timespec.
psychassert	- Drop in replacement for Matlabs assert().
psychlasterror	- Drop in replacement for Matlabs lasterror().
psychrethrow	- Drop in replacement for Matlabs rethrow().
PsychCV	- Miscellaneous C routines for computer vision and related stuff.
PsychDrawSprites2D	- Fast drawing of many 2D sprite textures.
PsychKinect	- Psychtoolbox driver for the Microsoft XBOX-360 Kinect.
PsychtoolboxDate	- Current version date, e.g. '1 August 1998'
PsychtoolboxVersion	- Current version number, e.g. 2.32

PsychWatchDog	- Watchdog mechanism and error handler for Psychtoolbox.
PsychTweak	- Tweak Psychtoolbox low-level operating parameters.
RemapMouse	- Map mouse position to stimulus position.
RestrictKeysForKbCheck	- Restrict operation of KbCheck et al. to a subset of keys on the keyboard.
Screen	- Control the video display. ** Type "Screen" for a list. **
SetMouse	- Set mouse position.
ShowCursor	- Show the cursor, and set cursor type.
Snd	- Play sounds.
VideoRefreshFromMeasurement	- Alternative calibration procedure to find exact video refresh interval.
WaitSecs	- Wait specified time.
WaitTicks	- Wait specified number of 60.15 Hz ticks.

## 10.2 Myo Mex SDK MATLAB Wrapper

Myo Mex SDK MATLAB Wrapper is a package that contains a simplified m-code class, MyoMex, that enables MATLAB users to stream data from Myo at up to 50Hz (Inertial Measurement Unit) and 200Hz (EMG and meta data), with only one command.

```
mm = MyoMex(); % Upon construction, MyoMex starts accumulating
streaming data in its myoData property
m = mm.myoData; % get MyoData object
% Data is now being pushed into log properties of m named,
% quat_log, gyro_log, accel_log, emg_log, etc.
% Data acquisition is non-blocking, too!
mm.delete(); % clean up
```

The IMU data includes estimated quaternion (orientation), three-axis gyroscope (angular velocity), and three-axis accelerometer (linear acceleration). The sEMG data includes 8 raw data channels plus the output of Myo's built-in gesture detection.

The package is available for download even from its repository on GitHub: <https://github.com/mark-toma/MyoMex>, where installation instructions and a tutorial are also available, or from the MathWorks File Exchange: <https://www.mathworks.com/matlabcentral/fileexchange/55817-myo-sdk-matlab-mex-wrapper>.

The first step toward interacting with the device involves the end user connecting to the physical Myo device using the Myo Connect desktop application and the included BLE dongle. Once connected, the API provided by Myo SDK enables third party code to interact with the device by calling into Myo Connect through a runtime library. Myo connect and Myo SDK must be downloaded from the site of

Thalmic Labs (<https://developer.thalmic.com/downloads> ) and installed. Following, a part from the "readme.txt" file attached to the downloaded package is quoted with instructions for its installation.

Proceed with installation of Myo Connect by launching the installed and

following its prompts.

Extract the SDK in your desired location in the filesystem, and take note

of the resulting file structure. For instance, you may choose to extract

the SDK contents to C:\ so that the resulting file structure looks like,

```
C:\myo-sdk-win-0.9.0\
```

```
bin\
```

```
...
```

```
include\
```

```
lib\
```

```
...
```

Following this example, we'll refer to "C:\myo-sdk-win-0.9.0" as the SDK\_PATH.

Next, add "SDK\_PATH\bin" to your PATH environment variable. This allows

your compiler to find the required DLL (i.e. myo32.dll or myo64.dll) when

linking against the Myo SDK. In this example, we just add

";C:\myo-sdk-win-0.9.0\bin" to the end of the current PATH variable.

```
# MATLAB PACKAGE INSTALLATION
```

Navigate to the location where you have extracted the contents of this package. Add the required directories to MATLAB's search path by typing,

```
>> install_myo_mex
```

Alternatively, you may choose to have this command save the path so that

```
>> install_myo_mex
```

Alternatively, you may choose to have this command save the path so that

you don't have to repeat this step in every new MATLAB session,

```
>> install_myo_mex save
```

```
# BUILDING MEX
```

Before you can build the mex file, you need to have a valid C++ compiler

installed on your system and configure mex to use this compiler. Assuming

that the former is already taken care of, type the following command and

follow the prompts to configure your C++ compiler.

```
>> mex -setup
```

To build the mex interface, you need to specify the location of the Myo

SDK. Recall your location for SDK\_PATH from above and type the command,

```
>> build_myo_mex SDK_PATH
```

Which in this example look like,

```
>> build_myo_mex C:\myo-sdk-win-0.9.0\
```

Now hopefully this completes without error. Upon success, you'll see command window output similar to the following,

```
>> build_myo_mex c:\myo-sdk-win-0.9.0
```

```

Changing directory to build directory:

'C:\path\to\matlab\package\Myo_SDK_MEX_Wrapper\MyoMex\myo_mex'

Evaluating mex command:

'mex -Ic:\myo-sdk-win-0.9.0\include -Lc:\myo-sdk-win-0.9.0\lib -
lmyo64 myo_mex.cpp'

Changing directory to original directory:

'C:\path\where\you\started'

MEX-file 'myo_mex' built successfully!

Possible errors are due to:

* Incorrect specification of SDK_PATH
* Corrupted Myo SDK file structure
* Failure to run 'install_myo_mex'
* Corrupted Myo_SDK_MEX_Wrapper file structure

If you did not add "SDK_PATH\bin" to the PATH environment variable, it
is
possible to build successfully but experience failures when using
MyoMex.

#####
#####

```

### 10.3 ASAM XIL API-dSPACE

dSPACE has its own user interface, ControlDesk, to monitor and control the experiments conducted using the dSPACE controller boards. However, the target experiment presented in Chapter 6 required to be monitored directly from the environment of MATLAB. Using the dSPACE ASAM XIL API .NET server in the M scripting language is the method dSPACE recommends in order to establish an interface between the dSPACE processor boards and MATLAB scripts, see Figure 10.1.

ASAM XIL API is a standard for the communication between test automation tools and test benches. It decouples the test software from real and virtual test systems. This makes it easy to reuse



test cases for different test systems. The standard also supports test benches at all stages of the development and testing process:

- Model-in-the-loop (MIL)
- Software-in-the-loop (MIL)
- Processor-in-the-loop (PIL)
- Hardware-in-the-loop (PIL)

dSPACE products can be used in all process phases and can work as a XIL API client as well as a XIL API server.

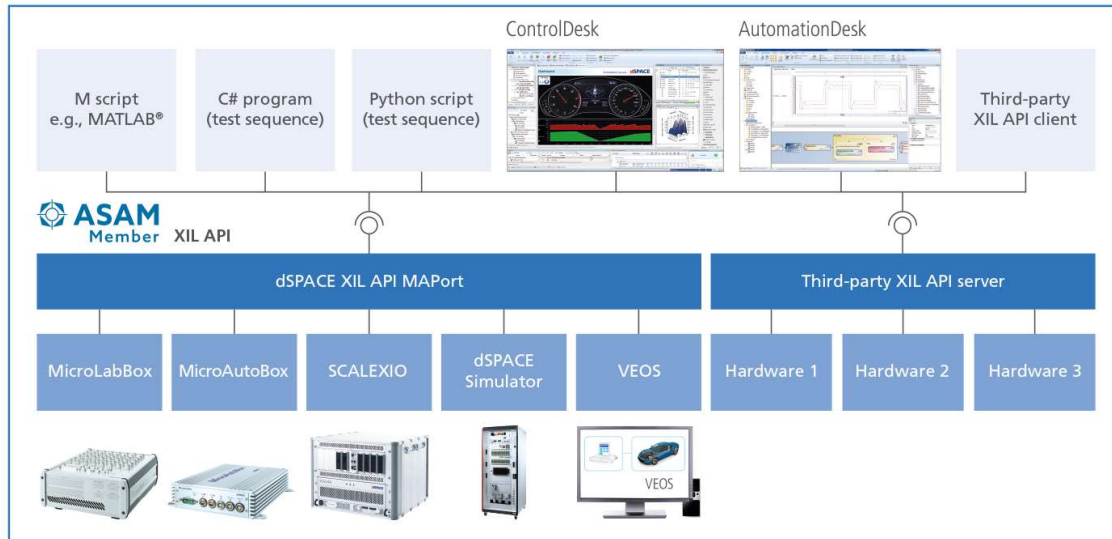


**Figure 10.1. Schematic diagram showing the connection between the dSPACE products and software tools.**

The dSPACE .NET Implementation of the ASAM XIL API 2.0.1 standard (dSPACE XIL API .NET server for short) currently covers large parts of the Model Access Port (MAPort) for access to real-time applications on dSPACE HIL and RCP platforms; larger parts of the common namespace of the XIL API, in which shared classes, data structures, and data types are defined for the XIL API Ports (especially the classes for acquisition data and real-time stimulation).

dSPACE XIL API gives the user the possibility to execute the following actions within the MATLAB environment, while a real time experiment runs:

- Reading and Writing Parameters
- Capturing
- Triggered measuring
- Processing the measurement results

Previously, the initialization of the XIL API .NET server and the creation of an MAPort configuration file have to be realized for the establishment of a successful connection between the dSPACE board and MATLAB. A complete tutorial can be downloaded from the following link of dSPACE: [https://www.dspace.com/support/patches/TASC/MLIB/discontinuation/MLIB\\_XIL\\_API\\_MigrationGuide/MLIB\\_XIL\\_API\\_MigrationGuide.pdf](https://www.dspace.com/support/patches/TASC/MLIB/discontinuation/MLIB_XIL_API_MigrationGuide/MLIB_XIL_API_MigrationGuide.pdf) .

The MAPort configuration file and the MATLAB script created for the conduction of the Classic EPP target experiment are demonstrated below as an example.

### **Configuration File**

With the following configuration file, the real-time application that is specified in the variable description file (SDF file) running on the modular system based on DS1103 can be accessed.

```
<?xml version="1.0" encoding="utf-8"?>
<PortConfigurations>
  <MAPortConfig>
    %Here the path of the Simulink model is set%

  <SystemDescriptionFile>C:\dSpace_test2\ClassicEpp\testclassic.sdf</SystemDescriptionFile>
  <PlatformName>ds1103</PlatformName>
</MAPortConfig>
</PortConfigurations>
```

### **XIL API .NET Initialization**

```
%Build the Simulink model
ModelName = 'TestClassic';
open_system(ModelName);
rtwbuild(ModelName);

% import XIL API .NET assemblies
NET.addAssembly('ASAM.XIL.Interfaces');
NET.addAssembly('ASAM.XIL.Implementation.TestbenchFactory');

import ASAM.XIL.Implementation.TestbenchFactory.Testbench.*;
import ASAM.XIL.Interfaces.Testbench.*;
import ASAM.XIL.Interfaces.Testbench.Common.Error.*;
import ASAM.XIL.Interfaces.Testbench.Common.ValueContainer.*;
import ASAM.XIL.Interfaces.Testbench.MAPort.*;

% The following lines must be adapted to the dSPACE platform used
%-----
% Set IsMPApplication to true if you are using a multiprocessor
platform
isMPApplication = true;
% Use an MAPort configuration file that is suitable for your platform
and
% simulation application See the folder Common\PortConfigurations for
some
% predefined configuration files
maPortConfigFile =
'C:\dSpace_test2\ClassicEpp\DemoMAPortConfiguration.xml';

% Set the name of the task here (specified in the application's TRC
file)
% Note: the default task name is "HostService" for PHS bus systems,
% "Periodic Task 1" for VEOS
task = 'HostService';
%-----
```

```

%-----
% Create a TestbenchFactory object; the TestbenchFactory is needed
to
% create the vendor-specific Testbench
%-----

myTestbenchFactory = TestbenchFactory();

%-----

% Create a dSPACE Testbench object; the Testbench object is the
central
% object to access factory objects for the creation of all kinds
of
% Testbench-specific objects
%-----

myTestbench =
myTestbenchFactory.CreateVendorSpecificTestbench('dSPACE GmbH', 'XIL
API', '2016-A');

%-----

% We need an MAPortFactory to create an MAPort and also a
ValueFactory
% to create ValueContainer objects
%-----

myMAPortFactory = myTestbench.MAPortFactory;
myValueFactory = myTestbench.ValueFactory;

%-----

% For multiprocessor platforms different tasknames and variable
names
% have to be used. Some variables are part of the subappliation
% "masterAppl", some belong to the subapplication "slaveAppl"
%-----

%-----

% Create and configure an MAPort object and start the simulation
%-----

fprintf('Creating MAPort...\n');
% Create an MAPort object using the MAPortFactory
demoMAPort = myMAPortFactory.CreateMAPort('DemoMAPort');
fprintf('...done\n');
% Load the MAPort configuration
maPortConfig = demoMAPort.LoadConfiguration(maPortConfigFile);
% Apply the MAPort configuration

```

## 10.4 Target Experiment Script

Here, the piece of code written in MATLAB for the realization the target experiments is quoted. According to the control topology tested this MATLAB script ace connection with the respective real time Simulink model.

```
%-----Initialize PsychToolbox-----%

RandStream.setGlobalStream(RandStream('mt19937ar','seed',sum(100*clock
))); % Seed rng stream
AssertOpenGL; % Ensure a compatible version of PTB is installed
GetSecs(); % Cache m-file for later, time-critical use
%-----%
%-----%

%-----Initialiaze MyoMex-----%
install_myo_mex; % adds directories to MATLAB search path
sdk_path = 'C:\myo-sdk-win-0.9.0'; % root path to Myo SDK
build_myo_mex(sdk_path); % builds myo_mex

mm = MyoMex(1); %MyoMex instant
ml = mm.myoData(1); %Get handle for MyoData
pause(0.5); %wait briefly for the first data frame to come in
ml.stopStreaming(); %stop the data streaminf
ml.clearLogs(); %clear the logs
%-----%
%-----%

%-----Constants-----%
%Color Constants
BG_COLOR = [255 255 255];
HIGH_COLOR = [255 0 0];
LOW_COLOR = [192 192 192];
TX_COLOR = [0 0 0];

%Pixel Constants
xCenter = 683; %x-center of the arc
yCenter = 384; %y-center of the arc
theta = 0 : 0.01 : pi; %angles of the arc
r = 300; %radius of the arc
x = r * cos(theta) + xCenter; %x-positions
y = r * sin(theta) + yCenter; %y-positions

targets = [35 62.5 90 130 170]'; %possible positions of the
targets
widths = [15 10 5 3 2]'; %possible widths of the targets
reps =15; %repetitions of distsance-width combination
%-----%
%-----%
```

```

%-----Path Construction-----%
ways = repmat([3 5; 5 1; 1 4; 4 2; 2 3],1,8)';
ways = reshape(ways,1,size(ways,1)*size(ways,2))';
ways((reps+1)*[1 2 3 4])=[];
path = targets(ways);
targetSizes = repelem(widths,length(path)-1); %Width Sequence
path = [path ;repmat(path(2:end),length(widths)-1,1)]; % Target
Sequecnce

distances = ones(length(path)-1,1); %Distance Sequence
for i = 1:length(distances)
    distances(i) = abs(path(i+1)-path(i));
end

a_sta = path(1:end-1); %Locations(angles) of the starting points
a_tar = path(2:end); %Locations(angles) of the target points

%Locations(pixels) of the starting points
locations_sta = [ r * cosd(a_sta) + xCenter, r * sind(a_sta) +
yCenter];
%Locations(pixels) of the target points
locations_tar = [ r * cosd(a_tar) + xCenter, r * sind(a_tar) +
yCenter];

%Matrix with all the prementioned variables
conditions = [targetSizes distances locations_sta a_sta
locations_tar a_tar];
%-----%
%-----%

%-----Variables Definition-----%
targetWidth =conditions(:,1);
s_r = r*targetWidth*(pi/180)/2; %length of the arc from the
beginning of a target to its center

radius = sqrt(2)*r*sqrt((1-cosd(targetWidth/2))); %radius of the
target in pixels/cosine law
j = 1;
remedialTrial = false;
out=0;
S_p=zeros(length(conditions),2); %Starting points
MT =zeros(length(conditions),1); %Movemnt time
DT=zeros(length(conditions),1); %Dwell time
success= zeros(length(conditions),1); %Success matrix
xy=[]; %Current position
Angles = 'Model Root/position s_deg/In1'; %Load the path name of
the slave motor position on the Simlulink model

%-----%
%-----%

```

```

%-----Beginning of the experiment-----%
try
    %Open experimental screen on last screen reported by Screens
    screen = max(Screen('Screens'));
    PsychImaging('PrepareConfiguration');
    PsychImaging('AddTask', 'General', 'UseVirtualFramebuffer');
    [windowPtr, rect] = PsychImaging('OpenWindow', screen, BG_COLOR);

    m1.startStreaming(); %Start streaming data from Myo

    while(j <= length(conditions))
        Screen('Flip',windowPtr); %Refresh the screen

        %Show if last trial was succesful or unsuccessful
        if j > 1
            if success(j-1) == 1
                DrawFormattedText(windowPtr,'Success','center',100,[0 255
0]);
            else
                DrawFormattedText(windowPtr,'Fail','center',100,[255 0 0
]);
            end
        end

        %First trial, show instructions
        DrawFormattedText(windowPtr,'Reach the highlighted target to
begin','center',rect(4) - 32,TX_COLOR);
        %Draw the arc
        Screen('FrameArc',windowPtr,[0 255 0],[xCenter-r yCenter-r
xCenter+r yCenter+r],90,180,2);

        %Render each node, target node is highlighted
        targetNode = conditions(j,6:7);
        nextNode = conditions(j,3:4);

        %Draw the starting node
        if(j <= length(conditions))
            Screen('Filloval',windowPtr,LOW_COLOR, ...
[nextNode(1) - radius(j), nextNode(2) - radius(j), ...
nextNode(1) + radius(j), nextNode(2) + radius(j)]);
        end

        %Draw the target node
        Screen('Filloval',windowPtr,HIGH_COLOR, ...
[targetNode(1) - radius(j), targetNode(2) - radius(j), ...
targetNode(1) + radius(j), targetNode(2) + radius(j)]);

        ShowCursor(0); %Show up the cursor
        [~, StimulusOnsetTime] = Screen('Flip',windowPtr,0,1);

        %Set the mouse on the starting node/Only at the beginning of the
experiment
        if (j==1)

```

```

        SetMouse(nextNode(1),nextNode(2));
        amor_st = 90; %Angle of the first starting node/Reference
angle
        amor = amor_st;
    end

    [startX,startY] = GetMouse(screen); %Co-ordinates of the mouse
position
    xy=[xy ; startX startY];

    S_p(j,:) = [startX,startY]; % Starting point of the next
movement

    %flags for beginning of movement, inside/outside target and
trial finish
    start = 0;
    out =1;
    finish = 0;

    %-----While next movement has non started-----%
    while ~start

        %Read the position of the Slave motor
        readVal = demoMAPort.Read(Angles);
        am = readVal.Value;

        %Check bounds
        if (am <=90 && am >= -75)
            amor = amor_st + am;
        end

        %Set the cursor at the point given by the position of the
        %slave motor
        pos = [r*cosd(amor)+xCenter r*sind(amor)+yCenter];
        SetMouse(pos(1),pos(2));
        [x,y,~] = GetMouse(screen);%Get the cursor position
        xy =[xy;x y];

        %Check if the movement has started
        if(x~=startX || y~=startY)
            start=1;
            StartingTime= GetSecs();
        end
    end

    %-----While next movement has not finished-----%
    while ~finish

        %Read the position of the Slave motor
        readVal = demoMAPort.Read(Angles);
        am = readVal.Value;

        %Check bounds

```

```

        if (am <=90 && am >= -75)
            amor = amor_st + am;
        end

        %Set the cursor at the point given by the position of the
        %slave motor
        pos = [r*cosd(amor)+xCenter r*sind(amor)+yCenter];
        SetMouse(pos(1),pos(2));
        [endX,endY,~] = GetMouse(screen);%Get the cursor position
        xy = [xy ; endX endY];

        %Check if the cursor has reached the target
        if(dist([pos(1),pos(2)],targetNode') <= s_r(j))

            finish = 1; %We have reached the target.We'll finish
            winners or losers,but we'll finish
            EndingTime= GetSecs(); %Get the moment that the cursor
            reached the target

            out =0; %Not out anymore
            time = EndingTime;

            %Check what happens while cursor is inside the
            target/Time Limit=1s
            while (time-EndingTime<=1)

                time = GetSecs();

                %Read the position of the Slave motor
                readVal = demoMAPort.Read(Angles);
                am = readVal.Value;
                amor = amor_st + am;

                %Set the cursor at the point given by the position of
                the

                %slave motor
                pos = [r*cosd(amor)+xCenter r*sind(amor)+yCenter];
                SetMouse(pos(1),pos(2));

                [endX,endY,~] = GetMouse(screen);%Get the cursor
                position

                xy =[xy; endX endY];

                %Check if the cursor overshoot the target and go to
                %the next target
                if (dist([pos(1),pos(2)],targetNode') > s_r(j))
                    out = 1;
                    timeout = GetSecs();
                    break;
                end

            end

        end

    end
end

```



```

end

    %Movement Time
    MT(j) = EndingTime - StartingTime;
    GoingTime = GetSecs();
    success(j)= ~out;
    %Duel Time
    DT(j) = GoingTime-EndingTime;

    j = j + 1;

end % End of sequence

    %Ens of experiment/Refresh the screen/Wait keyboard input for
    %exit
    Screen('Flip',windowPtr);
    DrawFormattedText(windowPtr,'Press any key to
continue','center','center',TX_COLOR);
    Screen('Flip',windowPtr,1,0);
    KbWait([],3);
    %end % End of condition
catch E
    On error
    Screen('CloseAll');
    disp(E.message);
    disp('You are in debug mode. Type ''return'' to exit');
    disp('*** DATA HAS NOT BEEN SAVED: TYPE ''return'' TO SAVE ***');
    keyboard;

end

%Close the screen
Screen('CloseAll');
%-----END of EXPERIMENT-----%
%-----%

%Angle of starting points
S_a = atand((S_p(:,2)-yCenter)./(S_p(:,1)-xCenter));
S_a(S_a<0)= S_a(S_a<0)+180;

%Position of ending points
R_p = [S_p(2:end,:); xy(end,1) xy(end,2)];

%Angle of ending points
R_a= atand((R_p(:,2)-yCenter)./(R_p(:,1)-xCenter));
R_a(R_a<0)= R_a(R_a<0)+180;

%Path of the cursor during experiment in angles
a = atand((xy(:,2)-yCenter)./(xy(:,1)-xCenter));
a(a<0)= a(a<0)+180;

%Real distances
De = abs(S_a-R_a);

    %Error between the center of the target node and the actual reaching
angle
    Werr = a_tar-R_a;

%Dispose MAPort
demoMAPort.Dispose();

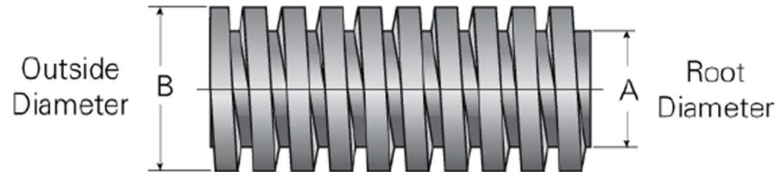
```

## 11 Appendix B

In this appendix, we present the datasheets of the most important electromechanical parts of the laboratory setup.

**Metric Lead Screw 4 mm x 1.22 mm Stainless Steel**

Call 855-HELIXLT or visit us online at [www.helixlinear.com](http://www.helixlinear.com) to configure and order your Metric Lead Screw 4 mm x 1.22 mm Stainless Steel today!



**Product Info**

Part Number	016048S
Thread Direction	RH/LH
Screw Material	Stainless Steel

**Details**

Lead [mm]	1.22
Starts	2
Pitch [mm]	0.6
Diameter [mm]	4
End Code for Types 1,2,3,5 [* Journals may show tracings of the thread]	2
End Code for Type 4 [* Journals may show tracings of the thread]	1
Diameter Code	016
Lead Code	048

**Dimensions**

A [mm]	2.34
B [mm]	3.84

**Performance Specifications**

Efficiency [%]	37-53
Lead Accuracy +/- [in/in]	0.0003





# Disc Couplings Clamping

For Servo Motors

**CPDW (Double Disc Type)**

**CPDT (Single Disc Type)**

**Parts:**

Main Body	Disc	Shaft	Key	Cap Screw
CPDW	CPDW	CPDW	CPDW	CPDW

Part Number	Type	d1, d2 Selection (d1=d2)										Unit Price
		D	d1	d2	F	G	H	I	J	K	L	
19	CPDW	19	4	5	6	7	8	9	10	11	12	CPDW/CPDT
25	CPDW	25	6	8	10	12	14	16	18	20	22	CPDW/CPDT
32	CPDW	32	8	10	12	14	16	18	20	22	24	CPDW/CPDT
40	CPDT	40	10	12	14	16	18	20	22	24	25	CPDT
50	CPDT	50	14	15	16	17	18	19	20	22	24	CPDT

## Characteristic Values

Part Number	Type	d1, d2 Selection (d1=d2)										Unit Price
		D	d1	d2	F	G	H	I	J	K	L	
19	CPDW	19	4	5	6	7	8	9	10	11	12	CPDW/CPDT
25	CPDW	25	6	8	10	12	14	16	18	20	22	CPDW/CPDT
32	CPDW	32	8	10	12	14	16	18	20	22	24	CPDW/CPDT
40	CPDT	40	10	12	14	16	18	20	22	24	25	CPDT
50	CPDT	50	14	15	16	17	18	19	20	22	24	CPDT

CPDW (Double Disc Type) and CPDT (Single Disc Type) are shown in the table. When multiple misalignments are occurring simultaneously, the allowable maximum value of each will be reduced to 1/2.

Part Number: CPDW40 - 12 - 14 - 16 - 18 - 20 - 22 - 24 - 25

# Disc Couplings "Servo-Fine"

High Rigidity Clamping / High Positioning Accuracy Clamping / Keywayed Bore

For Servo Motors

**SCPW (Double Disc Type)**

**SCPD (Single Disc Type)**

**Parts:**

Main Body	Disc	Shaft	Key	Cap Screw
SCPW	SCPW	SCPW	SCPW	SCPW

Part Number	Type	d1, d2 Selection (d1=d2)										Unit Price
		D	d1	d2	F	G	H	I	J	K	L	
19	SCPW	19	4	5	6	7	8	9	10	11	12	SCPW/SCPD
25	SCPW	25	6	8	10	12	14	16	18	20	22	SCPW/SCPD
32	SCPW	32	8	10	12	14	16	18	20	22	24	SCPW/SCPD
40	SCPD	40	10	12	14	16	18	20	22	24	25	SCPD
50	SCPD	50	14	15	16	17	18	19	20	22	24	SCPD

## Characteristic Values

Part Number	Type	d1, d2 Selection (d1=d2)										Unit Price
		D	d1	d2	F	G	H	I	J	K	L	
19	SCPW	19	4	5	6	7	8	9	10	11	12	SCPW/SCPD
25	SCPW	25	6	8	10	12	14	16	18	20	22	SCPW/SCPD
32	SCPW	32	8	10	12	14	16	18	20	22	24	SCPW/SCPD
40	SCPD	40	10	12	14	16	18	20	22	24	25	SCPD
50	SCPD	50	14	15	16	17	18	19	20	22	24	SCPD

SCPW (Double Disc Type) and SCPD (Single Disc Type) are shown in the table. When multiple misalignments are occurring simultaneously, the allowable maximum value of each will be reduced to 1/2.

Part Number: SCPW40 - 12 - 14 - 16 - 18 - 20 - 22 - 24 - 25

For Servo Motors

**SCPW (Double Disc Type)**

**SCPD (Single Disc Type)**

**Parts:**

Main Body	Disc	Shaft	Key	Cap Screw
SCPW	SCPW	SCPW	SCPW	SCPW

Part Number	Type	d1, d2 Selection (d1=d2)										Unit Price
		D	d1	d2	F	G	H	I	J	K	L	
19	SCPW	19	4	5	6	7	8	9	10	11	12	SCPW/SCPD
25	SCPW	25	6	8	10	12	14	16	18	20	22	SCPW/SCPD
32	SCPW	32	8	10	12	14	16	18	20	22	24	SCPW/SCPD
40	SCPD	40	10	12	14	16	18	20	22	24	25	SCPD
50	SCPD	50	14	15	16	17	18	19	20	22	24	SCPD

## Characteristic Values

Part Number	Type	d1, d2 Selection (d1=d2)										Unit Price
		D	d1	d2	F	G	H	I	J	K	L	
19	SCPW	19	4	5	6	7	8	9	10	11	12	SCPW/SCPD
25	SCPW	25	6	8	10	12	14	16	18	20	22	SCPW/SCPD
32	SCPW	32	8	10	12	14	16	18	20	22	24	SCPW/SCPD
40	SCPD	40	10	12	14	16	18	20	22	24	25	SCPD
50	SCPD	50	14	15	16	17	18	19	20	22	24	SCPD

SCPW (Double Disc Type) and SCPD (Single Disc Type) are shown in the table. When multiple misalignments are occurring simultaneously, the allowable maximum value of each will be reduced to 1/2.

Part Number: SCPW40 - 12 - 14 - 16 - 18 - 20 - 22 - 24 - 25

For Servo Motors

**SCPW (Double Disc Type)**

**SCPD (Single Disc Type)**

**Parts:**

Main Body	Disc	Shaft	Key	Cap Screw
SCPW	SCPW	SCPW	SCPW	SCPW

Part Number	Type	d1, d2 Selection (d1=d2)										Unit Price
		D	d1	d2	F	G	H	I	J	K	L	
19	SCPW	19	4	5	6	7	8	9	10	11	12	SCPW/SCPD
25	SCPW	25	6	8	10	12	14	16	18	20	22	SCPW/SCPD
32	SCPW	32	8	10	12	14	16	18	20	22	24	SCPW/SCPD
40	SCPD	40	10	12	14	16	18	20	22	24	25	SCPD
50	SCPD	50	14	15	16	17	18	19	20	22	24	SCPD

## Characteristic Values

Part Number	Type	d1, d2 Selection (d1=d2)										Unit Price
		D	d1	d2	F	G	H	I	J	K	L	
19	SCPW	19	4	5	6	7	8	9	10	11	12	SCPW/SCPD
25	SCPW	25	6	8	10	12	14	16	18	20	22	SCPW/SCPD
32	SCPW	32	8	10	12	14	16	18	20	22	24	SCPW/SCPD
40	SCPD	40	10	12	14	16	18	20	22	24	25	SCPD
50	SCPD	50	14	15	16	17	18	19	20	22	24	SCPD

SCPW (Double Disc Type) and SCPD (Single Disc Type) are shown in the table. When multiple misalignments are occurring simultaneously, the allowable maximum value of each will be reduced to 1/2.

Part Number: SCPW40 - 12 - 14 - 16 - 18 - 20 - 22 - 24 - 25

For Servo Motors

**SCPW (Double Disc Type)**

**SCPD (Single Disc Type)**

**Parts:**

Main Body	Disc	Shaft	Key	Cap Screw
SCPW	SCPW	SCPW	SCPW	SCPW

Part Number	Type	d1, d2 Selection (d1=d2)										Unit Price
		D	d1	d2	F	G	H	I	J	K	L	
19	SCPW	19	4	5	6	7	8	9	10	11	12	SCPW/SCPD
25	SCPW	25	6	8	10	12	14	16	18	20	22	SCPW/SCPD
32	SCPW	32	8	10	12	14	16	18	20	22	24	SCPW/SCPD
40	SCPD	40	10	12	14	16	18	20	22	24	25	SCPD
50	SCPD	50	14	15	16	17	18	19	20	22	24	SCPD

## Characteristic Values

Part Number	Type	d1, d2 Selection (d1=d2)										Unit Price
		D	d1	d2	F	G	H	I	J	K	L	
19	SCPW	19	4	5	6	7	8	9	10	11	12	SCPW/SCPD
25	SCPW	25	6	8	10	12	14	16	18	20	22	SCPW/SCPD
32	SCPW	32	8	10	12	14	16	18	20	22	24	SCPW/SCPD
40	SCPD	40	10	12	14	16	18	20	22	24	25	SCPD
50	SCPD	50	14	15	16	17	18	19	20	22	24	SCPD

SCPW (Double Disc Type) and SCPD (Single Disc Type) are shown in the table. When multiple misalignments are occurring simultaneously, the allowable maximum value of each will be reduced to 1/2.

Part Number: SCPW40 - 12 - 14 - 16 - 18 - 20 - 22 - 24 - 25

For Servo Motors

**SCPW (Double Disc Type)**

**SCPD (Single Disc Type)**

**Parts:**

Main Body	Disc	Shaft	Key	Cap Screw
SCPW	SCPW	SCPW	SCPW	SCPW

Part Number	Type	d1, d2 Selection (d1=d2)										Unit Price
		D	d1	d2	F	G	H	I	J	K	L	
19	SCPW	19	4	5	6	7	8	9	10	11	12	SCPW/SCPD
25	SCPW	25	6	8	10	12	14	16	18	20	22	SCPW/SCPD
32	SCPW	32	8	10	12	14	16	18	20	22	24	SCPW/SCPD
40	SCPD	40	10	12	14	16	18	20	22	24	25	SCPD
50	SCPD	50	14	15	16	17	18	19	20	22	24	SCPD

## Characteristic Values

Part Number	Type	d1, d2 Selection (d1=d2)										Unit Price
		D	d1	d2	F	G	H	I	J	K	L	
19	SCPW	19	4	5	6	7	8	9	10	11	12	SCPW/SCPD
25	SCPW	25	6	8	10	12	14	16	18	20	22	SCPW/SCPD
32	SCPW	32	8	10	12	14	16	18	20	22	24	SCPW/SCPD
40	SCPD	40	10	12	14	16	18	20	22	24	25	SCPD
50	SCPD	50	14	15	16	17	18	19	20	22	24	SCPD

SCPW (Double Disc Type) and SCPD (Single Disc Type) are shown in the table. When multiple misalignments are occurring simultaneously, the allowable maximum value of each will be reduced to 1/2.

Part Number: SCPW40 - 12 - 14 - 16 - 18 - 20 - 22 - 24 - 25

For Servo Motors

**SCPW (Double Disc Type)**

**SCPD (Single Disc Type)**

**Parts:**

Main Body	Disc	Shaft	Key	Cap Screw
SCPW	SCPW	SCPW	SCPW	SCPW





# Pulleys for Round Belts

## Set Screw Type

# Pulleys for Round Belts

## Clamping Type

**Technical Specifications:**

- U Groove:** Dimensions include  $\frac{1}{2}$  (1/2"),  $\frac{1}{4}$  (1/4"),  $\frac{1}{8}$  (1/8"),  $\frac{1}{16}$  (1/16"),  $\frac{1}{32}$  (1/32"),  $\frac{1}{64}$  (1/64").
- Trapezoidal Groove:** Dimensions include  $\frac{1}{2}$  (1/2"),  $\frac{1}{4}$  (1/4"),  $\frac{1}{8}$  (1/8"),  $\frac{1}{16}$  (1/16"),  $\frac{1}{32}$  (1/32"),  $\frac{1}{64}$  (1/64").
- Set Screw Type:** Dimensions include  $\frac{1}{2}$  (1/2"),  $\frac{1}{4}$  (1/4"),  $\frac{1}{8}$  (1/8"),  $\frac{1}{16}$  (1/16"),  $\frac{1}{32}$  (1/32"),  $\frac{1}{64}$  (1/64").

**Technical Specifications:**

- U Groove:** Dimensions include  $\frac{1}{2}$  (1/2"),  $\frac{1}{4}$  (1/4"),  $\frac{1}{8}$  (1/8"),  $\frac{1}{16}$  (1/16"),  $\frac{1}{32}$  (1/32"),  $\frac{1}{64}$  (1/64").
- Trapezoidal Groove:** Dimensions include  $\frac{1}{2}$  (1/2"),  $\frac{1}{4}$  (1/4"),  $\frac{1}{8}$  (1/8"),  $\frac{1}{16}$  (1/16"),  $\frac{1}{32}$  (1/32"),  $\frac{1}{64}$  (1/64").
- Clamping Type:** Dimensions include  $\frac{1}{2}$  (1/2"),  $\frac{1}{4}$  (1/4"),  $\frac{1}{8}$  (1/8"),  $\frac{1}{16}$  (1/16"),  $\frac{1}{32}$  (1/32"),  $\frac{1}{64}$  (1/64").

Part Number	Part Name	Material	Surface Treatment	U Groove	Trapezoidal Groove	Set Screw Type	Clamping Type	Unit Price
1	MBR100	EN 1.1191	Black Oxide	MBR100	MBR100	MBR100	MBR100	1
2	MBR200	EN 1.1191	Black Oxide	MBR200	MBR200	MBR200	MBR200	2
3	MBR300	EN 1.1191	Black Oxide	MBR300	MBR300	MBR300	MBR300	3
4	MBR400	EN 1.1191	Black Oxide	MBR400	MBR400	MBR400	MBR400	4
5	MBR500	EN 1.1191	Black Oxide	MBR500	MBR500	MBR500	MBR500	5
6	MBR600	EN 1.1191	Black Oxide	MBR600	MBR600	MBR600	MBR600	6
7	MBR700	EN 1.1191	Black Oxide	MBR700	MBR700	MBR700	MBR700	7
8	MBR800	EN 1.1191	Black Oxide	MBR800	MBR800	MBR800	MBR800	8
9	MBR900	EN 1.1191	Black Oxide	MBR900	MBR900	MBR900	MBR900	9
10	MBR1000	EN 1.1191	Black Oxide	MBR1000	MBR1000	MBR1000	MBR1000	10

Part Number	Part Name	Material	Surface Treatment	U Groove	Trapezoidal Groove	Set Screw Type	Clamping Type	Unit Price
1	MBR100	EN 1.1191	Black Oxide	MBR100	MBR100	MBR100	MBR100	1
2	MBR200	EN 1.1191	Black Oxide	MBR200	MBR200	MBR200	MBR200	2
3	MBR300	EN 1.1191	Black Oxide	MBR300	MBR300	MBR300	MBR300	3
4	MBR400	EN 1.1191	Black Oxide	MBR400	MBR400	MBR400	MBR400	4
5	MBR500	EN 1.1191	Black Oxide	MBR500	MBR500	MBR500	MBR500	5
6	MBR600	EN 1.1191	Black Oxide	MBR600	MBR600	MBR600	MBR600	6
7	MBR700	EN 1.1191	Black Oxide	MBR700	MBR700	MBR700	MBR700	7
8	MBR800	EN 1.1191	Black Oxide	MBR800	MBR800	MBR800	MBR800	8
9	MBR900	EN 1.1191	Black Oxide	MBR900	MBR900	MBR900	MBR900	9
10	MBR1000	EN 1.1191	Black Oxide	MBR1000	MBR1000	MBR1000	MBR1000	10

**Technical Specifications:**

- U Groove:** Dimensions include  $\frac{1}{2}$  (1/2"),  $\frac{1}{4}$  (1/4"),  $\frac{1}{8}$  (1/8"),  $\frac{1}{16}$  (1/16"),  $\frac{1}{32}$  (1/32"),  $\frac{1}{64}$  (1/64").
- Trapezoidal Groove:** Dimensions include  $\frac{1}{2}$  (1/2"),  $\frac{1}{4}$  (1/4"),  $\frac{1}{8}$  (1/8"),  $\frac{1}{16}$  (1/16"),  $\frac{1}{32}$  (1/32"),  $\frac{1}{64}$  (1/64").
- Set Screw Type:** Dimensions include  $\frac{1}{2}$  (1/2"),  $\frac{1}{4}$  (1/4"),  $\frac{1}{8}$  (1/8"),  $\frac{1}{16}$  (1/16"),  $\frac{1}{32}$  (1/32"),  $\frac{1}{64}$  (1/64").

**Technical Specifications:**

- U Groove:** Dimensions include  $\frac{1}{2}$  (1/2"),  $\frac{1}{4}$  (1/4"),  $\frac{1}{8}$  (1/8"),  $\frac{1}{16}$  (1/16"),  $\frac{1}{32}$  (1/32"),  $\frac{1}{64}$  (1/64").
- Trapezoidal Groove:** Dimensions include  $\frac{1}{2}$  (1/2"),  $\frac{1}{4}$  (1/4"),  $\frac{1}{8}$  (1/8"),  $\frac{1}{16}$  (1/16"),  $\frac{1}{32}$  (1/32"),  $\frac{1}{64}$  (1/64").
- Clamping Type:** Dimensions include  $\frac{1}{2}$  (1/2"),  $\frac{1}{4}$  (1/4"),  $\frac{1}{8}$  (1/8"),  $\frac{1}{16}$  (1/16"),  $\frac{1}{32}$  (1/32"),  $\frac{1}{64}$  (1/64").

**Description**

The AZBDC10A4 PWM servo drive is designed to drive brushless and brushed DC motors at a high switching frequency. To increase system reliability and to reduce cabling costs, the drive is designed for direct integration into your PCB. The AZBDC10A4 is fully protected against over-voltage, under-voltage, over-current, over-heating, and short-circuits. A single digital output indicates operating status. The drive interfaces with digital controllers that have digital PWM output. The PWM IN duty cycle determines the output current and DIR input determines the direction of rotation. This servo drive requires only a single unregulated isolated DC power supply, and is fully RoHS (Reduction of Hazardous Substances) compliant.

See Part Numbering Information on last page of datasheet for additional ordering options.

**Power Range**

Peak Current	10 A
Continuous Current	5 A
Supply Voltage	10 - 36 VDC

**Features**

- ▲ Four Quadrant Regenerative Operation
- ▲ Direct Board-to-Board Integration
- ▲ Lightweight
- ▲ High Switching Frequency
- ▲ Wide Temperature Range
- ▲ Differential Input Command
- ▲ Digital Fault Output Monitor
- ▲ Current Monitor Output
- ▲ Single Supply Operation
- ▲ Compact Size
- ▲ High Power Density
- ▲ 12VDC Operation

**HARDWARE PROTECTION**

- Over-Voltage
- Under-Voltage
- Over-Current
- Over-Temperature
- Short-circuit (phase-phase)
- Short-circuit (phase-ground)

**INPUTS/OUTPUTS**

- Digital Fault Output
- Digital Inhibit Input
- Analog Current Monitor
- Analog Command Input

**FEEDBACK SUPPORTED**

- Hall Sensors

**MODES OF OPERATION**

- Current

**COMMUTATION**

- Trapezoidal

**MOTORS SUPPORTED**

- Three Phase (Brushless)
- Single Phase (Brushed, Voice Coil, Inductive Load)

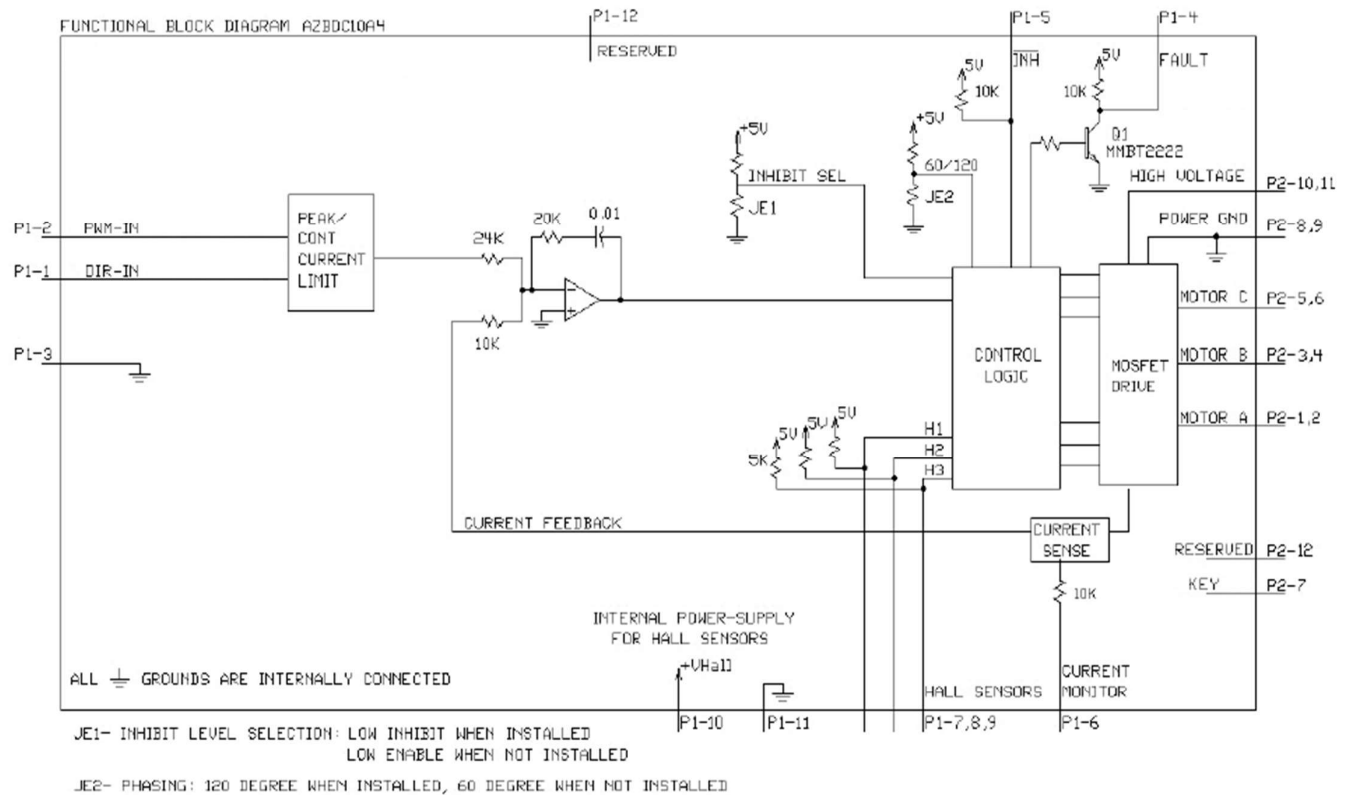
**COMMAND SOURCE**

- PWM

**COMPLIANCES & AGENCY APPROVALS**

- RoHS
- UL/cUL Pending
- CE Pending



**BLOCK DIAGRAM**

**Information on Approvals and Compliances**


RoHS (Reduction of Hazardous Substances) is intended to prevent hazardous substances such as lead from being manufactured in electrical and electronic equipment.

## SPECIFICATIONS

Power Specifications		
Description	Units	Value
DC Supply Voltage Range	VDC	10 - 36
DC Bus Under Voltage Limit	VDC	8
DC Bus Over Voltage Limit	VDC	40
Maximum Peak Output Current <sup>1</sup>	A	10
Maximum Continuous Output Current	A	5
Maximum Continuous Output Power	W	171
Maximum Power Dissipation at Continuous Current	W	9
Minimum Load Inductance (Line-To-Line) <sup>2</sup>	μH	100
Internal Bus Capacitance <sup>3</sup>	μF	23.5
Low Voltage Supply Outputs	-	+5 VDC (30 mA)
Switching Frequency	kHz	40
Control Specifications		
Description	Units	Value
Command Sources	-	PWM
PWM Input Frequency Range	-	10 - 25
Feedback Supported	-	Halls
Commutation Methods	-	Trapezoidal
Modes of Operation	-	Current
Motors Supported	-	Three Phase (Brushless), Single Phase (Brushed, Voice Coil, Inductive Load)
Hardware Protection	-	Invalid Commutation Feedback, Over Current, Over Temperature, Over Voltage, Under Voltage, Short Circuit (Phase-Phase & Phase-Ground)
Mechanical Specifications		
Description	Units	Value
Agency Approvals	-	RoHS, UL/cUL Pending, CE Pending
Size (H x W x D)	mm (in)	38.1 x 38.1 x 7.34 (1.50 x 1.50 x 0.29)
Weight	g (oz)	8.5 (0.3)
Operating Temperature Range <sup>4</sup>	°C (°F)	0 - 85 (32 - 185)
Storage Temperature Range	°C (°F)	-40 - 85 (-40 - 185)
Relative Humidity	-	0 - 90% Non-Condensing
Form Factor	-	PCB Mounted
P1 Connector	-	12-pin, 1.27 mm spaced header
P2 Connector	-	12-pin, 1.27 mm spaced header

### Notes

- Maximum duration of peak current is ~2 seconds. Peak RMS value must not exceed continuous current rating of the drive.
- Lower inductance is acceptable for bus voltages well below maximum. Use external inductance to meet requirements.
- Requires a minimum of 47 μF external bus capacitance between the DC Supply and Power Ground.
- Additional cooling and/or heatsink may be required to achieve rated performance.

## PIN FUNCTIONS

P1 - Signal Connector			
Pin	Name	Description / Notes	I/O
1	DIRECTION	Direction Input (+5V)	I
2	PWM / IN	10 – 25 kHz pulse width modulated digital input command (+5V). Input duty cycle commands the output current.	I
3	SIGNAL GND	Signal Ground (Common With Power Ground).	GND
4	FAULT OUT	TTL level (+5 V) output becomes high when power devices are disabled due to at least one of the following conditions: inhibit, invalid Hall state, output short circuit, over voltage, over temperature, power-up reset.	O
5	$\overline{\text{INHIBIT IN}}$	TTL level (+5 V) inhibit/enable input. Leave open to enable drive. Pull to ground to inhibit drive. Inhibit turns off all power devices.	I
6	CURRENT MONITOR	Current Monitor. Analog output signal proportional to the actual current output. Scaling is 2 A/V. Measure relative to signal ground.	O
7	HALL 3	Single-ended Hall/Commutation Sensor Inputs (+5 V logic level)	I
8	HALL 2*		I
9	HALL 1		I
10	+V HALL OUT	Low Power Supply For Hall Sensors (+5 V @ 30 mA). Referenced to signal ground. Short circuit protected.	O
11	SIGNAL GND	Signal Ground (Common With Power Ground).	GND
12	RESERVED	Reserved	-

P2 - Power Connector			
Pin	Name	Description / Notes	I/O
1	MOTOR A	Motor Phase Outputs. Current output distributed equally across 2 pins per motor phase, 3A continuous current carrying capacity per pin.	O
2	MOTOR A		O
3	MOTOR B		O
4	MOTOR B		O
5	MOTOR C		O
6	MOTOR C		O
7	NC (KEY)	No Connection. Keyed pin.	-
8	PWR GND	Power Ground (Common With Signal Ground). 3A Continuous Current Rating Per Pin	GND
9	PWR GND		GND
10	HV IN	DC Power Input. 3A Continuous Current Rating Per Pin. Requires a minimum of 47 $\mu$ F external capacitance between HV IN and PWR GND pins.	I
11	HV IN		I
12	RESERVED	Reserved	-

\*For use with Single Phase (Brushed) motors, ground Hall 2 and only connect motor leads to Motor A and Motor B.

**Note:** P1 and P2 are identical 12-pin headers. To avoid damage to the drive, be sure when plugging or soldering the drive into a PCB or interface card that the drive orientation is correct. P1 and P2 are labeled on the PCB silkscreen. Pin 7 on P2 is keyed to differentiate it from P1. Consult the mounting dimension drawing on page 6 of this datasheet for an illustration of the locations of P1 and P2.

## HARDWARE SETTINGS

### Jumper Settings

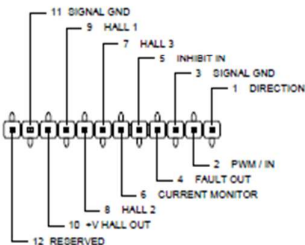
Jumpers are SMT, 0 ohm resistors located on the underside of the drive PCB. By default, the drive is configured with the jumpers installed. Typical drive operation will not require the jumpers to be removed. Please contact the factory before jumper removal.

Jumper		Description	Configuration	
		SMT Jumper (0 $\Omega$ Resistor)	Not Installed	Installed
JE1	Inhibit logic. Sets the logic level of inhibit pins. Labeled JE1 on the PCB of the drive.		Low Enable	Low Inhibit
JE2	Hall sensor phasing. Selects 120 or 60 degree commutation phasing. Labeled JE2 on the PCB of the drive.		60 degree	120 degree

## MECHANICAL INFORMATION

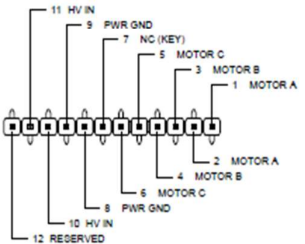
### P1 - Signal Connector

Connector Information	12-pin, 1.27 mm spaced header
Mating Connector	Details Samtec: RSM-112-02-L-S
	Included with Drive No

### P2 - Power Connector

Connector Information	12-pin, 1.27 mm spaced header
Mating Connector	Details Samtec: RSM-112-02-L-S
	Included with Drive No





## DRV8833 Dual H-Bridge Motor Driver

### 1 Features

- Dual-H-Bridge Current-Control Motor Driver
  - Can Drive Two DC Motors or One Stepper Motor
  - Low MOSFET ON-Resistance: HS + LS 360 mΩ
- Output Current (at  $V_M = 5\text{ V}$ ,  $25^\circ\text{C}$ )
  - 1.5-A RMS, 2-A Peak per H-Bridge in PWP and RTY Package Options
  - 500-mA RMS, 2-A Peak per H-Bridge in PW Package Option
- Outputs can be in Parallel for
  - 3-A RMS, 4-A Peak (PWP and RTY)
  - 1-A RMS, 4-A Peak (PW)
- Wide Power Supply Voltage Range: 2.7 to 10.8 V
- PWM Winding Current Regulation and Current Limiting
- Thermally Enhanced Surface-Mount Packages

### 2 Applications

- Battery-Powered Toys
- POS Printers
- Video Security Cameras
- Office Automation Machines
- Gaming Machines
- Robotics

### 3 Description

The DRV8833 device provides a dual bridge motor driver solution for toys, printers, and other mechatronic applications.

The device has two H-bridge drivers, and can drive two DC brush motors, a bipolar stepper motor, solenoids, or other inductive loads.

The output driver block of each H-bridge consists of N-channel power MOSFETs configured as an H-bridge to drive the motor windings. Each H-bridge includes circuitry to regulate or limit the winding current.

Internal shutdown functions with a fault output pin are provided for overcurrent protection, short-circuit protection, undervoltage lockout, and overtemperature. A low-power sleep mode is also provided.

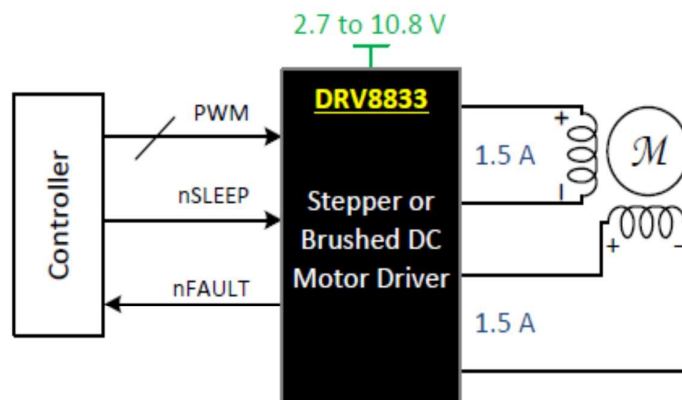
The DRV8833 is packaged in a 16-pin WQFN package with PowerPAD™ (Eco-friendly: RoHS & no Sb/Br).

#### Device Information<sup>(1)</sup>

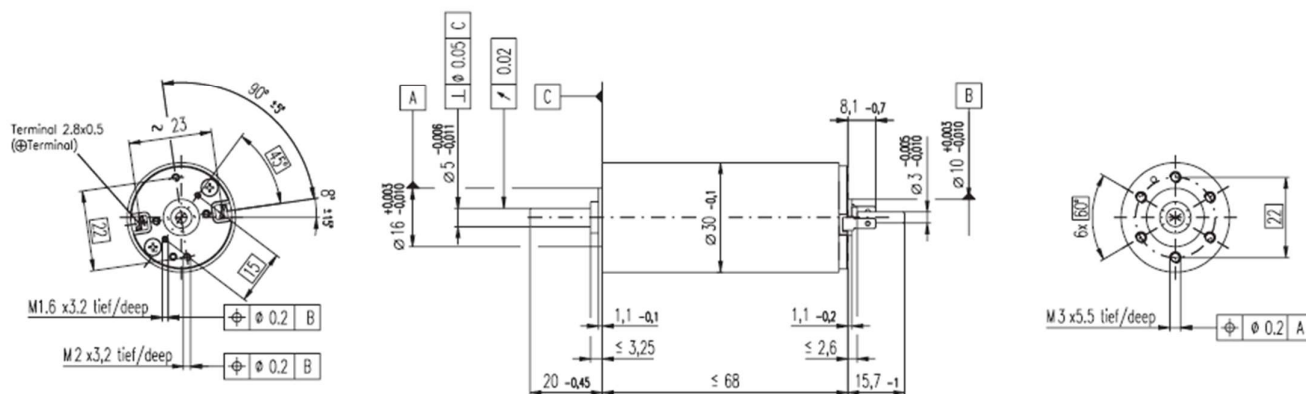
PART NUMBER	PACKAGE	BODY SIZE (NOM)
DRV8833	TSSOP (16)	5.00 mm × 4.40 mm
	HTSSOP (16)	5.00 mm × 4.40 mm
	WQFN (16)	4.00 mm × 4.00 mm

(1) For all available packages, see the orderable addendum at the end of the data sheet.

#### Simplified Schematic



# RE 30 Ø30 mm, Graphite Brushes, 60 Watt



M 1:2

- Stock program
- Standard program
- Special program (on request)

according to dimensional drawing  
shaft length 15.7 shortened to 8.7 mm

## Order Number

310005	310006	310007	310008	310009
268193	268213	268214	268215	268216

## Motor Data

Values at nominal voltage						
1	Nominal voltage	V	12.0	18.0	24.0	36.0
2	No load speed	rpm	8170	8590	8810	8590
3	No load current	mA	300	212	164	106
4	Nominal speed	rpm	7630	7900	8050	7810
5	Nominal torque (max. continuous torque)	mNm	51.7	75.5	85.0	83.4
6	Nominal current (max. continuous current)	A	4.00	4.00	3.44	2.20
7	Stall torque	mNm	844	991	1020	936
8	Starting current	A	60.5	49.8	39.3	23.5
9	Max. efficiency	%	86	87	87	87
Characteristics						
10	Terminal resistance	Ω	0.198	0.362	0.611	1.53
11	Terminal inductance	mH	0.0345	0.0703	0.119	0.281
12	Torque constant	mNm / A	13.9	19.9	25.9	39.8
13	Speed constant	rpm / V	685	479	369	240
14	Speed / torque gradient	rpm / mNm	9.74	8.71	8.69	9.22
15	Mechanical time constant	ms	3.42	3.25	3.03	3.17
16	Rotor inertia	gcm <sup>2</sup>	33.5	35.7	33.3	32.9

## Specifications

Thermal data	
17	Thermal resistance housing-ambient 6.0 K / W
18	Thermal resistance winding-housing 1.7 K / W
19	Thermal time constant winding 16.2 s
20	Thermal time constant motor 714 s
21	Ambient temperature -30 ... +100°C
22	Max. permissible winding temperature +125°C
Mechanical data (ball bearings)	
23	Max. permissible speed 12000 rpm
24	Axial play 0.05 - 0.15 mm
25	Radial play 0.025 mm
26	Max. axial load (dynamic) 5.6 N
27	Max. force for press fits (static) 110 N
28	Max. radial loading, 5 mm from flange 1200 N
28	Max. radial loading, 5 mm from flange 28 N

## Other specifications

29	Number of pole pairs	1
30	Number of commutator segments	13
31	Weight of motor	238 g

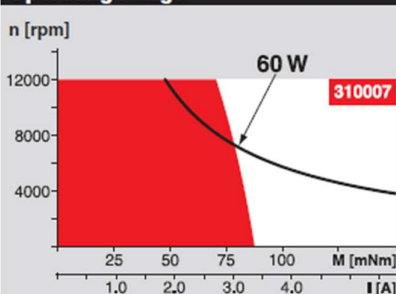
Values listed in the table are nominal.  
Explanation of the figures on page 49.

⚠ Tolerances may vary from the standard specification.

## Option

Preloaded ball bearings

## Operating Range



## Comments

■ **Continuous operation**  
In observation of above listed thermal resistance (lines 17 and 18) the maximum permissible winding temperature will be reached during continuous operation at 25°C ambient.  
= Thermal limit.

□ **Short term operation**  
The motor may be briefly overloaded (recurring).

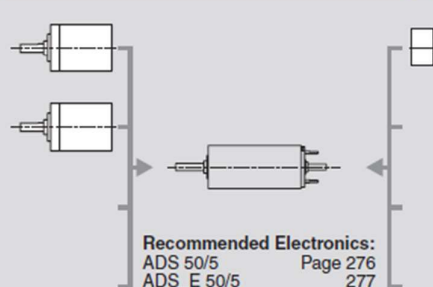
— Assigned power rating

## maxon Modular System

## Overview on page 16 - 21

**Planetary Gearhead**  
Ø32 mm  
0.75 - 4.5 Nm  
Page 239

**Planetary Gearhead**  
Ø32 mm  
1.0 - 6.0 Nm  
Page 240

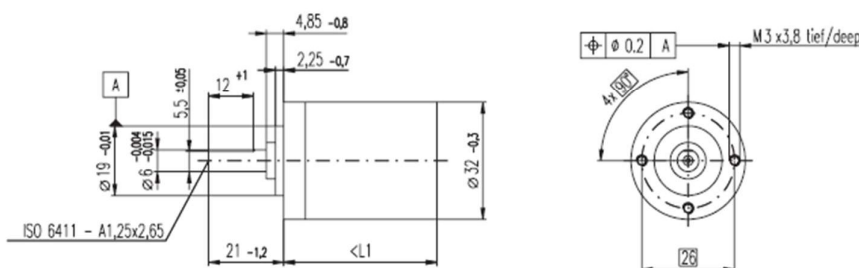


**Recommended Electronics:**  
ADS 50/5 Page 276  
ADS\_E 50/5 277  
EPOS 24/5 294  
EPOS2 50/5 295  
EPOS P 24/5 297  
Notes 18

**Encoder MR**  
256 - 1024 CPT  
3 channels  
Page 259



## Planetary Gearhead GP 32 C Ø32 mm, 1.0 - 6.0 Nm

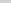
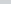


M 1:2

### Technical Data

Planetary Gearhead	straight teeth
Output shaft	stainless steel
Shaft diameter as option	8 mm
Bearing at output	ball bearing
Radial play, 5 mm from flange	max. 0.14 mm
Axial play	max. 0.4 mm
Max. radial load, 10 mm from flange	140 N
Max. permissible axial load	120 N
Max. permissible force for press fits	120 N
Sense of rotation, drive to output	=
Recommended input speed	< 8000 rpm
Recommended temperature range	-20 ... +100°C
Extended area as option	-35 ... +100°C

Option: Low-noise version

-  Stock program
-  Standard program
-  Special program (on request)

**Order Number**

		Standard program											
Special program (on request)		Special program (on request)											
		166930	166933	166938	166939	166944	166949	166954	166959	166962	166967	166972	166977
Gear Data													
1	Reduction	3.7 : 1	14 : 1	33 : 1	51 : 1	111 : 1	246 : 1	492 : 1	762 : 1	1181 : 1	1972 : 1	2829 : 1	4380 : 1
2	Reduction absolute	26/7	676/49	529/16	17576/343	13824/125	421824/1715	86112/175	19044/25	1012376/8675	8626176/1375	495144/175	109503/25
3	Max. motor shaft diameter	mm	6	6	3	6	4	4	3	3	4	3	3
Order Number		166931	166934		166940	166945	166950	166955	166960	166963	166968	166973	166978
1	Reduction	4.8 : 1	18 : 1		66 : 1	123 : 1	295 : 1	531 : 1	913 : 1	1414 : 1	2189 : 1	3052 : 1	5247 : 1
2	Reduction absolute	24/5	624/35		16224/245	6877/56	101062/343	331776/625	36501/40	2425488/1715	536406/245	1907712/625	839523/160
3	Max. motor shaft diameter	mm	4	4		4	3	3	4	3	3	3	3
Order Number		166932	166935		166941	166946	166951	166956	166961	166964	166969	166974	166979
1	Reduction	5.8 : 1	21 : 1		79 : 1	132 : 1	318 : 1	589 : 1	1093 : 1	1526 : 1	2362 : 1	3389 : 1	6285 : 1
2	Reduction absolute	23/4	299/14		3887/49	3312/25	389376/1225	20631/35	279841/256	9345024/6125	206668/675	474513/140	6436343/1024
3	Max. motor shaft diameter	mm	3	3		3	3	4	3	4	3	3	3
Order Number			166936		166942	166947	166952	166957		166965	166970	166975	
1	Reduction		23 : 1		86 : 1	159 : 1	411 : 1	636 : 1		1694 : 1	2548 : 1	3656 : 1	
2	Reduction absolute		57/6		14976/175	1587/40	359424/675	79488/125		1162213/686	7962624/125	457056/125	
3	Max. motor shaft diameter	mm		4		4	3	4	3		3	4	3
Order Number			166937		166943	166948	166953	166958		166966	166971	166976	
1	Reduction		28 : 1		103 : 1	190 : 1	456 : 1	706 : 1		1828 : 1	2623 : 1	4060 : 1	
2	Reduction absolute		138/5		3588/35	12167/64	89401/196	158171/224		2238912/1225	2056223/784	3637933/896	
3	Max. motor shaft diameter	mm		3		3	3	3		3	3	3	
4	Number of stages		1	2	2	3	3	4	4	5	5	5	5
5	Max. continuous torque	Nm	1	3	3	6	6	6	6	6	6	6	6
6	Intermittently permissible torque at gear output	Nm	1.25	3.75	3.75	7.5	7.5	7.5	7.5	7.5	7.5	7.5	7.5
7	Max. efficiency	%	80	75	75	70	70	60	60	50	50	50	50
8	Weight	g	118	162	162	194	194	226	226	258	258	258	258
9	Average backlash no load	°	0.7	0.8	0.8	1.0	1.0	1.0	1.0	1.0	1.0	1.0	1.0
10	Mass inertia	gcm <sup>2</sup>	1.5	0.8	0.8	0.7	0.7	0.7	0.7	0.7	0.7	0.7	0.7
11	Gearhead length L1	mm	26.4	36.3	36.3	43.0	43.0	49.7	49.7	56.4	56.4	56.4	56.4

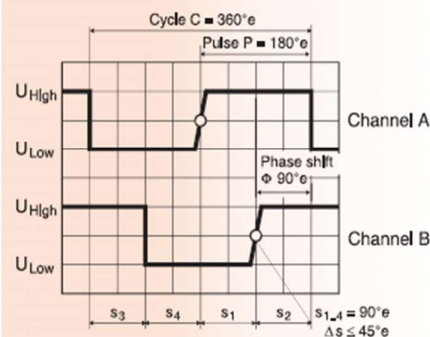
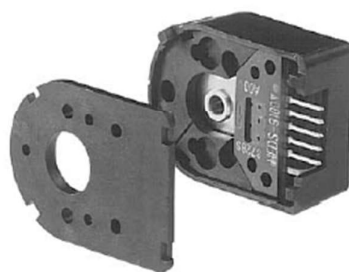
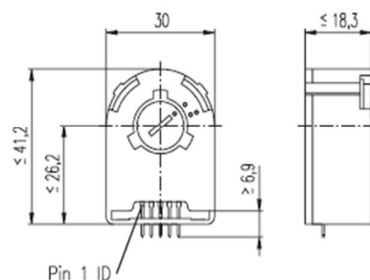


### Combination

Motor	Page	+ Tacho / Brake	Page	Overall length [mm] = Motor length + gearhead length + (tacho / brake) + assembly parts											
RE 25, 10 W	77			81.0	90.9	90.9	97.6	97.6	104.3	104.3	104.3	111.0	111.0	111.0	111.0
RE 25, 10 W	77	MR	258	92.0	101.9	101.9	108.6	108.6	115.3	115.3	115.3	122.0	122.0	122.0	122.0
RE 25, 10 W	77	Enc 22	260	95.1	105.0	105.0	111.7	111.7	118.4	118.4	118.4	125.1	125.1	125.1	125.1
RE 25, 10 W	77	HED_5540	262/264	101.8	111.7	111.7	118.4	118.4	125.1	125.1	125.1	131.8	131.8	131.8	131.8
RE 25, 10 W	77	DCT 22	271	103.3	113.2	113.2	119.9	119.9	126.6	126.6	126.6	133.3	133.3	133.3	133.3
RE 25, 20 W	78			69.5	79.4	79.4	86.1	86.1	92.8	92.8	92.8	99.5	99.5	99.5	99.5
RE 25, 20 W	79			81.0	90.9	90.9	97.6	97.6	104.3	104.3	104.3	111.0	111.0	111.0	111.0
RE 25, 20 W	79	MR	258	92.0	101.9	101.9	108.6	108.6	115.3	115.3	115.3	122.0	122.0	122.0	122.0
RE 25, 20 W	79	Enc 22	260	95.1	105.0	105.0	111.7	111.7	118.4	118.4	118.4	125.1	125.1	125.1	125.1
RE 25, 20 W	79	HED_5540	262/264	101.8	111.7	111.7	118.4	118.4	125.1	125.1	125.1	131.8	131.8	131.8	131.8
RE 25, 20 W	79	DCT 22	271	103.3	113.2	113.2	119.9	119.9	126.6	126.6	126.6	133.3	133.3	133.3	133.3
RE 25, 20 W	79	HED_5540 / AB 28	308	132.2	142.1	142.1	148.8	148.8	155.5	155.5	155.5	162.2	162.2	162.2	162.2
RE 26, 18 W	80			85.3	95.2	95.2	101.9	101.9	108.6	108.6	108.6	115.3	115.3	115.3	115.3
RE 26, 18 W	80	MR	258	96.3	106.2	106.2	112.9	112.9	119.6	119.6	119.6	126.3	126.3	126.3	126.3
RE 26, 18 W	80	Enc 22	260	102.7	112.6	112.6	119.3	119.3	126.0	126.0	126.0	132.7	132.7	132.7	132.7
RE 26, 18 W	80	HED_5540	262/264	103.7	113.6	113.6	120.3	120.3	127.0	127.0	127.0	133.7	133.7	133.7	133.7
RE 26, 18 W	80	DCT 22	271	106.3	116.2	116.2	122.9	122.9	129.6	129.6	129.6	136.3	136.3	136.3	136.3
RE 30, 60 W	81			94.5	104.4	104.4	111.1	111.1	117.8	117.8	117.8	124.5	124.5	124.5	124.5
RE 30, 60 W	81	MR	259	105.9	115.8	115.8	122.5	122.5	129.2	129.2	129.2	135.9	135.9	135.9	135.9
RE 35, 90 W	82			97.4	107.3	107.3	114.0	114.0	120.7	120.7	120.7	127.4	127.4	127.4	127.4
RE 35, 90 W	82	MR	259	108.8	118.7	118.7	125.4	125.4	132.1	132.1	132.1	138.8	138.8	138.8	138.8
RE 35, 90 W	82	HED_5540	262/264	118.4	128.3	128.3	135.0	135.0	141.7	141.7	141.7	148.4	148.4	148.4	148.4
RE 35, 90 W	82	DCT 22	271	115.5	125.4	125.4	132.1	132.1	138.8	138.8	138.8	145.5	145.5	145.5	145.5
RE 35, 90 W	82	AB 28	308	133.5	143.4	143.4	150.1	150.1	156.8	156.8	156.8	163.5	163.5	163.5	163.5
RE 35, 90 W	82	HEDS 5540 / AB 28	262/308	150.6	160.5	160.5	167.2	167.2	173.9	173.9	173.9	180.6	180.6	180.6	180.6
RE 36, 70 W	83			97.7	107.6	107.6	114.3	114.3	121.0	121.0	121.0	127.7	127.7	127.7	127.7
RE 36, 70 W	83	MR	259	109.1	119.0	119.0	125.7	125.7	132.4	132.4	132.4	139.1	139.1	139.1	139.1
RE 36, 70 W	83	HED_5540	262/264	118.7	128.6	128.6	135.3	135.3	142.0	142.0	142.0	148.7	148.7	148.7	148.7
RE 36, 70 W	83	DCT 22	271	115.8	125.7	125.7	132.4	132.4	139.1	139.1	139.1	145.8	145.8	145.8	145.8



## Encoder HEDS 5540, 500 Counts per turn, 3 Channels



- ☒ Stock program  
☐ Standard program  
☐ Special program (on request)

## Order Number

110511	110513	110515
--------	--------	--------

## Type

Counts per turn	500	500	500
Number of channels	3	3	3
Max. operating frequency (kHz)	100	100	100
Shaft diameter (mm)	3	4	6



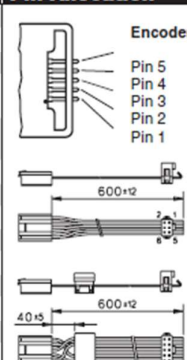
## Combination

+ Motor	Page	+ Gearhead	Page	+ Brake	Page	Overall length [mm] / • see: + Gearhead
RE 25, 10 W	77					75.3
RE 25, 10 W	77	GP 26, 0.5 - 2.0 Nm	235			•
RE 25, 10 W	77	GP 32, 0.4 - 2.0 Nm	237			•
RE 25, 10 W	77	GP 32, 0.75 - 6.0 Nm	238/240			•
RE 25, 20 W	79					75.3
RE 25, 20 W	79	GP 26, 0.5 - 2.0 Nm	235			•
RE 25, 20 W	79	GP 32, 0.4 - 2.0 Nm	237			•
RE 25, 20 W	79	GP 32, 0.75 - 6.0 Nm	238/240			•
RE 25, 20 W	79			AB 28	308	105.7
RE 25, 20 W	79	GP 26, 0.5 - 2.0 Nm	235	AB 28	308	•
RE 25, 20 W	79	GP 32, 0.4 - 2.0 Nm	237	AB 28	308	•
RE 25, 20 W	79	GP 32, 0.75 - 6.0 Nm	238/240	AB 28	308	•
RE 26, 18 W	80					77.2
RE 26, 18 W	80	GP 26, 0.5 - 2.0 Nm	235			•
RE 26, 18 W	80	GP 32, 0.4 - 2.0 Nm	237			•
RE 26, 18 W	80	GP 32, 0.75 - 6.0 Nm	238/240			•
RE 35, 90 W	82					91.9
RE 35, 90 W	82	GP 32, 0.75 - 6.0 Nm	239/240			•
RE 35, 90 W	82	GP 32, 8 Nm	242			•
RE 35, 90 W	82	GP 42, 3.0 - 15 Nm	244			•
RE 35, 90 W	82			AB 28	308	124.1
RE 35, 90 W	82	GP 32, 0.75 - 6.0 Nm	239/240	AB 28	308	•
RE 35, 90 W	82	GP 42, 3.0 - 15 Nm	244	AB 28	308	•
RE 36, 70 W	83					92.2
RE 36, 70 W	83	GP 32, 0.4 - 2.0 Nm	237			•
RE 36, 70 W	83	GP 32, 0.75 - 6.0 Nm	239/240			•
RE 36, 70 W	83	GP 42, 3.0 - 15 Nm	244			•
RE 40, 150 W	84					91.7
RE 40, 150 W	84	GP 42, 3.0 - 15 Nm	244			•
RE 40, 150 W	84	GP 52, 4.0 - 30 Nm	247			•
RE 40, 150 W	84			AB 28	308	124.2
RE 40, 150 W	84	GP 42, 3.0 - 15 Nm	244	AB 28	308	•
RE 40, 150 W	84	GP 52, 4.0 - 30 Nm	247	AB 28	308	•

## Technical Data

Supply voltage	5 V ± 10 %
Output signal	TTL compatible
Phase shift F (nominal)	90°e ± 45°e
Signal rise time (typical at C <sub>L</sub> = 25 pF, R <sub>L</sub> = 2.7 kΩ, 25°C)	180 ns
Signal fall time (typical at C <sub>L</sub> = 25 pF, R <sub>L</sub> = 2.7 kΩ, 25°C)	40 ns
Index pulse width (nominal)	90°e
Operating temperature range	-40 ... +100°C
Moment of inertia of code wheel	≤ 0.6 gcm <sup>2</sup>
Max. angular acceleration	250 000 rad s <sup>-2</sup>
Output current per channel	min. -1 mA, max. 5 mA

## Pin Allocation



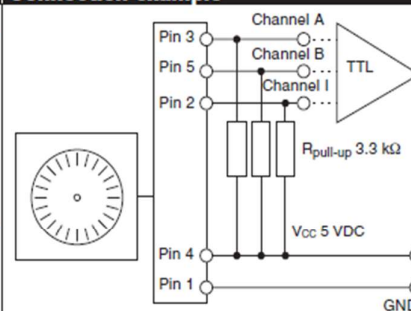
## Description

Pin no.	from 3409.506
1	Channel B
2	V <sub>CC</sub>
3	Channel A
4	Channel I
5	GND

**Cable with plug:**  
 maxon Art. No. 3409.506  
 The plug (Harting 0918506803) can be fixed in the required position.

**Cable with plug:** (compatible with Encoder HEDS5010)  
 maxon Art. No. 3409.504  
 The plug (3M 89110-0101) can be fixed in the required position.

## Connection example



Ambient temperature range  $\delta U = 25^\circ\text{C}$

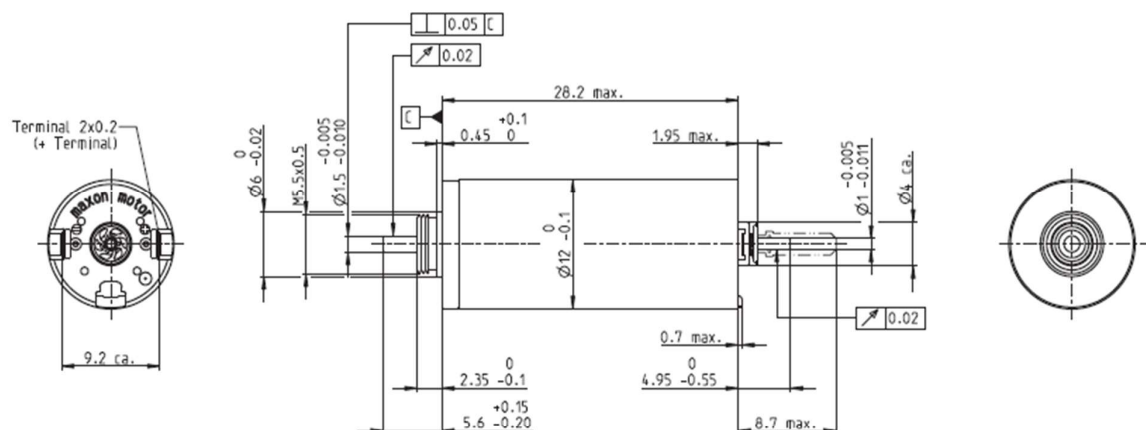
# DCX 12 L Precious Metal Brushes

## DC motor Ø12 mm

2.5/4.8 W 4.2 mNm 12000 rpm



maxon X drives



M 3:2

### Motor Data

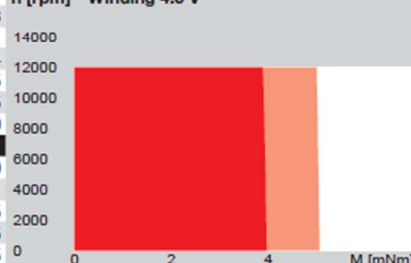
		3	4.5	6	9	12	18
1_ Nominal voltage	V	3	4.5	6	9	12	18
2_ No load speed	rpm	8800	8810	8810	8820	8810	8800
3_ No load current	mA	34.5	23	17.2	11.5	8.62	5.75
4_ Nominal speed	rpm	6360	5710	5600	5800	5600	5590
5_ Nominal torque (max. continuous torque)	mNm	2.88	4.07	3.92	4.16	3.92	3.89
6_ Nominal current (max. continuous current)	A	0.924	0.861	0.622	0.441	0.311	0.206
7_ Stall torque	mNm	10.4	11.6	10.8	12.2	10.8	10.7
8_ Stall current	A	3.24	2.4	1.68	1.26	0.842	0.554
9_ Max. efficiency	%	81	82	81	82	81	81
10_ Terminal resistance	Ω	0.927	1.87	3.58	7.12	14.3	32.5
11_ Terminal inductance	mH	0.031	0.071	0.125	0.282	0.502	1.13
12_ Torque constant	mNm/A	3.22	4.83	6.44	9.66	12.9	19.3
13_ Speed constant	rpm/V	2970	1980	1480	989	741	494
14_ Speed/torque gradient	rpm/mNm	854	766	823	729	821	831
15_ Mechanical time constant	ms	4.32	4.27	4.28	4.27	4.28	4.3
16_ Rotor inertia	gcm <sup>2</sup>	0.484	0.533	0.496	0.559	0.498	0.495

### Thermal data

17_ Thermal resistance housing-ambient	K/W	31
18_ Thermal resistance winding-housing	K/W	10.3
19_ Thermal time constant winding	s	10.1
20_ Thermal time constant motor	s	194
21_ Ambient temperature ball bearings	°C	-40...+85
Ambient temperature sleeve bearings	°C	-30...+85
22_ Max. winding temperature	°C	100

### Operating Range

n [rpm] Winding 4.5 V



■ Continuous operation  
■ Continuous operation with reduced thermal resistance  $R_{th}$  50%  
■ Intermittent operation

### Mechanical data ball bearings

23_ Max. speed	rpm	12000
24_ Axial play	mm	0...0.1
Preload	N	0.5
25_ Radial play	mm	0.015
26_ Max. axial load (dynamic)	N	0.5
27_ Max. force for press fits (static) (static, shaft supported)	N	8.8
28_ Max. radial load [mm from flange]	N	120

### Mechanical data sleeve bearings

23_ Max. speed	rpm	12000
24_ Axial play	mm	0...0.15
Preload	N	0
25_ Radial play	mm	0.015
26_ Max. axial load (dynamic)	N	0.1
27_ Max. force for press fits (static) (static, shaft supported)	N	30
28_ Max. radial load [mm from flange]	N	120

### Other specifications

29_ Number of pole pairs		1
30_ Number of commutator segments		7
31_ Weight of motor	g	16
32_ Typical noise level	dBA	44

### maxon Modular System

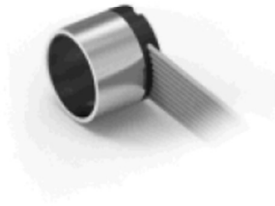
maxon gear	Stages	maxon sensor	maxon motor control
116_GPX 12 A/C	1-4	146_ENX 10 EASY	416_ESCON Module 24/2
117_GPX 12 LN/LZ	1-4	146_ENX 10 QUAD	416_ESCON 36/2 DC
118_GPX 12 HP	2-4		424_EPOS2 24/2 (DC/EC)
119_GPX 14 A/C	3-4		424_EPOS2 Module 36/2
120_GPX 14 LN/LZ	3-4		
121_GPX 14 HP	4		

### Configuration

Bearing: Sleeve bearings/ball bearings preloaded  
 Commutation: Precious metal brushes with or without CLL  
 Flange front/back: Standard flange/Flange with thread holes/no flange  
 Shaft front/back: Length  
 Electric connection: Terminals or cable/cable length/connector type

xdrives.maxonmotor.com

## Sensor - ENX10 EASY 512IMP



Type	
Counts per turn	512
Number of channels	3
Line Driver	RS422
Max. outer diameter	10 mm
Max. housing length	8.5 mm
Max. electrical speed	90000 rpm
Max. speed	30000 rpm

Technical data	
Supply voltage, typical	5 V
Supply voltage tolerance +/-	10 %
Output signal driver	Differential, EIA RS 422
Current per cable	-20...20 mA
Min. state length	45 °el
Min. state length	135 °el
Signal rise time/Signal fall time	20/20 ns
Min. state duration	125 ns
Direction of rotation	A for B, CW
Index position	A low & B low
Index synchronously to AB	yes
Index pulse width	90 e°
Typical current draw at standstill	23 mA
Max. moment of inertia of code wheel	0.05 gcm <sup>2</sup>
Weight (Standard cable length)	7.1 g
Operating temperature range	-40...100 °C
Number of autoclave cycles	0

Datasheet: [http://www.maxonmotor.com/medias/CMS\\_Downloads/DIVERSES/ENXEASY\\_en.pdf](http://www.maxonmotor.com/medias/CMS_Downloads/DIVERSES/ENXEASY_en.pdf)